Substrate Aggregation and Ubiquitination Dictate the Fate of Misfolded Proteins for Endoplasmic Reticulum Associated Degradation over Post Endoplasmic Reticulum Degradation

by

Zhihao Sun

BS in Biotechnology, Qingdao University, 2010

MS in Biochemistry and Molecular Biology, Zhejiang University, 2013

Submitted to the Graduate Faculty of the

Dietrich School of Arts and Sciences in partial fulfillment

of the requirements for the degree of

Doctor of Philosophy

University of Pittsburgh

2019

UNIVERSITY OF PITTSBURGH

THE KENNETH P. DIETRICH SCHOOL OF ARTS AND SCIENCES

This dissertation was presented

by

Zhihao Sun

It was defended on

May 3, 2019

and approved by

Jon P. Bolye, Ph.D., Associate Professor, Department of Biological Sciences

Graham F. Hatfull, Ph.D., Professor, Department of Biological Sciences

Adam D. Linstedt, Ph.D., Professor, Department of Biological Sciences

Andrew P. VanDemark, Ph.D., Associate Professor, Department of Biological Sciences

Dissertation Advisor: Jeffrey L. Brodsky, Ph.D., Professor, Department of Biological Sciences

Substrate Aggregation and Ubiquitination Dictate the Fate of Misfolded Proteins for Endoplasmic Reticulum Associated Degradation over Post Endoplasmic Reticulum Degradation

Zhihao Sun, PhD

University of Pittsburgh, 2019

Protein folding is inherently dynamic and error prone. Even with an elaborate network of cellular factors, protein misfolding occurs frequently. To maintain protein homeostasis, eukaryotes have evolved a hierarchy of protein quality control checkpoints along the secretory pathway, including endoplasmic reticulum associated degradation (ERAD) and post-ER quality control (QC). Although most aberrant proteins are eliminated by ERAD, some misfolded proteins do exit the ER and are turned over by lysosomal proteases. To date, it remains elusive how misfolded membrane proteins are selected for different fates: ERAD versus post-ERQC. To address this question, a novel model substrate, SZ*, was designed and utilized in this study. SZ* is a single-pass membrane chimeric protein bearing cytosolic folding lesion. I first investigated its degradation fate in yeast and found that SZ* is eliminated by both the proteasome via the ERAD pathway and vacuolar proteases via the Golgi-QC pathway. The post-ER degradation of SZ* occurs after ER exit and requires the multivesicular body pathway. I then interrogated cells with different stress treatment to test how various conditions affect the fate of SZ*. My results showed that both heat-shock and substrate overexpression increase ERAD targeting, which both lead to substrate aggregation. Therefore, a misfolded membrane protein with a higher aggregation propensity is preferentially retained in the ER and targeted for ERAD. Next, I sequentially inhibited different steps in the ERAD pathway and tested SZ* ER export efficiency both *in vivo* and *in vitro*. I discovered that inhibiting steps required for ubiquitination, including substrate recognition and ubiquitination, facilitate ER exit of SZ* through coat protein complex

(COP) II transport. These studies suggest that ERAD substrates can be rescued for ER export by eliminating ubiquitination. In line with this evidence, I fused SZ* to four tandem ubiquitin moieties that are not efficiently degraded by ERAD and found that this substrate could not exit the ER even when ERAD was inhibited. Together, these data provide evidence that substrate aggregation and ubiquitination can be sufficient for ER retention.

TABLE OF CONTENTS

LIST OF TABLES

LIST OF FIGURES

PREFACE

This research work is the culmination of my graduate studies, and the most significant accomplishments by far in my science career. Such accomplishment would never be possible without the supports and contributions of many wonderful people in my life.

First and foremost, I would like to express my sincerest gratitude to my mentor and research advisor, Dr. Jeffrey L. Brodsky. It is my great honor to join his lab, and become one of his students. Jeff is such a great mentor and friend who helped me all the way to guide my life and research to the right track. As an international student, I have to overcome many challenges, and homesick is one of the biggest. I still remember that he asked me to go back home to see my parents and friends although I just joined the lab for one month at that time. I also remember when my baby girl was born, Jeff directly told me to take days off however long I want. I am so grateful for his support in every aspect in my life. In science, I am deeply impressed by his sharp mind and great width of knowledge. Whenever I got stuck in my research, Jeff will always give me great idea and encourage me to keep moving. He is my role model in both research and life. The skills and lessons I learned from Jeff will be of great significance in my life to guide both my research and life in the future.

I would also like to thank all the Brodsky lab members. Dr. Patrick Needham is my good friend and rotation advisor who chaperoned me into the protein quality control field and taught me all the basic skills about yeast work. Dr. Chris Guerriero is both my good friend and research “big brother”, who is always there to help me solve my problems in both research and life. Dr. Teresa Buck is my research “Big sister”, who is always happy to share her expertise both in science and life. I would also like to thank Dr. Annette Chiang, who helped me most aspects in

my life. I still remember my first Christmas in Annette's house with her family, which swept away my loneliness and homesickness. Thank you Jennifer Goeckeler-Fried for being a wonderful lab manager. My research couldn't be so smooth without your support. Thank you Dr. Timothy Mackie for being a great friend and lab mate. You taught me a lot about interesting American history and yeast genetics. Thanks for your quick response and great help even after you left Pittsburgh. Thank you the rest Brodsky lab members including Dr. Michael Preston, Dr. Lynley Doonan, Dr. Sara Sannino, Sam Estabrooks, Deepa Kumari, Katie Nguyen, and Grant Daskivich. Thanks for creating a friendly and positive lab environment where I can enjoy my research. Thank you Sam Estabrooks and Deepa Kumari for being my great friends. The jokes and friendship we had made my life colorful in the lab. Thank you Danica Pratta, my undergraduate researcher. Thanks for working with me for about two and half years, and for your wonderful gift for Riley. Thank you all the undergraduate lab aids!

Next, I would like to express my sincere thanks to my committee member Dr. Jon Boyle, Dr. Graham Hatfull, Dr. Adam Linstedt, and Dr. Andrew VanDemark for their insightful and encouraging support throughout my gradate career. It is my great honor to have the opportunity to rotate in the Hatfull lab and VanDemark lab. Thanks for being such a great committee chair, Jon! Thanks for all the helpful reagent and suggestions, Adam!

Finally, I would like to thank my family and friends. I am the second person in our family who received bachelor degree, the first person in our family to receive the master degree and the doctor degree in the next a few months. My sister and I are the first two persons in our family who received the higher education. For these, I would like to first thank my parents, Guihan Sun and Fenglan Zhu. I could never have this accomplishment without your endless support and love. You always encourage me to learn as much as I can and never to worry about financial issue. I

will never forget that my Mom would always wait by the cellphone for my video call each day just to check if I had a good day. I will always remember how much you worried about me that day when I fell asleep forgetting to log off our chatting software. You always encourage me to pursue a career in research in the United States, although I know how much you miss me. You are the greatest parents in the world, who give me all but ask for nothing. Thanks Dad, and thanks Mom! I would also like to express my gratitude to my sister, Zhihong Sun who would do everything she could to help me and my brother-in-law, Yunpeng Ji, who also gave me great support during my graduate career. Thank you my parents-in-law and brother-in-law, who brought to me my beloved wife and gave me great support during my graduate study. To my wife, Ning, I would never achieve this without your help and accompany. Thanks for your love and understanding! Thanks for being always by my side! Thanks for bringing to me such a lovely and beautiful girl Runxin. The past seven months with my daughter taught me so much. Thanks for being my biggest motivation, Runxin! To my friends especially Xuecheng Jiang, Houfu Zhang, Ching-Chung Ko, thanks for listening, offering me advice, and supporting me through my entire graduate career. Thanks for all my friends including my college roommates in Qingdao University, graduate roommates in Zhejiang University. Those are my life-long treasure of memory.

1.0 INTRODUCTION

In eukaryotes, about one-third of the proteome is synthesized at the ER. These proteins first enter the ER through a protein translocon in an unfolded state (Rapoport et al., 2017). To gain functional activity and traffic to their final destinations, these proteins must fold into defined tertiary and in some cases quaternary structures. During the folding process, a myriad of chaperones are recruited to assist folding intermediates to overcome energy barriers before the energetically favorable conformation can be reached (Balchin et al., 2016). Protein folding in the ER is also guided by post-translational modifications, including glycosylation, disulfide bond formation, and lipidation (Braakman and Hebert, 2013). At this point, monomeric and multi-subunit protein complexes can then continue their journey along the secretory pathway through COPII vesicle-mediated transport.

Despite the enormous investment of cellular resources dedicated to protein folding, about 12%-15% of newly synthesized polypeptides in human cells, and 1-5% in yeast are co-translationally eliminated through ubiquitin-proteasome system (Duttler et al., 2013; Wang et al., 2013). This percentage becomes even higher for post-translational protein degradation, as new proteins face even more challenges such as post-translational modifications, genetic mutations, defined metabolic states and environmental stress (Chen et al., 2011; Shao and Hegde, 2016; Trombetta and Parodi, 2003). In the cell, protein misfolding is toxic due to either loss-of-function or gain-of-function activities. In one example, loss-of-function mutations can arise as a result of genetic mutation that makes the protein susceptible to degradation by one of several cellular quality control (QC) machineries. Mutant variants of proteins such as the cystic fibrosis transmembrane conductance regulator (CFTR) and aquaporin 2 represent examples of disease-

causing proteins that are trapped in the ER and are then efficiently disposed of by the endoplasmic reticulum-associated degradation (ERAD) pathway, which give rise to cystic fibrosis and alpha 1 antitrypsin deficiency, respectively (Guerriero and Brodsky, 2012; Stoller and Aboussouan, 2012; Veit et al., 2016). Other proteins, when mutated, can have detrimental gain-of-function effects by forming protein aggregates or polymers. These aggregation-prone proteins can engage in promiscuous interactions with other cellular components and accumulate in toxic cellular protein inclusions that sequester essential cellular components or organelles (Eisele et al., 2015). Proteins in the cytosol that exhibit this phenomenon include mutant Huntington protein (Htt) and alpha-synuclein, which in turn lead to Hungtington's disease and Parkinson's disease, respectively (Sweeney et al., 2017). As the analysis of genomic and patient databases becomes more widespread, the number of conformational diseases that are related to protein misfolding and/or aggregation is growing (Guerriero and Brodsky, 2012; Tao and Conn, 2018).

To counteract protein misfolding and maintain protein homeostasis "proteostasis", eukaryotes have evolved multiple QC mechanisms in the cytosol and along the secretory pathways, including cytoplasmic QC, ERAD, ER-phagy, Golgi QC (GQC) and plasma membrane QC (PMQC). For each of these processes, the unfolded protein response (UPR) and the heat shock response respectively serve as master regulators by adjusting protein synthesis, chaperone induction, and protein degradation pathways (Karagoz et al., 2019; Li et al., 2017; Preissler and Ron, 2018; Travers et al., 2000).

ERAD clears most misfolded secretory proteins during or soon after proteins enter the ER by a step-wise mechanism: substrate recognition, retrotranslocation and ubiquitination, and proteasomal degradation (Berner et al., 2018; Hwang and Qi, 2018; Needham et al., 2019;

Ruggiano et al., 2014; Vembar and Brodsky, 2008). The activity of ERAD needs to be tightly regulated as both hyperactive and hypoactive ERAD result in human disease (Guerriero and Brodsky, 2012; Hebert and Molinari, 2007). Notably, ER-phagy (see below) back-ups ERAD when folding is challenged by stress, or when protein aggregates/polymers arise in the ER that cannot be handled by the ERAD pathway. For example, alpha-1 antitrypsin deficiency is caused by degradation of mutant forms of alpha-1 antitrypsin (AT) in the ER, even though the protein retains residual function (Perlmutter, 2011). Interestingly, AAT with lower aggregation propensity or is present at lower levels are mostly degraded by ERAD, whereas accumulation of the most aggregation prone variant, AT-Z, is eliminated by ER-phagy (Fregno et al., 2018; Kruse et al., 2006; Teckman and Perlmutter, 1996; Teckman and Perlmutter, 2000). Nevertheless, some misfolded or unassembled proteins evade ERAD and ER-phagy, exit the ER, and become GQC substrates that are routed to the vacuole (in yeast) or lysosome (in higher cells) for degradation (Arvan et al., 2002). Of note, some native membrane proteins with polar residues in their transmembrane domain (TMD) mimic protein misfolding events and are recognized by a Golgi-resident E3 ubiquitin ligase, Tul1, and sorted to the vacuole for maturation/degradation (Reggiori and Pelham, 2002). Compared to other substrates, GQC substrates may be less toxic so they can escape the ER and are recognized in the Golgi, which may operate with higher or perhaps altered specificity. Therefore, the ER acts as an initial triage center, selecting out the direst cases for ERAD/ER-phagy. In this chapter, I will review the mechanisms underlying ERAD, ER-phagy, and GQC, and highlight the “decisions” made in the ER to triage misfolded proteins for degradation, especially by ERAD versus post-ERQC.

1.1 ENDOPLASMIC RETICULUM ASSOCIATED DEGRADATION

ERAD is the primary defense mechanism in the ER to recognize and target terminally misfolded proteins for degradation. Initially, the ER was assumed to harbor the proteolytic activity for misfolded ER proteins (Needham and Brodsky, 2013). However, subsequent research revealed the cytosolic proteasome as the degradation machinery for misfolded ER proteins (Hampton et al., 1996; Hiller et al., 1996; Jensen et al., 1995; McCracken and Brodsky, 1996; Sommer and Jentsch, 1993; Ward et al., 1995; Werner et al., 1996). Therefore, the ER membrane establishes a physical barrier to separate the ER folding and degradation environments, protecting folding intermediates from premature degradation. The identification of ERAD components in multiple systems revealed an evolutionarily conserved process. Despite the immense structural and topological diversity of proteins that enter the secretory pathway, work primarily in the budding yeast, *S. cerevisae*, revealed simple principles under which ERAD operates: misfolded ER proteins are recognized and ubiquitinated by one of three branches, ERAD-L (lumen), ERAD-C (cytoplasm) or ERAD-M (membrane), depending on the localization of the folding lesion relative to the ER membrane (Carvalho et al., 2006; Huyer et al., 2004b; Vashist and Ng, 2004). The key players required for substrate ubiquitination are the E3 ubiquitin ligases Hrd1 (ERAD-L/M) and Doa10 (ERAD-C). However, the assignment of mammalian ERAD substrates to three ERAD classes (ERAD-L/C/M) is less straightforward due to the existence of multiple E3 ligases that can work both individually and in concert with one another (Christianson and Ye, 2014). Therefore, I will mostly focus on studies in yeast. Nevertheless, common in both yeast and man are the critical early steps during ERAD, which include substrate recognition, retrotranslocation and ubiquitination, which in yeast differ between

each branch. Later steps during ERAD, including Cdc48/p97-mediated retrotranslocation and proteasomal degradation, are common to all three branches (Figure 1).

1.1.1 ERAD-L

To protect proteostasis, the ERAD-L machinery must recognize proteins that fail to acquire ER-specific post-translational modifications as well as terminally misfolded proteins with lesions within the ER. These latter substrates must be distinguished from folding intermediates that exhibit similar misfolded conformations. The requirement to monitor protein folding along with the acquisition of post-translational modifications makes ERAD-L unique and the most complicated of the three ERAD branches.

The typical and best-characterized ERAD-L substrates are misfolded glycoproteins, as recognition requires both an *N*-linked glycan and protein determinants that are misfolded. During glycoprotein folding, a core glycan, Glc3Man9GlcNAc2, is first appended to an asparagine in the N-X-(S/T) consensus motif (Helenius and Aebi, 2004). This N-linked glycan is subsequently trimmed by a cascade of enzymes, which act in concert with chaperones and lectins to monitor glycoprotein folding. The three terminal glucose residues are cleaved sequentially by glucosidase I and II, generating Man9GlcNAc2 (Hitt and Wolf, 2004; Jakob et al., 1998). Further trimming by mannosidase I (Mns1) removes the α-1,2-mannose from the B-branch, yielding Man8GlcNAc2 (Camirand et al., 1991). This is the rate-limiting step during ERAD-L, which provides sufficient time to fold proteins that may be folding-competent (Jakob et al., 1998). Strikingly, Man8GlcNAc2 glycan is shared by both well-folded proteins exiting the ER and ERAD-L substrates, indicating that the Mns1 mannosidase does not discriminate between folded and misfolded proteins (Gauss et al., 2011). To instead generate an ERAD glycan signal, an

exposed α-1,6-mannose is generated by Htm1 (EDEM in mammals) in complex with protein disulfide isomerase Pdi1 (Gnann et al., 2004; Nishikawa et al., 2001). After the exposure of α-1,6-mannose, misfolded glycoproteins are captured by the Yos9 (OS-9 and XTP-3B in mammals) lectins and molecular chaperones, which together deliver substrates to Hrd3 (Sel1 in mammals), a component of Hrd1 complex (Denic et al., 2006; Plemper et al., 1999; Xie et al., 2009).

Besides the ERAD glycan signal, another feature common in most terminally misfolded proteins and folding intermediates is exposed hydrophobic patches that are otherwise buried inside folded proteins. In addition to assisting in the delivery of substrates to Hrd3 (see above), these proteins are maintained in a soluble state by binding to ER-resident molecular chaperones, including the Hsp70 Kar2 (BiP in mammals) and Hsp40 partners Scj1 and Jem1 (Brodsky et al., 1999; Gauss et al., 2011; Jakob et al., 1998; Nishikawa et al., 2001).

Recent work suggests the involvement of another type of glycosylation event during ERAD, *O*-mannosylation of Ser/Thr residues by Pmt1/Pmt2 (Xu and Ng, 2015a; Xu and Ng, 2015b; Xu et al., 2013). This modification is important to terminate futile folding cycles of certain misfolded lumenal protein and thus facilitate ERAD (Xu et al., 2013). Both *N*-glycan trimming and *O*-mannosylation are slow process, which lead to substrate lingering in the ER. In principle, this provides enough time for protein folding and re-folding, but on the other hand this potentially presents folding intermediates to the ERAD machinery since some chaperones are involved in both protein folding and turnover (Preston and Brodsky, 2017). This conundrum was recently solved by the discovery of a guardian complex, Slp1-Emp65, that plays an important role in protecting folding intermediates from premature degradation (Sun and Brodsky, 2017; Zhang et al., 2017).

After being selected, ERAD-L substrates are delivered to the Hrd1 complex, which includes Yos9, Hrd3, Der1, Usa1 and Hrd1. Since the Really Interesting New Gene (RING) domain in the Hrd ubiquitin ligase is localized on the cytosolic side of the ER membrane, soluble ERAD-L substrates need to be retrotranslocated or dislocated from the ER lumen to the cytosol to be modified. The identity of the proteinaceous "retrotranslocon" has been controversial.

Sec61 and Hrd1 are currently the major candidates that function as the ERAD retrotranslocon. Because of its function as a protein-conducting channel for the ER, Sec61 was first suggested as the retrotranslocon during ERAD. Evidence supporting this hypothesis includes coimmunoprecipitation experiments demonstrating interaction between Sec61 and ERAD substrates as well as the proteasome (Kalies et al., 2005; Schafer and Wolf, 2009; Wiertz et al., 1996b). Some ERAD substrates, such as Apolipoprotein B, are retrotranslocated when translocation into the ER through Sec61 is interrupted, indicating that Sec61 has the potential to move proteins in either direction (Mitchell et al., 1998). Nevertheless, strong evidence implicating the Hrd1 ubiquitin ligase as the retrotranslocon has grown over recent years, at least for some substrates. First, the function of this 8 transmembrane protein during ERAD-L requires its oligomerization, which is mediated by Usa1, and Hrd1 interacts with substrates at an early retrotranslocation stage (Carvalho et al., 2010). Additional evidence for its activity as a retrotranslocation channel came from a recent *in vitro* reconstitution assay that recapitulated retrotranslocation with proteoliposomes containing both Hrd1 and an ERAD-L substrate. In the *in vitro* assay, an ERAD-L substrate tethered via a single transmembrane domain was poly-ubiquitinated after addition of other components of the ubiquitin machinery outside the reconstituted vesicles. These data demonstrate substrate retrotranslocation across a lipid membrane (Baldridge and Rapoport, 2016). The identity of Hrd1 as a retrotranslocon was further

corroborated by a recent cryo-electron microscopy (cryo-EM) structure of Hrd1 in complex with Hrd3 (Schoebel et al., 2017). In the structure, Hrd1 forms a dimer within the membrane with Hrd3, which is associated on the lumenal side of the ER membrane. Five of eight transmembrane segments of Hrd1 form a funnel that extends from the cytosol almost to the lumenal side of the membrane. In addition, the aqueous cavity formed by Hrd1 is reminiscent of that formed by Sec61.

Another early candidate for the retrotranslocon was Der1, which is a multi-spanning membrane protein that is also required for elimination of ERAD-L substrates (Knop et al., 1996; Mehnert et al., 2014; Vashist and Ng, 2004). As a component of the Hrd1 complex, Der1 receives ERAD-L substrates from the recognition factors Yos9/Hrd3 and transfers them to the Hrd1 ligase through the Hrd1 scaffold protein Usa1 (Horn et al., 2009; Mehnert et al., 2014). In one study, Der1 (Derlin-1 in mammals) was shown to directly facilitate the retrotranslocation of mutant pro-α-factor *in vitro* using mammalian microsomes loaded with the substrate (Wahlman et al., 2007). Mutant pro-α-factor is a non-canonical substrate whose degradation is ubiquitin-independent, potentially bypassing the requirement of Hrd1 as both an E3 ligase and retrotranslocon (Werner et al., 1996). Therefore, Der1 may act both as a mediator to recruit ERAD-L substrates to the membranous Hrd1 complex and as retrotranslocon for non-ubiquitinated ERAD substrates, like pro-α-factor and possibly cholera toxin (Kothe et al., 2005). More recent evidence indicated that Der1 intimately contacts ERAD substrates as they exit the ER, and it was proposed to facilitate the solubilization of membrane proteins, which could increase access to Hrd1 (Mehnert et al., 2014). Overall, several integral membrane components in the ER remain as strong candidates as the retrotranslocon for ERAD-L substrates.

1.1.2 ERAD-M

ER membrane proteins with folding lesions within transmembrane domains are recognized and eliminated by ERAD-M, in which the Hrd1 complex plays a major role. In contrast to recognition of ERAD-L substrates, the identification of folding lesions within the lipid bilayer is especially challenging as these lesions not be accessible to any known chaperone. In fact, the composition of the Hrd1 complex for ERAD-M—only Hrd1 and Hrd3—is significantly simpler than the Hrd1 complex for ERAD-L.

HMG-CoA reductase (Hmg2 in yeast and HMGR in mammals) is the best-characterized ERAD-M substrate, which in fact led to the identification of Hrd1 (HMG-CoA reductase degradation) (Hampton et al., 1996). During sterol biosynthesis, this enzyme is the rate-limiting step and thus HMG-CoA reductase stability undergoes stringent regulation in response to cellular sterol levels (Wangeline et al., 2017). When sterol levels are low, Hmg2 is stabilized by a sterol-dependent chaperone, the insulin-induced gene proteins (INSIGs). When sterol levels are high, Hmg2 appears to adopt a conformation that is recognized by the ERAD-M machinery and is rapidly degraded by ERAD (Theesfeld and Hampton, 2013). Unlike ERAD-L substrates, ERAD-M substrates such as Hmg2, Sec61-2, and Pdr5* appear to be directly recognized by the Hrd1 ubiquitin ligase via the transmembrane domain (Sato et al., 2009). Specifically, site-directed mutagenesis supported the view that Hrd1 recognizes misfolded lesions in transmembrane domain. Because ERAD-M substrates are already anchored in the ER membrane, they may directly enter the Hrd1 retrotranslocon sideways from the lipid bilayer for retrotranslocation and coupled ubiquitination.

Recently, the ERAD-C ubiquitin ligase, Doa10 (see below), was also shown to be involved in the turnover of a specific ERAD-M substrate: the unassembled Sec61β homologue 2

(Sbh2), which presents an exposed transmembrane degron (Habeck et al., 2015). In addition, some ERAD-M substrates, like Sec61-2, can mislocalize to the inner nuclear membrane, a specialized ER subdomain, and are instead recognized by the Asi complex for proteasomal degradation. During this process, the Asi complex seems to recognize folding lesions within the transmembrane domain, similarly to Hrd1 (Foresti et al., 2014; Khmelinskii et al., 2014). Yet another class of non-canonical ERAD-M substrates are single-pass membrane proteins, such as unassembled α, β T-cell receptor subunits, whose transmembrane domains are less hydrophobic. These subunits can completely enter the ER lumen before retrotranslocation, and are recognized by the ER lumenal Hsp70 (BiP) for ERAD (Feige and Hendershot, 2013). Therefore, ERAD-M substrates with different types of folding lesions may employ diverse mechanisms for recognition prior to the proteasomal degradation.

1.1.3 ERAD-C

ERAD-C deals with misfolded membrane proteins with folding lesions located in their cytosolic domain, which requires a different set of chaperones and E3 ubiquitin ligases compared to ERAD-L substrates. The common feature of ERAD-C substrates is the exposure of hydrophobic patches that are otherwise buried inside the native conformation. To prevent protein aggregation, cytosolic chaperones including cytoplasmic isoforms of Hsp70 (Ssa1-4 in yeast), Hsp40 (Ydj1 and Hlj1 in yeast), nucleotide exchange factors (NEFs), Hsp90, and small heat shock proteins (sHsps) are engaged for efficient clearance of ERAD-C substrates (Ahner et al., 2007; Huyer et al., 2004b; Park et al., 2007; Youker et al., 2004). Hsp70 captures hydrophobic patches exposed in folding intermediates and ERAD-C substrates to sequester them from the aqueous environment, thereby preventing protein aggregation and assisting protein folding

(Vembar and Brodsky, 2008). In turn, the peptide binding and release cycle of Hsp70 is intrinsically slow and is regulated by both the Hsp40 co-chaperone and dedicated NEFs. In terms of ERAD-C substrates that are terminally misfolded, futile folding cycles must be prevented so the substrate can be targeted for degradation. Chaperones including Hsp70 (Ssa1) and Hsp40 (Ydj1 and Hlj1) have been shown as recognition factors for a growing number of ERAD-C substrate in yeast, such as CFTR, Pma1-D378S, Ste6*, Chimera A*, and SZ* (Guerriero et al., 2017; Han et al., 2007; Huyer et al., 2004b; Sun and Brodsky, 2017; Youker et al., 2004). Moreover, an *in vitro* ubiquitination system was used to show that Hsp70 (Ssa1) and Hsp40 (Ydj1 and Hlj1) are required for both substrate recognition and E3 ubiquitin ligase recruitment (Nakatsukasa et al., 2008). Although it is not understood how the same set of chaperones dictate proteins to different fates (i.e., folding versus degradation), prolonged chaperone engagement might provide enough time for recruitment of the E3 ubiquitin ligase, Doa10, to tag ERAD-C substrates with a poly-ubiquitin chain.

Unlike ERAD-L substrates that undergo retrotranslocation-coupled ubiquitination, ERAD-C substrates are ubiquitinated prior to retrotranslocation because their cytosolic domains gain easy access to the cytosolic RING domain in Doa10. During ubiquitination, a cascade of ubiquitin enzymes, including the E1 ubiquitin-activating enzyme, the E2 ubiquitin-conjugating enzyme, and an E3 ubiquitin ligase are required to deliver the ubiquitin moiety to the substrates (Oh et al., 2018). For ubiquitination of ERAD-C substrates, two E2 ubiquitin-conjugation enzymes, Ubc6 and Ubc7, are involved. Recently, it was shown that Ubc6 can attach a single ubiquitin not only to lysine residue but also to hydroxylated amino acids, which can act as primers for subsequent poly-ubiquitination by Ubc7, thus expanding the substrate range of Doa10 (Weber et al., 2016). In addition to Doa10, another cytosolic/nuclear E3 ligase

responsible for *N*-end rule degradation, Ubr1, also contributes to the turnover of ERAD-C substrates, like Ste6* and CFTR in yeast (Prasad et al., 2018; Stolz et al., 2013). Because polytopic membrane proteins may bear multiple folding lesions, different branches of ERAD may also coordinate with each other during substrates recognition and ubiquitination for efficient clearance of misfolded proteins in the ER.

1.1.4 Protein Retrotranslocation and Proteasomal Degradation

Following substrate ubiquitination or retrotranslocation-coupled ubiquitination, all three ERAD branches converge on the Cdc48/p97-mediated retrotranslocation step, during which ubiquitinated ERAD substrates are extracted from the ER/the ER membrane and are transferred to the 26S proteasome. After being marked with a poly-ubiquitination chain, ERAD substrates recruit the cytosolic Cdc48 (p97 in mammals) complex by interacting with the ubiquitin-interacting Cdc48 cofactors Ufd1/Npl4 (Braun et al., 2002; Jarosch et al., 2002; Ye et al., 2003). The recruitment of the Cdc48 complex is further facilitated by an ER integral membrane protein, Ubx2, which also interacts with Ufd1/Npl4 (Neuber et al., 2005; Schuberth and Buchberger, 2005). The Cdc48 complex next provides the driving force for retrotranslocation via ATP hydrolysis and “pulls” ubiquitinated substrates out of the ER membrane and into the cytosol prior to proteasomal degradation (Ye et al., 2003).

Cdc48 is a member of the ATPases Associated with various cellular Activities (AAA+ ATPase) family, which use ATP hydrolysis to exert force on macromolecules (Snider et al., 2008). Members of this family form hexamers with two stacked ATPases rings (D1 and D2) surrounding a central pore, which is reminiscent of the protein unfolding/disaggregating channel Hsp104 (Gates et al., 2017) as well as a bacterial disaggregase, ClpB (Mogk et al., 2015).

Although it has long been known that Cdc48 extracts proteins from the ER membrane during ERAD, a more detailed mechanism of substrate processing by Cdc48 was recently revealed by an *in vitro* reconstitution system (Blythe et al., 2017; Bodnar and Rapoport, 2017). During retrotranslocation, a substrate bearing a K48 linked poly-ubiquitin chain first binds to Ufd1/Npl4, and is locally denatured in the D1 ring in the Cdc48 complex. The unfolded loop of the substrate reaches to the central pore of the Cdc48 complex, and as it travels further into the pore it is pulled by pore loops in the D2 ring upon ATP hydrolysis. During entry, the binding of poly-ubiquitinated substrates by Ufd1/Npl4 is weakened or diminished by the trimming of a poly-ubiquitin chain on the substrate, thus releasing the substrate and facilitating further threading through the central pore of Cdc48. The trimming of poly-ubiquitin chains is mediated by a deubiquitinase (DUB), which generates heterologous retrotranslocated substrates with different ubiquitin chain lengths. At this stage, substrates with ubiquitin chains that are too short to be degraded by the proteasome will be rescued by the Cdc48 cofactor Ufd2, an E4 ubiquitin elongation enzyme (Koegl et al., 1999). For ERAD-L substrates bearing *N*-linked glycans, another Cdc48 binding partners, Png1, may remove the carbohydrates before proteasome delivery. Of note, Png1 binds to C-terminus of Cdc48 and probably functions only on unfolded substrates after their translocation (Li et al., 2006).

After being retrotranslocated from the ER, ERAD substrates are then delivered to the proteasome for degradation, which is facilitated by the shuttling factors Rad23 and Dsk2 and that contain both ubiquitin- and proteasome-binding domains (Kim et al., 2004; Medicherla et al., 2004). In higher eukaryotes, a chaperone holdase complex, including Bag6, Ubl4A, and Trc35, associates with retrotranslocated ERAD substrates to prevent their aggregation and facilitate degradation (Wang et al., 2011b). The engagement of chaperone holdases is rather important for

retrotranslcoated membrane proteins such as those in ERAD-C substrates, which contain hydrophobic transmembrane domains and are thus aggregation prone in the cytoplasm. However, Bag6 lacks a yeast ortholog. The best candidate for this holdase in yeast is Hsp104, which was recently shown to facilitate the retrotranslocation of insoluble ERAD substrate via its ATPase activity (Preston et al., 2018). It is also possible that retrotranslocated membrane substrates undergo an autonomous conformational change to bury aggregation prone domains without the need of a holdase chaperone.

1.1.5 Protein Quality Control versus Quantity Control by ERAD

Besides misfolded or damaged proteins, normal proteins that are deemed unnecessary are also turned over by ERAD, which is termed quantity control. In order for quantity control substrates to be recognized by ERAD, they have to display signals that mimic misfolded proteins in response to a cellular signal or the presence of an adaptor.

During sterol biosynthesis, Hmg2 (see above) is susceptible to ERAD-M in response to the accumulation of a pathway intermediate, isoprene geranylgeranyl pyrophosphate (GGPP) (Wangeline et al., 2017). On the contrary, low lipid levels serve as a signal for quantity control of ApoB: ApoB that fails to become lipidated misfolds and is eliminated by ERAD (Doonan et al., 2018). Some transporters are also regulated by ERAD quantity control by ligand binding. The cadmium exporter, Pca1, contains a cytosolic degron that targets Pca1 for ERAD in the absence of cadmium. When cellular cadmium levels are high, Pca1, is stabilized and escapes ERAD to act rapidly in response to cadmium (Adle et al., 2009). Therefore, cells employ ERAD quantity control to selectively degraded unnecessary proteins to save energy and building blocks to synthesize other proteins.

In contrast to metabolic regulation of ERAD quantity control, adaptor protein-mediated quantity control is also prevalent. For example, a yeast ER intramembrane protease, Ypf1, was identified as an adaptor to mediate ERAD of a zinc transporter, Zrt1, under zinc replete condition (Avci et al., 2014). Clipping of Zrt1 by Ypf1 introduces a misfolding signal that recruits Dfm1 (a Der1 homolog) and Doa10, thus targeting Zrt1 for ERAD. Another example of adaptor-mediated quantity control occurs when ERAD is hijacked by a virus. The human cytomegalovirus (CMV) encodes membrane adaptor proteins US2 and US11, which independently bind to newly synthesized major histocompatibility class I (MHC-1) molecules and recruit the ERAD machinery (Loureiro et al., 2006; Stagg et al., 2009; Wiertz et al., 1996a). Surface display of MHC-1 is reduced, thereby disabling the host immune response. A similar strategy is used by the HIV-encoded adaptor protein Vpu, which targets human CD4 for ERAD (Fujita et al., 1997; Schubert et al., 1998).

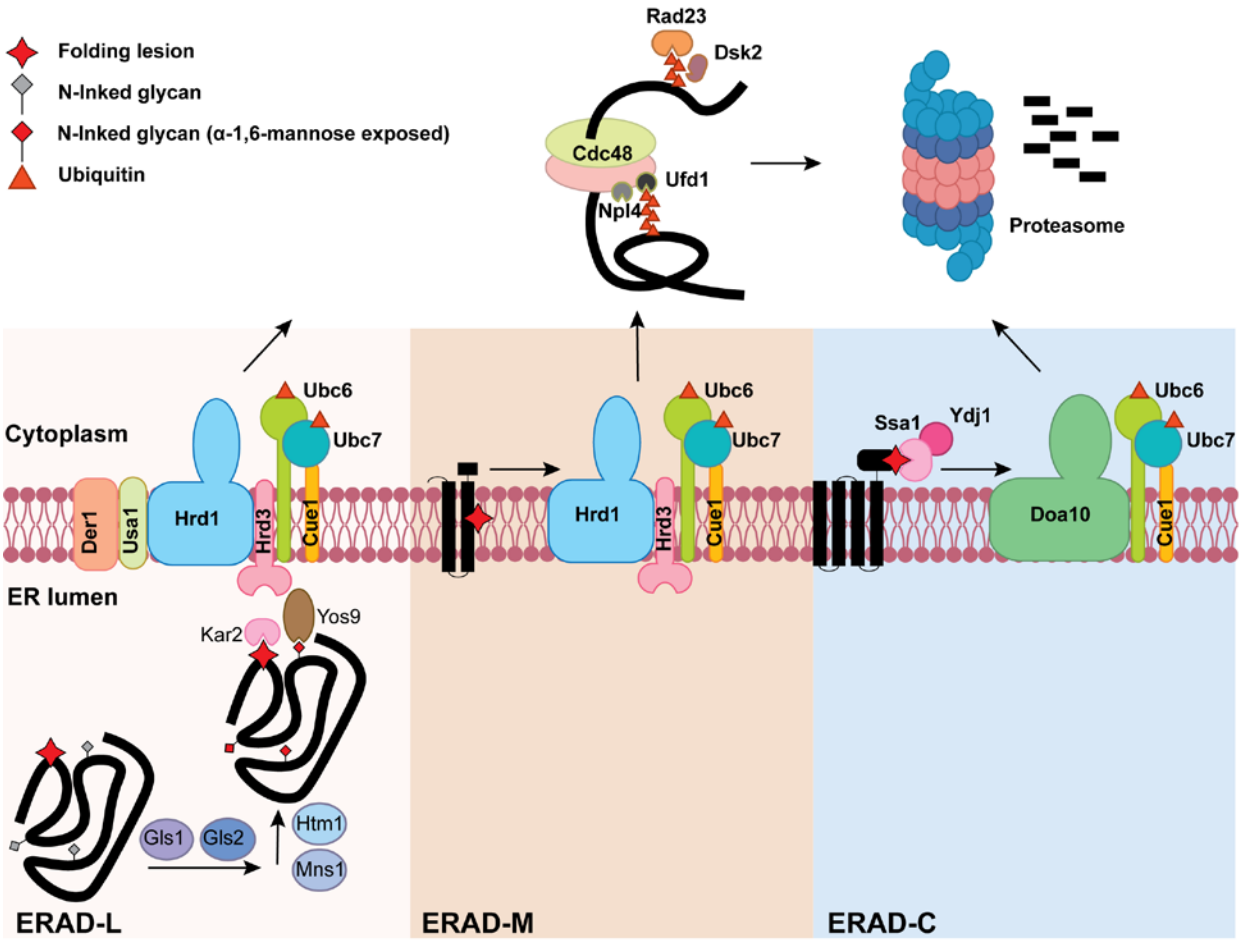

Figure 1 Three branches of ERAD pathway in yeast

Lower panel defines the different steps in substrate recognition and ubiquitination for ERAD-L/M/C substrates. ERAD-L substrates containing lumenal folding lesion (red star) and N-linked glycan (grey diamond) are recognized and processed by a cascade of enzymes to generate ERAD glycan signal (red diamond). Chaperones (Kar2) and lectins (Yos9) then capture the ERAD-L substrates and transfer it to the Hrd1 complex for retrotranslocation coupled ubiquitination (red triangle). ERAD-M substrates containing a membranous folding lesion (red star) are directly recognized and ubiquitinated by Hrd1 complex. ERAD-C substrates containing cytosolic folding lesion are recognized by cytosolic chaperones (eg. Ydj1 and Ssa1), which then bridge the interaction between ubiquitin ligase Doa10 and substrates for ubiquitination. All three ERAD branches converge in the retrotranslocation step mediated by Cdc48 complex including Cdc48 and its cofactor Ufd1 and Npl4 that interact with ubiquitin (red triangle) on

substrates (upper panel). Cdc48 provides the molecular force via ATP hydrolysis to extract substrates from the ER to the cytosol. Following retrotranslocation, substrates are escorted to the 26S proteasome for degradation by shuttling factors Rad23 and Dsk2.

1.2 ER-PHAGY

The diameter of the pore of the ERAD retrotranslocon may prevent misfolded oligomeric or aggregated proteins, or proteins that are only partially unfolded, from being retrotranslocated. Because these substrates may become even more toxic as they accumulate, the ER is equipped with a backup QC mechanism to clear misfolded proteins that cannot be disposed of by ERAD, ER-phagy. Like other autophagy pathways, ER-phagy can exhibit selectivity to discriminate between functional proteins and damaged non-functional proteins, as well as act as a nonselective pathway to eliminate bulky ER materials that accumulate upon ER stress. ER-phagy can be classified into micro-ER-phagy (non-selective) and macro-ER-phagy (selective) (Lipatova and Segev, 2015).

1.2.1 Micro-ER-phagy

The term “ER-phagy” was firstly used by the Walter group upon the discovery of ER whorls (Bernales et al., 2006; Bernales et al., 2007). Treatment with dithiothreitol (DTT) and tunicamycin, which disrupt protein disulfide bond formation and glycosylation in the ER lumen, respectively, and induce the unfolded protein response (UPR), results in massive ER expansion

followed by the formation of the whorls. The ER whorls are then selectively engulfed into the vacuole by invagination and inward budding of the vacuolar membrane, which occurs independently of the core autophagy machinery. This is reminiscent of the process of microautophagy. However, micro-ER-phagy differs from microautophagy in the fact that none of the microautophagy-related components, including the EGO complex, the vacuolar transporter chaperone complex (VTC) and the endosomal sorting complexes required for transport (ESCRT) (see below), is required for micro-ER-phagy (Dubouloz et al., 2005; Sahu et al., 2011; Uttenweiler et al., 2007). The trigger for micro-ER-phagy seems instead to be ER expansion rather than the accumulation of misfolded proteins in the ER, because expansion of the ER by directly knocking out *OPI1*, the lipid biosynthesis transcriptional repressor, is sufficient to induce micro-ER-phagy (Schuck et al., 2014; Schuck et al., 2009). Therefore, micro-ER-phagy may remove ER subdomains in the vacuole to re-establish pre-stress ER volume and content. Thus far, this phenomenon has only been reported in yeast. It also remains largely illusive how ER expansion triggers micro-ER-phagy, and if a receptor is required during this process.

1.2.2 Macro-ER-phagy

Compared to micro-ER-phagy, macro-ER-phagy is a conserved mechanism which is induced in response to cellular stress induced by nitrogen starvation, rapamycin treatment, and protein aggregation in the ER (Grumati et al., 2018). Also in contrast to micro-ER-phagy, macro-ER-phagy coopts the autophagy core machineries. The discovery of various ER-phagy receptors also indicates that macro-ER-phagy is a highly selective and regulated mechanism that helps maintain ER homeostasis.

In budding yeast, macro-ER-phagy is induced by nitrogen starvation and rapamycin treatment, during which two ER-phagy receptors are required (Mochida et al., 2015). Atg39 localizes to the perinuclear ER and induces ER-phagy of a nuclear subdomain. Atg40 mainly localizes to the cortical and cytoplasmic ER and instead mediates the autophagic sequestration of ER subdomains. Both Atg39 and Atg40 contain an Atg8 family interacting motif, which engages Atg8 on the phagophore membrane (the precursor of the autophagosome). In addition, another autophagosome scaffold protein, Atg11, which recruits the autophagosome-formation machinery onto the receptor-target complex, binds both Atg39 and Atg40 (Mochida et al., 2015; Okamoto, 2014). Of note, nitrogen starvation or rapamycin treatment enhances the expression of both Atg39 and Atg40, which forms a feedback loop to regulate nitrogen starvation or rapamycin-induced ER-phagy. Overexpression of a membrane protein, Snc1, can also trigger macro-ER-phagy, during which autophagy related genes including Atg1, atg8, atg9 and a small GTPase Ypt1 are required (Lipatova and Segev, 2015). Overexpression of Snc1 results in its sequestration first into ER-to-autophagy membranes (ERAM), and Ypt1-dependent recruitment of select proteins to ERAM forms the autophagosome, which fuse with the lysosome. ATZ expressed in yeast undergoes both ERAD (see above) as well as autophagy-dependent degradation, indicating the potential for protein-mediated ER-phagy in yeast (Kruse et al., 2006). In mammalian cells, ATZ is sorted into an autophagosome for ER-phagy by the ER-phagy receptor FAM134B (Fregno et al., 2018). In contrast, the yeast ER-phagy receptors for either overexpressed Snc1 or ATZ remain enigmatic.

In mammalian cells, macro-ER-phagy is induced by nutrient deprivation, accumulation of misfolded and/or aggregated proteins, and some pathogens (Dikic, 2018; Grumati et al., 2018; Loi et al., 2018). ER-phagy also provides a backup mechanism for ERAD to dispose of ERAD-

resistant misfolded proteins, such as intracisternal granules (ICGs), mutant dysferlin, procollagen, ATZ, and a gonadotropin-releasing hormone receptor mutant (Fujita et al., 2007; Hidvegi et al., 2010; Houck et al., 2014; Ishida et al., 2009; Kruse et al., 2006; Tooze et al., 1990).

The identification of ER-phagy receptors, including FAM134B, RTN3, Sec62, and CCPG1, has greatly advanced our understanding of macro-ER-phagy in mammalian cells and expanded its function to both counteract cellular stress and re-establish ER volume and content after stress (Fumagalli et al., 2016; Grumati et al., 2017; Khaminets et al., 2015; Smith et al., 2018). The first characterized receptor, FAM134B, mediates starvation-induced ER-phagy in mammalian cells (Khaminets et al., 2015). It localizes at the edge of ER sheets via a reticulon homology domain (RHD), which can promote curvature of the ER membranes during autophagosome formation. The presence of a LIR at the cytosolic C-terminus confers upon FAM134B the ability to recruit LC3 and/or GABARAP at the limiting membrane of growing phagophores. Both the RHD and LIR of FAM134B are required to complete ER-phagy. Downregulation of the gene encoding FAM134b leads to ER expansion as a result of defective ER-phagy under both basal and starvation conditions. In contrast, overexpression results in ER fragmentation and lysosomal degradation. These data position FAM134B as a regulator of ER size under basal and stressed conditions.

After the identification of FAM134B, an increasing number of misfolded proteins have been identified as cargo. For example, collagen is the main structural component of the extracellular matrix, and ~20% of newly synthesized type I procollagens (PC1) is degraded in the lysosome due to inefficient PC1 folding (Bienkowski et al., 1986; Ishida et al., 2009). Collagen mutants are associated with several matrix-associated diseases, including osteogenesis

imperfecta (Marini et al., 2007). Mutations in PC1 or the Hsp47 collagen chaperone form ERAD-resistant protein aggregates, which are eliminated by ER-phagy in an FAM134B-dependent manner (Forrester et al., 2019; Fregno et al., 2018; Ishida et al., 2006). Moreover, an ERAD-L component, calnexin, was found as a co-receptor that recognizes misfolded PC1 in the ER and interacts with FAM134B, linking ERAD and selective ER-phagy. Since FAM134B lacks domains that reside in the ER lumen, it makes sense that ER-phagy employs ERAD-L components to recognize and dispose of misfolded proteins in the ER lumen.

Recently, another FAM134B substrate was identified as a misfolded transmembrane glycoprotein, I1061T NPC1 (Schultz et al., 2018). Unlike other ER-phagy substrates that are ERAD-resistant, I1061T NPC1 can be degraded by both ERAD and ER-phagy (Gelsthorpe et al., 2008; Schultz et al., 2018). Because the components involved in the ERAD of I1061T NPC1 are not well characterized, the misfolded lesion in I1061T NPC1 either transmits this conformational change to its membrane or cytosolic domain or engages other ERAD-L components, like calnexin, to recruit FAM134B.

Several other ER-phagy receptors and facilitators of ER-phagy also exist. For example, RTN3 is an RHD-containing protein that has the potential to induce membrane curvature and thus localizes at ER tubules (Yang and Strittmatter, 2007). RTN3 exists in various splicing isoforms, but only the longest one carries LIR domains and functions as an ER-phagy receptor (Grumati et al., 2017). Under amino acid starvation condition, RTN3 oligomerizes to engage and cluster LC3 to form autophagosomes from ER tubules for lysosome delivery and degradation (Grumati et al., 2017). In addition, Sec62 was recently discovered as a receptor for “recovER-phagy” that is independent of its function during protein translocation (Fumagalli et al., 2016). During the UPR, eukaryotes expand their ER to protect protein homeostasis. Unlike yeast that

utilize micro-ER-phagy to regulate the shape and size of the ER during ER stress (see above), mammalian cells activate recovER-phagy as ER stress is resolved and to reset ER volume and content. Through the C-terminal LIR domain, mammalian Sec62 acts as the receptor for recovER-phagy. Compared to the mammalian homolog, Sec62 in yeast lacks a putative LC3-interacting region (LIR), based on which I speculate that the loss of LIR on yeast Sec62 may explain the dispensability of autophagy core machineries during micro-ER-phagy. It is unclear if yeast lost the LIR domain or whether this domain was gained during evolution as diverse mechanisms for ER-phagy evolved.

Similar to Sec62, Cell-Cycle Progression Gene 1 (CCPG1) is another ER-phagy receptor associated with the UPR (Smith et al., 2018). CCPG1 contains both LIR and FIP200-interacting regions, which bind independently to LC3 as well as FIP200, a component that associates with the autophagy machinery. During ER stress, CCPG1 expression is upregulated to remove portions of the ER harboring insoluble proteins. ER-phagy mediated by CCPG1 plays an important role in protecting pancreatic acinar cells against protein aggregation in the ER lumen and subsequent UPR induction (Smith et al., 2018). However, it is still unknown how CCPG1 recognizes and clusters aggregated proteins for ER-phagy. Because of its large ER lumenal domain, CCPG1 may either work on its own or with ERAD-L components to recognize its substrates. Overall, even though the identification of these ER-phagy receptors has helped define how cargos are selected, how the ER-phagy machinery “decides” where and when to degrade a misfolded protein is an important future undertaking.

1.3 GOLGI QUALITY CONTROL

Folded and mature proteins in the ER travel along the secretory pathway to the Golgi via COPII vesicle transport. The COPII coat consist of five subunits: Sar1, Sec23/24 dimer, and Sec13/31 tetramer (Barlowe et al., 1994). In brief, the formation of COPII vesicles is initiated by activating the small GTPase Sar1 upon association with a guanine nucleotide exchange factor (GEF), Sec12. Activation induces a conformational change in Sar1 (Sar1-GTP), exposing hydrophobic elements that insert into the ER membrane. A Sec23/24 heterodimer is then recruited to the ER by Sar1-GTP to form the inner COPII coat, to which the outer coat formed by the Sec13/31 heterotetramer, is recruited via direct interaction between Sec31 and Sec23/Sar1. The formation of this coat complex then stimulates the GTPase activating activity of Sec23 to promote Sar1 GTP hydrolysis, thus switching Sar1 back to the inactive state (Barlowe and Helenius, 2016). During this process, transport-competent cargo transiently accumulate or concentrate at specialized ER subdomains called ER exit sites (ERES) (Lee et al., 2004). Due to the size limit of COPII vesicles (usually less than 90 nm in diameter), the packaging of large cargos like procollagen and apolipoproteins requires expansion of COPII by the formation of large vesicles or a tunnel between the ER and the ER-Golgi intermediate compartment (ERGIC)/Golgi (Jin et al., 2012; McCaughey et al., 2019; Raote and Malhotra, 2019; Raote et al., 2018). Recently, a novel mechanism termed autoregulation of ER export (AREX) has been discovered in human cells that monitors and regulates the secretory flux of folded cargos in the ER through COPII (Subramanian et al., 2019). In response to an elevated amount of folded secretory cargos, AREX components are activated to both facilitate cargo export and attenuate protein synthesis, thus preventing the accumulation of folded and potentially harmful cargo in the ER (Subramanian et al., 2019). As the next station in the protein secretory pathway, the Golgi

apparatus not only functions as a protein post-translational modification factory--adding modifications such as glycosylation, acetylation, phosphorylation, sulfation, palmitoylation, methylation, and proteolytic cleavage--but also as a QC step to protect protein homeostasis along the secretory pathway (Arvan et al., 2002; Potelle et al., 2015).

A growing number of misfolded proteins have been identified that escape ERAD and are delivered to the vacuole/lysosome for degradation after selection in the Golgi. These data suggested the existence of a quality control mechanism in this compartment. Surprisingly, some misfolded proteins entering the Golgi can also be targeted for proteasomal degradation after delivery back to the ER. Thus, based on where they are targeted for degradation, GQC can be divided into proteasome-targeted GQC and lysosome/vacuole-targeted GQC (Figure 2).

1.3.1 Proteasome-targeted GQC

Some misfolded proteins can escape ERAD and ER-phagy and can be packaged into COPII vesicles for anterograde trafficking to the Golgi (Caldwell et al., 2001; Taxis et al., 2002; Vashist and Ng, 2004). Proteasome-targeted GQC captures the escaped substrates most likely in the *cis*-Golgi and cycles them back to the ER for ERAD. A fully competent ER to Golgi trafficking pathway, therefore, is required for efficient ERAD of some misfolded proteins.

Evidence from both yeast and mammalian studies support the involvement of the Golgi during ERAD. In budding yeast, efficient elimination of some ERAD-L substrates (CPY*, PrA*, KHN and KWW) requires a functional early secretory pathway (Caldwell et al., 2001; Taxis et al., 2002; Vashist et al., 2001; Vashist and Ng, 2004), and blocking anterograde trafficking inhibited ERAD-L. Erv29, which cycles between ER and Golgi, was identified as the COPII vesicle cargo receptor for CPY* and PrA* (Caldwell et al., 2001; Vashist et al., 2001). As

anticipated, COPI vesicle transport, which mediates retrograde trafficking from the Golgi to the ER, was involved in efficient degradation of CPY* and KHN (Vashist et al., 2001). In addition to ERAD-L substrates, some misfolded proteins with mutated transmembrane domains were also retrieved from the Golgi to the ER via a known retrieval receptor, Rer1 (Letourneur and Cosson, 1998). Because both Erv29 and Rer1 are general receptors that do not distinguish between misfolded and normal cargos, the escaped ERAD substrates are probably packaged into COPII and retrieved via COPI vesicles along with proteins that normally reside in the ER.

In mammals, unassembled MHC class I proteins expose polar residues in the transmembrane domain that are otherwise shielded by a partner protein, which leads to ERAD (Hughes et al., 1997). However, instead of being retained in the ER, unassembled MHC class I molecules advance to the *cis*-Golgi before retrieval back to the ER (Hsu et al., 1991). A similar result was also shown for the MHC class II β subunit, which can cycle between the Golgi and ER. The accelerated proteasomal degradation of β subunit upon brefeldin A treatment, is consistent with Golgi cycling during ERAD (Dusseljee et al., 1998). Consistent with findings in yeast, COPI vesicle transport also plays an important role in cycling an unassembled TCR α chain back to the ER (Yamamoto et al., 2001). Moreover, the ER chaperone BiP and the HDEL receptor helped retrieve proteins, such as a vesicular stomatitis virus G protein (VSVG) mutant and an unassembled TCR α chain (Hammond and Helenius, 1994; Yamamoto et al., 2001). Consistent with data in yeast, the human ortholog of Rer1 was also involved in the Golgi retrieval process for misfolded proteins with lesions in a transmembrane domain, such as the G51R rhodopsin mutant and a chimeric protein, $CD8^{TMD*}$ (Briant et al., 2017; Yamasaki et al., 2014).

Regardless of the mechanism by which substrates are retrieved, the ERGIC and *cis*-Golgi seem to be the location where GQC occurs due to the following reasons. First, all currently identified retrieval receptors, including the HDEL receptor, Rer1, and Erv29, are primarily localized in the *cis*-Golgi under steady-state conditions. Second, proteasome-targeted GQC substrates, such as N153D tissue-non-specific alkaline phosphatase (TNSALP), MHC class I molecules, and MHC class II β subunit, fail to acquire Golgi modifications, which happens in the *medial*-Golgi in mammalian cells, as indicated by sensitivity to Endo H cleavage (Dusseljee et al., 1998; Hsu et al., 1991; Ito et al., 2002). Thus, proteasome-targeted GQC may act as the first barrier to prevent escaped ERAD substrates from entering steps in the secretory pathway beyond the *cis*-Golgi. Notably, knockdown of mammalian Rer1 resulted in transport of the G51R rhodopsin mutant and the chimeric $CD8^{TMD*}$ protein to the lysosome, probably through the lysosomal/vacuole-targeted GQC pathway (see below) (Briant et al., 2017; Yamasaki et al., 2014). Because proteasome-targeted GQC occurs independently of substrate ubiquitination or the multivesicular body (MVB) pathway, this QC event is simply a gatekeeping checkpoint in which the *cis*-Golgi is equipped with multiple retrieval receptors that identify escaped ERAD substrates that may also be bound to ER chaperones. The existence of proteasome-targeted GQC, nevertheless, raises more questions than answers. Future research will be needed to address why ER-Golgi trafficking is required for efficient ER degradation of some substrates, what structural features dictate ER exit versus ER retention of select substrates, and does the entire population of escaped substrates undergo ER-Golgi trafficking or is only a subset of these substrates retained in the ER and directly targeted for ERAD?

1.3.2 Lysosome/vacuole-targeted GQC

Most commonly, the term GQC refers to an event that targets misfolded protein for lysosomal degradation. In contrast to the QC checkpoint in ERGIC and *cis*-Golgi that retrieves back misfolded proteins for ERAD (Section 1.3.1), I have used the term lysosome/vacuole-targeted GQC to describe this more common, canonical form of GQC, which sorts misfolded proteins for lysosomal/vacuolar degradation or maturation in higher cells and in yeast, respectively. Data on this pathway have primarily arisen from studies in yeast and have revealed two routes to target misfolded proteins from the Golgi to the lysosome: receptor-mediated sorting and ubiquitin ligase mediated sorting.

Receptor-mediated GQC

Vps10 is a type I membrane receptor localized in the Golgi and sorts the vacuolar hydrolases proteinase A (PrA) and carboxypeptidase Y (CPY) (Bowers and Stevens, 2005). Loss of Vps10 results in secretion of more than 90% of newly synthesized CPY and 50% of PrA (Cooper and Stevens, 1996; Marcusson et al., 1994). Upon binding to its sorting receptor at the Golgi, CPY is transported from the late Golgi to endosomes in a clathrin and dynamin-related GTPase Vps1-dependent manner (Deloche et al., 2001). In addition to folded cargo proteins, Vps10 also recognizes and sorts misfolded proteins for lysosomal degradation, including misfolded lambda repressor-invertase chimeras and β-lactomase (Holkeri and Makarow, 1998; Hong et al., 1996; Wang and Ng, 2010). Analysis of the mutant lambda repressor-invertase chimera was the first observation that supported GQC of a lumenal/soluble protein. The chimeras were constructed by fusing invertase to either wild-type or mutant lambda repressor. In contrast to the wild-type version that was mostly secreted, the mutant was delivered to the vacuole in a

Vps10-dependent fashion (Hong et al., 1996). Similarly, β-lactamase, when expressed in *S. cerevisiae,* was transported in a Vps10-dependent manner from the Golgi to the vacuole for degradation (Holkeri and Makarow, 1998). Deletion of *VPS10* not only blocked vacuolar sorting of the chimera as well as β-lactamase but also led to secretion. Moreover, overexpression of the misfolded substrate increased the percentage of its secretion, indicating a saturable process (Hong et al., 1996). However, the mechanism of how Vps10 recognizes both folded and misfolded proteins remains unknown. One possibility is that folded and misfolded substrates engage two different sites on Vps10 (Jorgensen et al., 1999).

A similar sorting mechanism was subsequently discovered in mammalian cells. Sortilin is a mammalian type I membrane receptor homologous to Vps10. Sortilin resides in both the Golgi and plasma membrane and mediates lysosomal cargo sorting, including sphingolipid activator proteins, ApoB, lipoprotein lipase, and neurotensin (Amengual et al., 2018; Lefrancois et al., 2003; Nielsen et al., 1999; Nielsen et al., 2001). Similar to its yeast counterpart, sortilin also mediates lysosomal sorting of misfolded proteins, such as aggregated GPP130. After manganese treatment, GPP130 undergoes oligomerization/aggregation followed by lysosomal degradation, which requires both clathrin and sortilin (Tewari et al., 2015; Venkat and Linstedt, 2017). Interestingly, while Golgi protein oligomerization/aggregation induced by a tandem FKBP domain was sufficient to trigger lysosomal degradation, trafficking was sortilin-independent, suggesting that protein aggregation is necessary but not sufficient for sortilin-mediated lysosomal sorting (Venkat and Linstedt, 2017) The finding that sortilin recognizes protein aggregates in the Golgi lumen and facilitates lysosomal degradation is reminiscent of a previous study in which a type I membrane protein, furin, became progressively aggregated in Golgi leading to its lysosomal delivery (Wolins et al., 1997). Because these substrates are mostly

lumenal protein and may not be accessible to the cytosolic ubiquitination machinery, and because delivery to the lysosome is MVB-independent, the structural features and machinery that define this non-canonical, Vps10/sortillin-specific form of QC remain unclear.

Ubiquitin ligase mediated GQC

In contrast to Vps10/sortillin-receptor sorting, ubiquitin ligase-mediated GQC is better defined. Studies in yeast identified two ubiquitin ligase in the Golgi that directly and indirectly recognize misfolded proteins for degradation in the lysosome: Tul1 and Rsp5. To date, all the identified substrates of Tul1 and Rsp5 are membrane proteins. In this case, the MVB pathway is required after substrate ubiquitination and for lysosomal delivery.

Tul1 is a RING domain ubiquitin ligase with multiple transmembrane segments. It was first identified as an ubiquitin ligase that recognizes and marks misfolded proteins with mutant transmembrane domains for vacuole-dependent degradation. Known substrates include Pep12(D), CPS1, and Phm5 (Reggiori and Pelham, 2002). These substrates are all single pass membrane proteins with polar residues in the membrane-spanning portion of the protein, which is recognized by Tul1. Tul1 functions with the E2 ubiquitin conjugating enzyme, Ubc4, to add poly-ubiquitin chains onto the cytosolic portion of the substrate, thereby acting as a sorting signal for the MVB pathway. Unlike CPY, which is a folded, soluble protein that engages Vps10 for lysosomal sorting, the membrane proteins CPS1 and Phm5 use another strategy: Both CPS1 and Phm5 possess polar residues and mimic misfolded Tul1 substrates, so they are ubiquitinated and delivered to the vacuole via MVB capture. Moreover, the scope of Tul1 substrates can be further expanded under stress conditions, such as amino acid starvation or TOR inactivation. Under these conditions, specific Golgi proteins including Yif1, Tlg2, Btn1, Kex2 and

unpalmoylated Tgl1 become Tul1 substrates and are directed to the vacuole, which helps counteract nitrogen depletion (Dobzinski et al., 2015).

Tul1 was later characterized as a component of the Dsc complex, which consists of Tul1, Dsc2, Dsc3, Dsc4, and Ubx3 in fission yeast (Stewart et al., 2011). The overall structure of the Dsc complex mirrors that of the Hrd1 complex. Strikingly, Tul1, Dsc2, and Dsc3 are homologous to Hrd1, Der1 and Usa1, respectively (Stewart et al., 2012; Stewart et al., 2011). Each of these components, except for Dsc4, also exists in budding yeast, but the involvement of Cdc48 in the fission yeast Dsc complex suggests that a unique form of GQC is at-play. Under conditions where ergosterol and/or oxygen is limited, the Dsc complex in fission yeast binds and cleaves the membrane-bound sterol regulatory element binding protein (SREBP) in the Golgi, liberating its cytosolic transcriptional factor domain to activate genes required for lipid synthesis and uptake. To this end, the ubiquitin-proteasome system is employed (Stewart et al., 2011).

More Tul1 substrates in budding yeast have been identified that localize in other compartments besides the Golgi, indicating extended function of the Dsc complex in other organelles. New Tul1-dependent substrates include the vacuolar zinc transporters, such as Cot1 (which mediates influx) and Zrt3 (which mediates efflux). Both transporters are regulated in response to intracellular zinc. Specifically, high levels of zinc induce Zrt3 degradation, whereas low levels of zinc trigger the degradation of Cot1. The degradation of both transporters depends on vacuolar membrane recycling and requires Tul1 (Li et al., 2015). In contrast, two novel Dsc complex subunits were identified that target the complex to different organelles: Gld1 directs the Dsc complex to the Golgi and endosome, whereas Vld1 targets the Dsc complex to the vacuolar membrane (Yang et al., 2018). Therefore, as the critical component of Dsc complex, Tul1 is a

versatile E3 ligase that can complex with different subunits to protect protein fidelity in the late secretory pathway: i.e., the Golgi, endosome, and vacuole.

Rsp5 is another versatile E3 ubiquitin ligase involved in lysosome/vacuole-targeted GQC and harbors three domains: the N-terminal C2 domain, the central WW domain, and the C-terminal catalytic HECT domain, which possesses ubiquitin ligase activity (Belgareh-Touze et al., 2008; MacGurn et al., 2012). The WW domain of Rsp5 is the protein-protein interaction module that binds a short recognition motif, PPXY. Rsp5 can recognize the PPXY motif residing in either substrates or adaptors, which facilitate its broad substrate range and accessibility. Indeed, the existence of multiple Rsp5 adaptors that localize in different organelles can target Rsp5 to the plasma membrane, to endosomes, to the vacuole, or to the Golgi, indicative of its broad role in several QC processes (Belgareh-Touze et al., 2008; Sardana et al., 2019). For example, during vacuolar targeted GQC, Rsp5 is recruited by the Bul1 and Bul2 adaptors to ubiquitinate misfolded membrane proteins, such as a mutated form of the plasma membrane proton ATPase, Pma1, for subsequent vacuole delivery (Chang and Fink, 1995; Luo and Chang, 1997; Pizzirusso and Chang, 2004). An obligate GQC substrate, Wsc1*, is another Rsp5 substrate that is routed from the Golgi to the vacuole through the MVB pathway (Wang and Ng, 2010; Wang et al., 2011c). The absence of a PPXY motif on Wsc1* suggests the existence of an as-yet unidentified adaptor. Another example demonstrating the utility of Rsp5 regards the fate of some ERAD substrates, which under some conditions may even exit the ER and advance to the Golgi for subsequent vacuolar degradation. The classic ERAD-L substrate, CPY*, when overexpressed, is routed for vacuolar degradation after Golgi transit (Haynes et al., 2002; Spear and Ng, 2003). Surprisingly, CPY* delivery doesn't utilize Vps10, which is evident for wild type CPY. Instead, the degradation of overexpressed CPY* employs Rsp5 for ubiquitin-dependent

sorting into the vacuole (Haynes et al., 2002). Furthermore, Rsp5 can regulate the fate of newly synthesized transporters in response to environmental conditions. The yeast amino acid transporter Gap1 is directed from the Golgi to the vacuole in an Rsp5-dependent manner in the presence of high ammonia (De Craene et al., 2001). Another example comes from the yeast siderophore transporter Sit1, which is transported to the vacuole in a similar manner in the absence of its substrate, ferrioxamine B (Froissard et al., 2007). Overall, Rsp5 can dispose of both misfolded membrane proteins in the Golgi and unnecessary transporters, which is reminiscent of protein quantity control in the ER (see Section 1.1.5).

After ubiquitination by Tul1, Rsp5 or another uncharacterized ubiquitin ligase, misfolded membrane proteins undergo an inward budding process to form intraluminal vesicles. During this process, ESCRT is recruited to induce the invagination of endosomal limiting membrane. Briefly, ESCRT-0 is first recruited to the endosomes by binding ubiquitin on substrates and then directs the assembly of the downstream complexes. ESCRT-I clusters ubiquitinated proteins and acts as a bridge between ESCRT-0 and ESCRT-II. ESCRT-II with its GLUE domain has high affinity for endosome-enriched phospholipid phosphatidylinositol-3-phsophate (PI3P) and is assembled on the late endosomal membrane. ESCRT-III is then recruited and oligomerized to induce the inward budding and intraluminal vesicles invagination. Finally, an ATPase, Vps4, strips other ESCRT components from the membrane and directs membrane scission (Christ et al., 2017; Henne et al., 2011). The late endosomes with intraluminal vesicles are termed multivesicular bodies (MVB), which are then fused with lysosome/vacuole for delivery of its cargos for degradation (Piper and Katzmann, 2007).

Our early understanding of Rsp5 function arose primarily from its role during the endocytosis and vacuole-dependent degradation of damaged or dispensable plasma membrane

transporters (Belgareh-Touze et al., 2008; MacGurn et al., 2012). However, Rsp5 was recently found to clear mislocalized vacuolar membrane proteins (Sardana et al., 2019). In contrast, the mammalian ortholog of Rsp5, NEDD4, is involved in neither GQC nor plasma membrane QC, but instead down-regulates functional plasma membrane proteins, such as the epithelial sodium channel and voltage-gated calcium and sodium channels, via ubiquitin-dependent endocytosis (Fotia et al., 2004; Rougier et al., 2011; Staub et al., 1996).

Together, Golgi is armed with two QC checkpoints to dispose of misfolded proteins that advance to the Golgi: proteasome-targeted GQC in the *cis*-Golgi and lysosome/vacuole-targeted GQC which most likely takes place in the *trans*-Golgi. Based on the severity of the lesion, misfolded proteins are either retrieved for ERAD via receptors or are directed for lysosomal degradation via the Vps10 receptor (e.g., misfolded lumenal/soluble proteins) and/or a ubiquitin ligase complex (e.g., misfolded membrane proteins). Furthermore, while both proteasome-targeted GQC and receptor-mediated GQC appear to be conserved between yeast and mammals, the existence of a mammalian GQC ubiquitin complex remains unidentified.

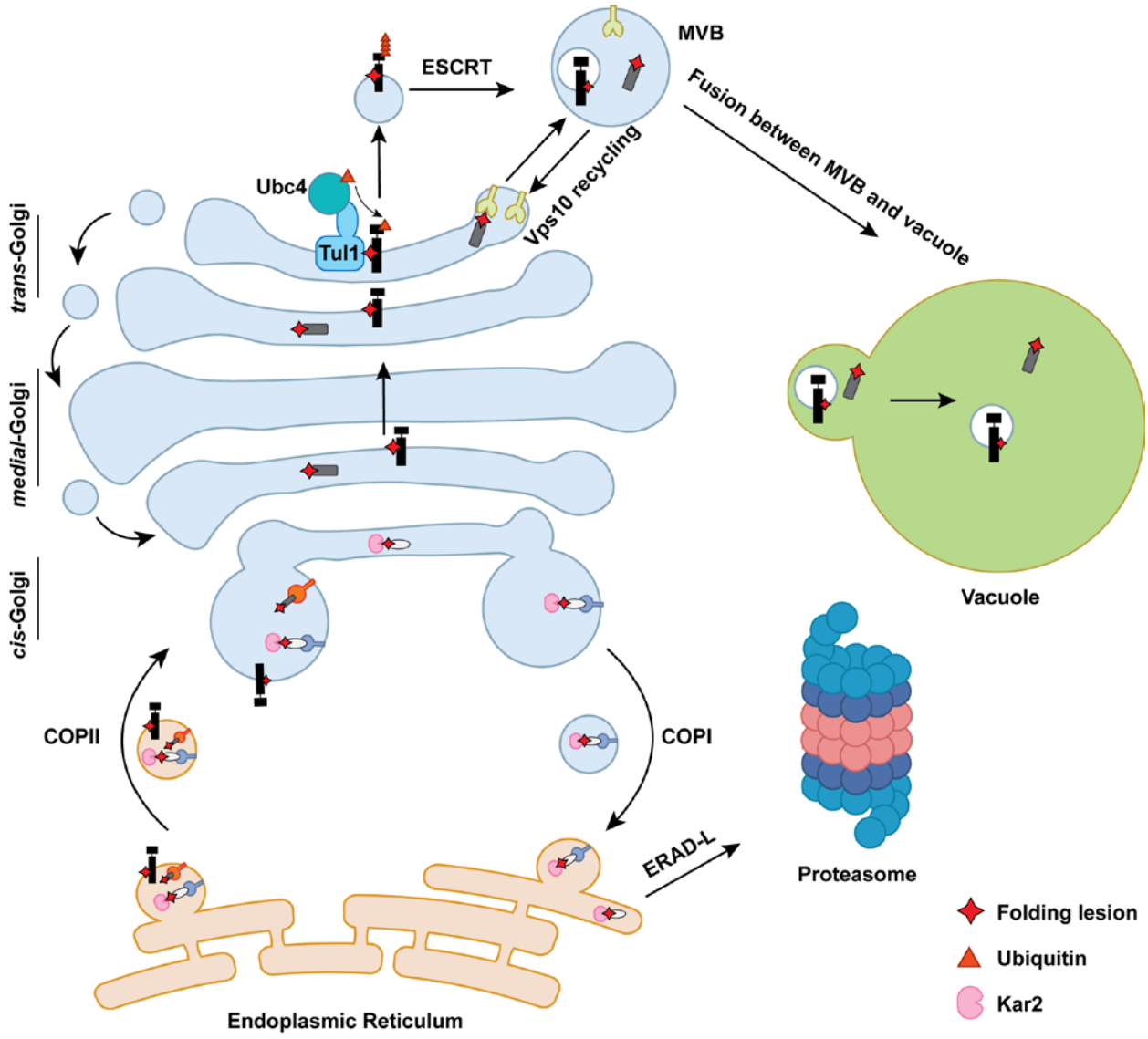

Figure 2 Golgi quality control pathway

Misfolded proteins targeted for GQC are first transported to the *cis*-Golgi via COPII vesicle transport. Proteasome-targeted GQC: ER chaperones and retrieval receptors in the *cic*-Golgi bind and retrieve some misfolded proteins back to the ER through COPI vesicle transport. These substrates are then eliminated by the proteasome via ERAD-L. Lysosome/vacuole-targeted GQC: Misfolded proteins that travel further to the *trans*-Golgi are sorted to the MVB via Vps10 receptor or a ubiquitin ligase and ESCRT. Following MVB sorting, misfolded proteins are delivered to the vacuolar lumen for degradation.

1.4 COOPERATION AMONG ERAD, ER-PHAGY, AND GQC

The ER serves as a hub for both protein synthesis and quality control. As discussed in section 1.1, the primary QC machinery, ERAD, is an elaborate and efficient mechanism that can monitor the protein-folding state and clear misfolded proteins with folding lesions located at different positions relative to ER membrane. The ubiquitin proteasome system is employed by ERAD to ensure that only terminally misfolded proteins that are marked with poly-ubiquitin are eliminated. However, the capacity and ability of ERAD is restricted by the specific functions of ERAD components, which may not be able to recognize or handle all aberrant proteins. This necessitates additional QC machineries that cooperate with ERAD to maintain ER protein homeostasis: ER-phagy and GQC. The two additional QC machineries expand both the ability and capacity of ER to recognize and clear misfolded proteins.

GQC may deal with substrates that exhibit more minor folding lesions. Substrates for either proteasome-targeted GQC or lysosome/vacuole-targeted GQC undergo anterograde trafficking from the ER to Golgi, which often requires a functional ER exit signal (Kawaguchi et al., 2010; Kincaid and Cooper, 2007). The prolonged engagement of ER chaperones, such as BiP and/or calnexin, may distinguish proteasome-targeted GQC substrates from lysosome/vacuole-targeted GQC substrates. Proteasome-targeted GQC substrates possess both a functional ER exit signal and a misfolding lesion that signals ERAD. In contrast, lysosome/vacuole-targeted GQC substrates may display more subtle misfolded lesions but still contain a functional ER exit signal, which reside in substrates such as Pep12(D), CPS1, Phm5, and Wsc1*. For substrates that display both an ERAD signal and a functional ER exit signal, the ERAD and ER exit machineries can compete for these misfolded proteins (Kincaid and Cooper, 2007). However, ERAD can also recognize more subtle defects or different lesions in protein as it can degrade

substrates that might fold and function later in the secretory pathway if folding is artificially induced (Lukacs and Verkman, 2012; Ward et al., 1995; Welsh and Smith, 1993). Therefore, under normal conditions, ERAD outcompetes the ER exit machinery. In contrast, when ERAD is compromised, misfolded substrates with functional ER exit signals can undergo forward trafficking at a higher level (Kincaid and Cooper, 2007; Spear and Ng, 2003; Wang et al., 2011a). Even for ERAD substrates, such as CPY*, whose ER exit signal may only be partially functional, compromising some ERAD component still increases ER exit (Kincaid and Cooper, 2007). Furthermore, under specific conditions when CPY* is overexpressed, which saturates the ERAD pathway, CPY* can advance to the Golgi and becomes a lysosome/vacuole-targeted GQC substrate (Spear and Ng, 2003). So far, most lysosome/vacuole-targeted GQC substrates contain folding lesions in either the lumenal domain or a transmembrane domain, which is consistent with the finding that ERAD substrates with lumenal folding lesions are able to advance to the Golgi before ER degradation, while those with cytosolic folding lesions are statically retained in the ER (Vashist and Ng, 2004). It is also possible that cytosolic folding lesions may directly disturb the ER exit signal and that the cytosolic chaperones may be more strict in binding their substrates, thus directly competing with COPII-mediated ER exit. Recently, I reported on a novel substrate, SZ*, with a cytosolic folding lesion that can be targeted for both ERAD and vacuole-targeted GQC. I discovered that substrate aggregation also changes the balance between ERAD and vacuole-dependent degradation (Sun and Brodsky, 2018).

In contrast to GQC, ER-phagy may deal with more severely misfolded substrates that display folding lesions in the ER but cannot be disposed of by ERAD due to their aggregation state or the absence of a recognizable ERAD signal, which is most cases remains mysterious. Protein misfolding and aggregation may also bury ER exit signals, preventing anterograde

transport. It was recently shown that an ERAD-L component, calnexin, might play a critical role in terminating ERAD and directing substrates for ER-phagy by recruiting ER-phagy receptor FAM134B (Forrester et al., 2019). This discovery potentially bridges the gap between two distinct QC machineries, ERAD and ER-phagy, and suggests a discrimination point in ERAD. However, the identification of a detergent soluble ER-phagy substrate, GnRHR, suggests instead that even soluble misfolded substrates may be targeted for ER-phagy (Houck et al., 2014). The signal for GnRHR ER-phagy is unknown.

Under stress conditions, when misfolded proteins accumulate in the ER, ERAD alone is insufficient to maintain ER homeostasis. Under these conditions, the UPR is induced to both attenuate protein translation and enhance protein folding and degradation (Karagoz et al., 2019). Enhanced degradation resulted from transcriptional activation of genes involved in ERAD, ER-phagy and GQC, suggesting collaboration between these three QC machineries to protect ER proteome fidelity (Smith and Wilkinson, 2017; Smith et al., 2018; Travers et al., 2000). ERAD, ER-phagy and GQC are further connected during ER stress to more generally maintain ER homeostasis. It has long been recognized that ERAD is enhanced upon UPR induction to clear misfolded proteins in the ER. Several ERAD-L components are up-regulated by the UPR, including Hrd1, Der1, Hrd3 and Ubc7 (Travers et al., 2000). Erv29 is also up-regulated during UPR and is required to transport both folded and misfolded cargo. Although another ERAD-targeting GQC receptor, Rer1 (see above), is not directly up-regulated during UPR, but loss of Rer1 induces ER stress in both yeast and worms, suggesting the involvement of proteasome-targeted GQC in maintaining ER homeostasis (Ghavidel et al., 2015). The enhanced anterograde and retrograde trafficking between ER and Golgi during UPR may further facilitate both proteasome-targeted GQC and lysosome/vacuole-targeted GQC indirectly. In line with this result,

the identification of Tul1 as a GQC ubiquitin ligase further confirmed the involvement of GQC during the UPR as Tul1 is specifically induced by UPR but not by the heat-shock response (Reggiori and Pelham, 2002; Roth et al., 1998; Travers et al., 2000). Besides ERAD and GQC, autophagy flux is further enhanced during the UPR (Senft and Ronai, 2015). Under ER stress conditions, multiple autophagy-related genes (ATG) are transcriptionally up-regulated, and one of the UPR branches in metazoan, the PERK-eIF2α pathway, is essential for autophagy induction (B'Chir et al., 2013). Strikingly, one ER-phagy receptor, CCPG1, is also up-regulated in response to ER stress, suggesting an important role of ER-phagy to counteract ER stress (Smith et al., 2018). Furthermore, micro-ER-phagy in yeast and its mammalian counterpart, Sec62-mediated recovER-phagy, are both required to re-establish pre-stress ER condition by eliminating excessive ER membranes and folding factors that are generated during the UPR (Bernales et al., 2006; Fumagalli et al., 2016; Schuck et al., 2014). Recently, a conserved Atg8-binding adaptor, Ubx5 in yeast (PUX proteins in plant) was identified that targets mutated, non-functional Cdc48/p97 for autophagic degradation, which if stabilized could compromise ERAD (Marshall et al., 2019). Additionally, another ERAD component, the proteasome, when inactivated also becomes an autophagy substrate, suggesting the involvement of autophagy in monitoring ER quality control by turning over inactive ERAD components (Marshall et al., 2015). Despite the distinct machineries employed by ERAD, ER-phagy and GQC, their synchronized up-regulation during ER stress indicates their cooperative potential to counteract ER stress and maintain ER protein homeostasis (Figure 3).

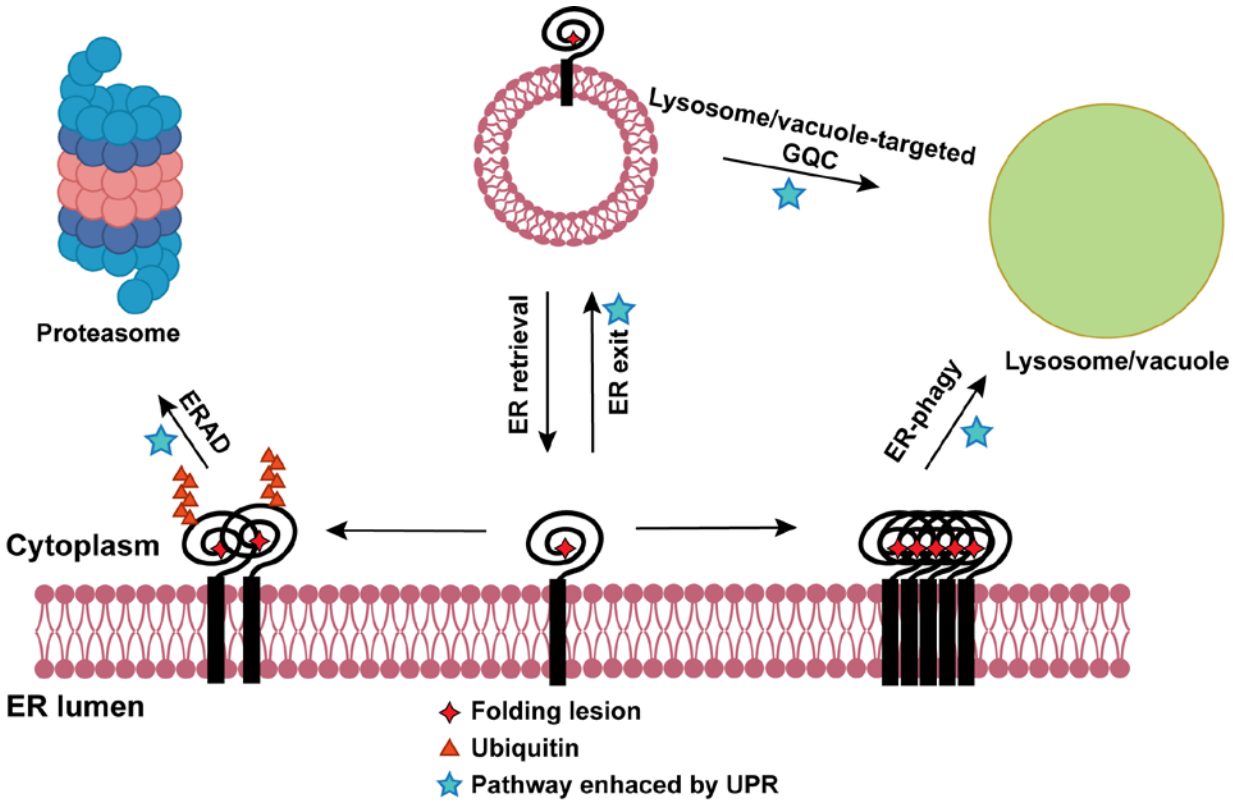

Figure 3 Degradation fate of misfolded proteins in the ER

Misfolded proteins in the ER can be targeted for multiple quality control pathways. Most of the misfolded proteins in the ER are eliminated by ERAD via the ubiquitin-proteasome system. Some misfolded proteins exit the ER and are sorted en route to the lysosome/vacuole for degradation. Upon severe aggregation, some misfolded proteins are targeted for lysosomal/vacuolar degradation via ER-phagy. All three quality control machineries act in coordination to safeguard the ER proteosatsis, especially upon ER stress, during which all three pathways are upregulated (blue star) to enhance the protein turnover in the ER through different routes.

1.5 THESIS SUMMARY

In this thesis, I investigated features of misfolded secretory pathway proteins that dictate their degradation fate in yeast: ERAD versus post-ER degradation. Despite the incomplete conservation between yeast and mammals, the reduced level of gene redundancy and conservation of major protein quality control components make yeast a good model organism for my research. To this end, I first designed a novel substrate, SZ*, and demonstrated that SZ* is degraded by both the proteasome through the ERAD pathway and by vacuolar proteases through the post-ER degradation pathway (Chapter 2). This phenomenon is similar to that seen with ApoB, ROMK, and Kir2.1 (Amengual et al., 2018; Hrizo et al., 2007; Kolb et al., 2014; Mackie et al., 2018). Through an interrogation of cells with different stress, I was able to demonstrate that heat-shock and substrate overexpression can increase ERAD targeting of SZ*, which correlated with substrate aggregation. Next, I investigated whether inhibiting distinct steps during ERAD affected the anterograde transport of SZ* from the ER (Chapter 3). I demonstrated that inhibiting pre-ubiquitination steps during the ERAD of SZ* allows ER exit. In order to confirm that ubiquitination acts as an ER retention signal, I attached four tandem ubiquitin molecules to SZ* and showed that poly-ubiquitin is sufficient to retain SZ* in the ER even when ERAD is compromised. Based on these efforts, I discovered that substrate aggregation and ubiquitination dictate the fate of misfolded membrane proteins for ERAD versus post-ER degradation.

2.0 A NOVEL MODEL SUBSTRATE WHOSE DEGRADATION IS DETERMINED BY AGGREGATION PROPENSITY

The contents of this chapter are adapted from a recently published article in *Molecular Biology of the Cell* (Sun and Brodsky, 2018). The figures and text have been edited for clarity and flow.

2.1 INTRODUCTION

In eukaryotes, one third of the proteome enters the ER, thus making the ER a rather crowded environment. Because of genetic mutations, translational errors, and cellular stress, protein misfolding occurs quite frequently (Berner et al., 2018; Needham et al., 2019). Accumulation of misfolded and/or aggregation-prone proteins not only endangers cellular health but also causes human diseases such as Huntington's disease, Alzheimer's disease, and Parkinson's diseases (Hartl, 2017). To protect proteome fidelity and maintain cellular homeostasis, eukaryotes have evolved multiple QC mechanisms that operate along the secretory pathway including ERAD, ER-phagy, GQC and plasma membrane QC (Arvan et al., 2002; Dikic, 2018; MacGurn et al., 2012; Vembar and Brodsky, 2008). Therefore, proteins—especially membrane proteins with complex topologies and subunits of multimeric assemblies—are subject to sequential QC checkpoints before reaching to their final destinations (Houck and Cyr, 2012; Okiyoneda et al., 2011).

Most secreted and membrane proteins that fail to pass the ERQC checkpoint are eliminated by ERAD, during which misfolded proteins are proteolyzed in a step-wise mechanism. Briefly, ERAD substrates are first recognized by molecular chaperones, residing in both the ER lumen and cytoplasm, as well as by chaperone-like lectins (Braakman and Bulleid, 2011; Nakatsukasa et al., 2008). Depending on the location of the folding lesion, ERAD substrates are then ubiquitinated by distinct E3 ubiquitin ligases that associate with a non-overlapping group of protein partners in the ER (Carvalho et al., 2006; Vashist and Ng, 2004). Despite the existence of three ERAD branches, ERAD-C, ERAD-L and ERAD-M, they all converge on the substrate retrotranslocation step. During substrates retrotranslocation, the ubiquitinated substrates are extracted from the ER to the cytoplasm in an ATP- and Cdc48/p97-dependent manner (Ye et al., 2003). Finally, the retrotranslocated substrates with poly-ubiquitin tags are delivered to the 26S proteasome for degradation (Meusser et al., 2005).

When the ERAD pathway is compromised or overwhelmed by the accumulation of misfolded proteins in the ER, the UPR is induced to counteract ER stress by attenuating protein translation, increasing protein folding capacity and enhancing protein degradation (Preissler and Ron, 2018). Enhanced protein degradation results from up-regulation of UPR targets that are involved in ERAD, ER-phagy, and GQC (Bernales et al., 2006; Preissler and Ron, 2018; Reggiori and Pelham, 2002; Schuck et al., 2014; Travers et al., 2000). Additionally, the cytoplasmic heat-shock response can also alleviate ER stress by altering multiple ER-associated activities, such as protein translocation, folding, and anterograde transport along the secretory pathway (Liu and Chang, 2008). Even with a robust ERAD machinery and the UPR that responds to stressful condition, misfolded proteins can escape ERAD and advance to the Golgi, suggesting the existence of post-ERQC mechanisms.

Like ERQC, post-ERQC, including GQC and plasma membrane QC, employs key components to targets misfolded proteins for clearance by the proteasome (proteasome-targeted GQC) and the lysosome (lysosome/vacuole-targeted GQC and plasma membrane QC). GQC is equipped with two QC checkpoints, which reside in the *cis*-Golgi (proteasome-targeted GQC) and *trans*-Golgi (lysosome/vacuole-targeted GQC) to protect later steps in the secretory pathway by inspecting the folding state of a protein and triaging misfolded proteins to different proteolytic machineries for turnover. Briefly, proteasome-targeted GQC substrates are transiently trafficked to the *cis*-Golgi and then retrieved for proteasomal degradation (Caldwell et al., 2001; Taxis et al., 2002; Vashist et al., 2001). In contrast, misfolded proteins that travel further to the *trans*-Golgi are monitored by lysosome/vacuole-targeted GQC and modified by E3 ubiquitin ligases, such as Tul1 and Rsp5, and can be selected by the Vps10 receptor for vacuolar/lysosomal degradation. Canonical substrates directed for vacuolar/lysosomal degradation by GQC include membrane proteins harboring polar residues in their transmembrane domains, such as Pep12(D), Phm5 and Cps1, as well as membrane proteins with lumenal folding lesions, like Wsc1* (Reggiori and Pelham, 2002; Wang and Ng, 2010; Wang et al., 2011c). QC at the plasma membrane ensures the fidelity of the proteome at the cell surface through the ART-Rsp5 ubiquitin ligase network (Zhao et al., 2013). When cells are subject to stresses (such as heat-shock stress), changes in nutrient levels, or altered environmental conditions, cell surface proteins undergo dynamic regulation, during which the ART-Rsp5 network recognizes and ubiquitinates select proteins and targets them for lysosomal degradation in response to these stimuli (MacGurn et al., 2012). For membrane proteins, both the GQC and plasma membrane QC pathways converge at the MVB pathway, where ubiquitinated proteins are invaginated into the endosomal lumen with the help of endosomal sorting complexes required for transport

(ESCRT), thus forming multivesicular bodies for vacuolar/lysosomal delivery (Christ et al., 2017; Henne et al., 2013).

In the early secretory pathway, ERAD and GQC work in tandem to prevent misfolded proteins from moving to later steps in the secretory pathway. Misfolded membrane proteins that escape ERAD and become GQC substrates bear folding lesions in either transmembrane or lumenal domains but not cytosolic domain. In addition, it has been recognized that misfolded membrane proteins with cytosolic folding lesions (ERAD-C substrates) are retained in the ER but the underlying reason for this event remains elusive (Vashist et al., 2001). Considering the fact that multiple human disease-causing mutant proteins bear cytosolic folding lesions that are trapped in the ER for ERAD, it is vital to establish if misfolded membrane proteins with cytosolic folding lesions can exit the ER and what features dictate ER retention versus ER exit (Guerriero and Brodsky, 2012; Houck and Cyr, 2012).

In this chapter, I sought to define how a membrane protein with a cytoplasmic misfolded domain might be selected for ERAD versus post-ERQC. To this end, I first designed a novel misfolded membrane protein, SZ*, which is a simplified version of a well-characterized ERAD substrate, Ste6-166 (Loayza et al., 1998). The substrate was constructed by appending a single pass membrane span from a plasma membrane protein, Wsc1, to a cytosolic misfolded domain NBD2*, which on its own is a substrate for ubiquitin-proteasome-mediated degradation (Guerriero et al., 2013). I first characterized the degradation requirements of SZ* and then found that SZ* was selected for efficient degradation by both ERAD and vacuole/lysosome-targeted GQC, the latter of which requires the MVB pathway. By interrogating how various conditions affect the degradation fate of SZ*, I discovered that heat-shock and substrate overexpression enhance ERAD targeting of SZ*, which correlated with increased substrate aggregation.

Together, these data provide a new tool to investigate the mechanism underlying degradation pathway selection and add new insights into the rules that govern ERAD substrate selection.

2.2 MATERIALS AND METHODS

2.2.1 Yeast growth conditions, strains, and plasmid construction

Yeast cells were grown at 26°C unless otherwise indicated. Temperature-sensitive strains were grown at room temperature for propagation and then shifted to 37°C. The *Saccharomyces cerevisiae* strains employed in this chapter are provided in Table 1 (Appendix A). Liquid and solid selective media were prepared as previously described (Michaelis and Herskowitz, 1988). Yeast transformation was conducted using lithium acetate method (Ito et al., 1983).

Both triple HA-tagged SZ and SZ* are generated by overlapping PCR. Briefly, SZ* was amplified through overlap PCR from plasmid pRP12 using primers OSZ01, OSZ02, OSZ03, and OSZ04 (all plasmids and primers used in this chapter were listed in Table 2, and Table 3 (Appendix A), respectively) (Prasad et al., 2012). The SZ* fragment was cloned into the p416TEF plasmid at the SpeI/XhoI sites, thus generating plasmid pSZ01. Similarly, SZ was PCR amplified from plasmid pSZ01 and pCG01 by overlapping PCR again using primers OSZ01, OSZ06, OSZ05, and OSZ07, thus generating plasmid pSZ02. To construct GFP tagged SZ*, SZ* with a 15 amino acid $((GGGGS)_3)$ flexible linker right after the NBD2* first constructed with primers OSZ08 and OSZ09 and inserted into the p416TEF plasmid at XhoI/BamHI site. Superfolder GFP was then inserted next to the SZ*-linker at the BamHI/EcoRI sites, generating SZ*-GFP (pSZ03) (Lee et al., 2013). W-N was amplified by overlap PCR using primers OSZ07,

OSZ10, OSZ11, and OSZ12 and plasmid pSW148 and pSZ02 as templates. Similarly, W-N* was amplified by overlap PCR using primers OSZ04, OSZ10, OSZ11, and OSZ12 and plasmid pSW148 and pSZ01. Then, the fragments encoding W-N and W-N* were inserted into the p416TEF plasmid at the SpeI and XhoI sites, generating pSZ04, and pSZ05, respectively. 3HA-NBD2* was PCR amplified with primers OSZ13 and OSZ04 using pCG03 as a template. The 3HA-NBD2* fragment was then inserted into the p416TEF (low expression) and p426TEF (high expression) plasmids, generating pSZ06 and pSZ07, respectively. A high expression vector for SZ* (pSZ08) was created by subcloning into p426TEF at the SpeI/XhoI sites. The DNA sequences of all constructs were confirmed by Genewiz.

2.2.2 Carbonate extraction

To liberate soluble protein that are loosely associated with membrane, carbonate extraction assay was performed. A total of 30 ODs of wild-type yeast cells expressing the indicated substrates were lysed with glass beads in 400µl of Buffer 88 (20mM HEPES, pH 6.8, 150mM KOAc, 5mM MgOAc, 250mM sorbitol) with 1mM DTT and protease inhibitors (1.5µg/ml pepstatin A, 3mM PMSF, and 3µg/ml leupeptin). Unbroken cells and cell debris were pelleted at 800g at 4°C for 5 min. Next, 300µl of the crude lysate (supernatant) was mixed with same volume of 200mM Na_2CO_3 (pH 11.5) and the mixture was incubated on ice for 30 min. The samples were then centrifuged at 100,000g for 30 min at 4°C. A trichloroacetic acid (TCA) precipitation was used to isolate proteins in the supernatant, and 80µl of TCA sample buffer (80mM Tris, pH 8, 8mM EDTA, 15% glycerol, 0.08% Tris base, 0.01% bromphenol blue 3.5% SDS, supplemented with freshly added β-mercaptoethanol to a final concentration of 4%) was added to solubilize the proteins from supernantant and pellet fractions (Zhang et al., 2001). Both

the supernatant (S) and pellet (P) were then resolved by 10% SDS-PAGE, followed by Western blot analysis.

2.2.3 Proteinase accessibility assay

ER microsomes containing SZ or SZ* were prepared as previously described (Nakatsukasa et al., 2008). In brief, 100 ODs of the indicated cells expressing SZ or SZ* from the p416TEF plasmid were harvested and lysed with glass beads in Buffer 88 with protease inhibitors (3mM PMSF, 1.5µg/ml pepstatin A, and 3µg/ml leupeptin). Unbroken cells and cell debris were pelleted at 800g for 5 min at 4°C, and the supernatant was removed and centrifuged at 18,000g for 30 min at 4°C to isolate a crude microsome fraction. After two washes with Buffer 88, the microsomes were again collected and resuspended, and equal amounts were treated in the presence or absence of proteinase K (Sigma-Aldrich, final concentration 5µg/ml), or proteinase K in the presence of 1% Triton-100. After 15 min on ice, PMSF (final concentration 10mM) was added to terminate the reaction. Total protein was TCA precipitated, as above, and SDS-PAGE and Western blot analysis were performed.

2.2.4 Detection of steady-state protein levels

Cells expressing the indicated substrates were grown to log phase (A_{600} ~1.0), and equal numbers of cells were harvested. Total protein was precipitated with TCA. When temperature sensitive strains were examined, cells were shifted to 37°C for 30 min to induced the mutant phenotype before cells were harvested. The total TCA precipitated material was then subject to SDS-PAGE and Western blot analysis as described above.

2.2.5 Stress treatments and measurements of ERAD-dependent degradation

pdr5Δ cells expressing SZ* were grown to early log phase (A_{600} ~0.8) and the following stressors were added to the culture media before the cells were incubated at 30°C for 1 h: Tunicamycin (4μg/ml), H_2O_2 (1mM), $CdCl_2$ (50μM), Canavanine (1mM) and calcofluor white (CFW; 100μg/ml). For heat-shock treatments, cells were grown at 37°C for 1 h in the absence of any other treatment. After a 1 h treatment, MG132 (100 μM) or DMSO was added to the culture and the cells were incubated with shaking at 26°C (or 37°C to induce heat-stress) in a waterbath for 40 min. Finally, 1ml of cells were taken from each culture, snap frozen in liquid nitrogen, and total protein was obtained by TCA precipitation. The indicated proteins were resolved by 10% SDS-PAGE, followed by Western blot analysis as described above

2.2.6 Assays to measure protein degradation

Cycloheximide chase assays were preformed to measure protein stability as described (Guerriero et al., 2013). In brief, the indicated yeast strains expressing the desired substrate were grown in SC (synthetic complete) medium lacking uracil (-ura) and containing glucose to mid-log phase (A_{600} ~1.0), and cycloheximide was added to the culture to a final concentration of 150 μg/ml. A 1ml aliquot was taken for the zero time point, and the culture was incubated at 26°C or 37°C, as indicated, in a shaking water bath. At each time point, 1 ml aliquots were taken and the cells were snap-frozen in liquid nitrogen. For total protein extraction, TCA precipitation was used and protein pellets were solubilized with TCA sample buffer. Prior to SDS-PAGE, insoluble material was removed by centrifugation at 10,000 rpm in a microcentrifuge at room temperature. Samples were resolved via 10% SDS-PAGE, and subject to Western blot analysis,

as described above.

Pulse chase assays were also performed to test the stabilities of distinct proteins, as described(Tansey, 2007). In brief, yeast expressing W-N and W-N* were grown in SC (synthetic complete) medium lacking uracil (-ura) and methionine (-met) but containing glucose to early log phase (A_{600} ~0.5), and S-35 (PerkinElmer) was added to each culture to a final concentration of 100 μCi/ml for 10 min. After labeling, the cells were washed with pre-warmed culture medium and then resuspended in culture medium supplemented with 13mM methionine, 40mM cysteine, and 0.2mg/ml cycloheximide. A 1ml aliquot of the culture was immediately taken as the zero time point, which was then mixed with 400μl of quench buffer (80mM Cys, 80mM Met, and 100mM NaN_3) and placed on ice. The rest of the culture was incubated at 26°C in a shaking water bath, and at each subsequent time point 1 ml aliquots were taken and similarly mixed with quench buffer. Cells were lysed by glass bead beating and W-N and W-N* were immunoprecipitated from these samples with protein A sepharose (GE healthcare) and anti-HA antibody (Roche). After the pellets were washed and proteins were subject to SDS-PAGE, gels were dried and exposed to a phosphorimager screen. The protein substrates were detected by phosphorimager analysis on a Typhoon FLA 7000 (GE Healthcare).

2.2.7 Detergent solubility assays

The solubility of the indicated proteins was measured in dodecyl maltoside (DDM) as described previously (Zhao et al., 2013). In brief, ER microsomes from wild-type yeast expressing the indicated substrates were prepared as described above and incubated at indicated temperature for 30 min in Buffer 88 with protease inhibitors (see above) in the presence or absence of 1% DDM (EMD Millipore). The mixture was then centrifuged at 18,000g for 30 min

at 4°C, and the detergent soluble fraction (i.e., the supernatant) was precipitated with TCA (see above). Proteins from both the soluble and insoluble fractions were resuspended in TCA sample buffer and resolved by 10% SDS-PAGE, and Western blot analysis was performed as described above.

2.2.8 Assays to detect the heat-shock response

W303-A wild-type yeast were transformed with the HSE-LacZ reporter plasmid along with the Hsf1-R206S plasmid (Santoro et al., 1998; Sewell et al., 1995), where indicated, and were grown to log phase (A_{600} ~1.0). A total of 5 ODs of cells were harvested and lysed in Buffer 88 with protease inhibitors (3mM PMSF, 1.5µg/ml pepstatin A, and 3µg/ml leupeptin) by bead beating. Unbroken cells and cell debris were removed as described above. The supernatant was then collected and cleared by centrifugation at 18,000g for 10 min (4°C). The overall protein concentration of the cleared lysate was determined by BCA protein assay kit (ThermoFisher). A total of 100 µl of cleared lysate (25-80µg) was added to 0.9 ml of Z buffer (60mM Na_2HPO_4, 40mM NaH_2PO_4, 10mM KCl, 1mM $MgSO_4$, 50mM β-mercaptoethanol, pH 7.0). Next, the mixture was incubated at 30°C for 5 min and the reaction was initiated by adding 200µl ONPG (4mg/ml in Z buffer). The reaction was incubated at 30°C until the mixture acquired a pale yellow color and then terminated with 500µl 1M Na_2CO_3. The optical density was measured at A_{420nm} and beta-galactosidase activity was calculated by using the following formula: OD_{420}*1.7/(0.0045*total protein*time).

2.2.9 Indirect immunofluorescence microscopy

Yeast expressing HA-tagged SZ* from the p416TEF plasmid were grown in SC-ura medium with glucose to an A_{600} of 0.5-0.8, fixed for 1 h in 4% formaldehyde at 30°C, and the cell walls were digested by incubation with Zymolyase 20T (MP Biomedicals) at 37°C for 30 min. The cells were applied to polylysine pretreated slides and were then permeabilized with methanol/acetone. The slides were blocked for 1 h at 37°C with blocking buffer (0.5% BSA, 0.5% ovalbumin, 0.6% fish skin gelatin in PBS buffer) and incubated with the following primary antibodies at 4°C: anti-HA at a 1:250 and anti-Kar2 at a 1:500. After washing, the primary antibodies were conjugated with Alexa Fluor 488 goat anti-mouse and Alexa Fluor 568 goat anti-rabbit (ThermoFisher), both at 1:500, and nuclei were stained with DAPI. The slides were mounted with Prolong Antifade Gold (Invitrogen) and imaged with an Olympus FV1000-100 confocal microscope.

2.2.10 Live-cell fluorescence microscopy

The indicated yeast cells expressing GFP-tagged SZ* were grown to log phase (A_{600}~0.8), and cells were incubated at 30°C in the presence of FM4-64 (ThermoFisher) for 30 min. Unbound FM4-64 was removed by washing the cells with SC media. The treated cells were then harvested by centrifugation and imaged by fluorescent microscopy on an Olympus FV1000-100 confocal microscope.

2.2.11 Western blot analysis

Trichloroacetic acid (TCA) precipitation was used to first pellet yeast total proteins, which were then resolved by SDS-PAGE. After SDS-PAGE, proteins were transferred onto nitrocellulose (BioTrace NT, Pall Corp.) using the overnight wet transfer system (Amersham Biosciences), and Western blot analysis was performed as described previously (Guerriero et al., 2013) with the following primary antibodies: polyclonal rabbit anti-Sec61p (Stirling et al., 1992) at 1:5000, rabbit anti-glucose-6-phosphate dehydrogenase (G6PD) (A9521, Sigma-Aldrich) at 1:5000, monoclonal mouse anti-GFP antibody (Roche) at 1:5,000, rat anti-HA-peroxidase (Roche) at 1:10,000, and mouse anti-Pma1 which was a gift from Amy Chang (University of Michigan, Ann Arbor, MI) at 1:1,000. Secondary antibodies used in this study were: HRP-conjugated goat anti-rabbit or anti-mouse secondary antibody at 1:5000 (Cell Signaling Technology). Proteins were visualized using SuperSignal Chemiluminescence (Thermo Scientific). Images of the blots were taken on a BIO-RAD ChemiDoc^{TM}XRS Image Station and quantified using ImageJ version1.48v software (National Institutes of Health). Where indicated, protein half-life was calculated using PRISM GraphPad version 7.0C (GraphPad Software, Inc).

2.3 RESULTS

2.3.1 Design and characterization of a new ERAD substrate

To investigate if membrane proteins with cytosolic folding lesions are able to exit the ER and be degraded by other QC machineries, I used a truncated cytosolic nucleotide-binding domain (NBD2*) derived from Ste6-166 as the degron (Guerriero and Brodsky, 2012; Loayza et al., 1998). There are multiple advantages of using NBD2*: (1) Under appropriate conditions, this truncated domain can be targeted to different locations, namely the cytoplasm or the ER membrane (Guerriero et al., 2017; Guerriero et al., 2013; Prasad et al., 2012; Preston et al., 2018); (2) Cytoplasmic folding lesions seem to be more easily detected than lumenal and transmembrane domain folding lesions. Namely, while some ERAD-L substrates can exit the ER before being retrieved back for ER degradation (Caldwell et al., 2001; Taxis et al., 2002; Vashist et al., 2001), vacuole/lysosome-targeted GQC substrates bearing folding lesions in the membrane (Pep12(D)) and lumenal domain (Wsc1*) escape ERAD detection and are instead delivered for lysosomal degradation (Reggiori and Pelham, 2002; Wang and Ng, 2010); (3) NBD2* is a well-characterized degron, which on its own is efficiently degraded by the ubiquitin proteasome system (Guerriero et al., 2013); (4) NBD2* possesses two putative di-acidic ER-exit motifs, TLEVENN and QDEILEIEMYD, which may engage COPII machinery for its ER exit (Watanabe and Riezman, 2004). To further facilitate substrate ER exit and minimize ER retention, I chose a single-pass transmembrane domain from a yeast plasma membrane protein (Wsc1), and a triple-HA tag as the only lumenal portion of the protein. In parallel, a “wild-type” version of our substrate, SZ, which instead deposits full length NBD2 in the cytoplasm and is similarly attached to the single-pass transmembrane domain, was also designed. (Figure 4A).

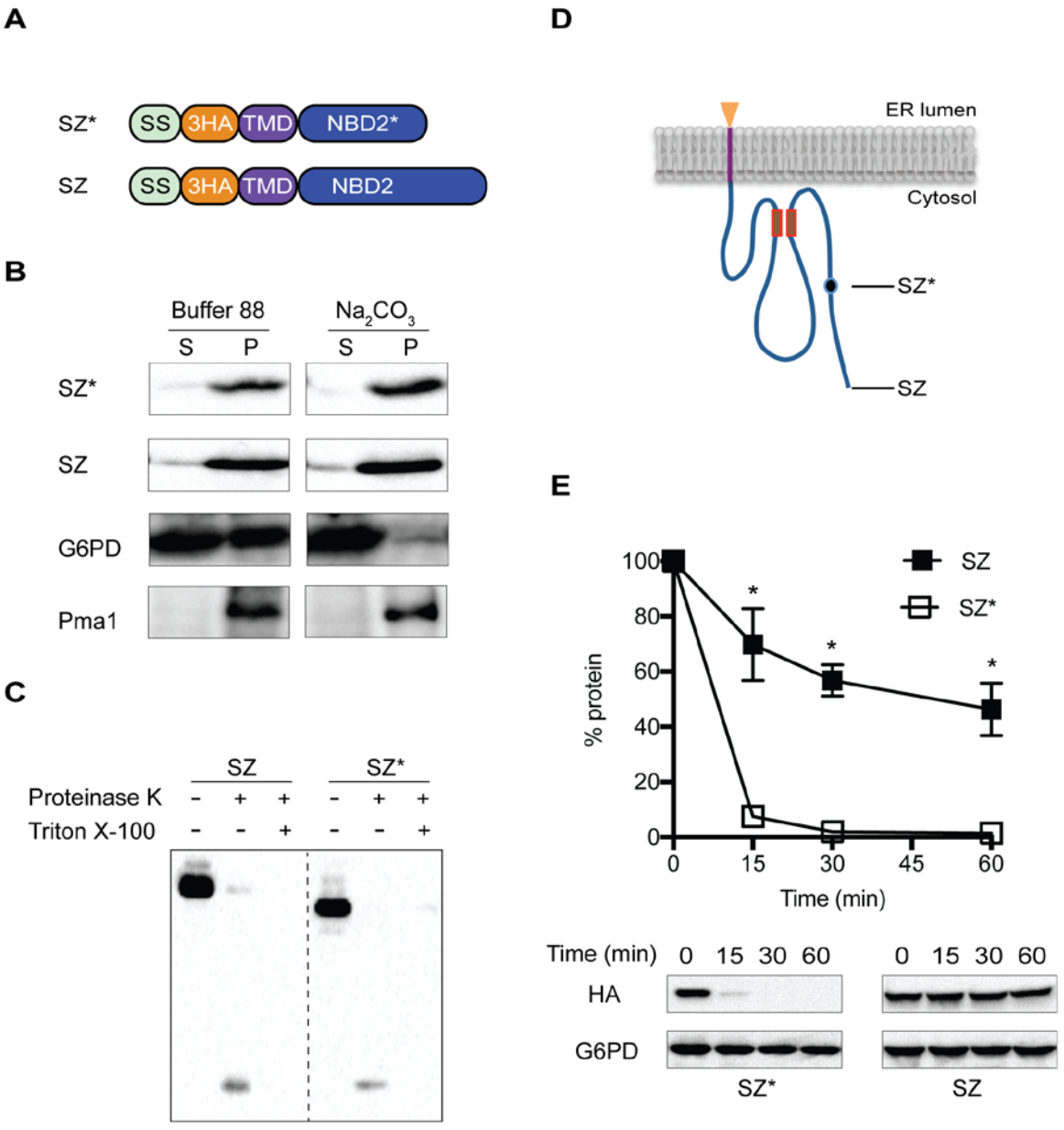

Figure 4 Characterization of a novel ERAD substrate

(A) Domain schematics of SZ and SZ* (SS: signal sequence of Kar2; 3HA: triple HA tag; TMD: transmembrane domain; NBD2: full-length nucleotide binding domain 2 from Ste6p; NBD2*: truncated NBD2 from Ste6-166). (B) Microsomes from wild-type (*BY4742*) yeast containing SZ* or SZ were treated with or without 0.1M sodium carbonate and protein residence in the supernatant (S) and pellet (P)

fractions was analyzed after centrifugation (100,000g for 30 min) and immunoblotting (G6PD: soluble protein marker; Pma1: membrane protein marker). (C) Microsomes from wild-type yeast containing SZ* or SZ were treated with proteinase K in the presence or absence of Triton X-100 and protein remaining in the microsomes was analyzed by immunoblotting with anti-HA antibody. (D) Predicted topology of SZ and SZ*. Closed circle indicates the truncation position in SZ*. The Walker A and Walker B motifs are indicated as two small boxes, and the HA epitope is depicted as a triangle. (E) The stabilities of SZ and SZ* were measured by cycloheximide chase analysis. Data represent the means ±SE of three to six independent experiments; * denotes $p<0.05$.

Carbonate extraction assay was conducted to first confirm that SZ and SZ* are integral membrane proteins. After treatment, both SZ and SZ* resided in the pellet with the integral membrane protein marker Pma1 (Figure 4B). In contrast, the cytosolic enzyme G6PD localized almost completely in the supernatant. I next determined the membrane topology of SZ* and SZ using a protease accessibility assay. Treatment of ER enriched microsomes with limiting concentrations of proteinase K led to the generation of a ~7KDa peptide, corresponding to the expected size of the protease inaccessible triple HA tag and the appended TMD (Figure 4C). In addition, both SZ* and SZ migrated at their expected molecular masses (35KDa and 39KDa, respectively), suggesting that the four cryptic glycosylation sites in NBD2 failed to enter the ER (Figure 4C). Therefore, I concluded that both SZ* and SZ are type-I membrane proteins with NBD2 facing to the cytoplasmic side of the ER and triple HA tag deposited in the lumen (Figure 4D).

The stabilities of SZ* and SZ were next determined by a cycloheximide chase assay in a wild-type yeast strain. Similar to what was found for its cytosolic counterpart, NBD2* and NBD2, respectively, SZ* is highly unstable with a half-life of ~3.8 min, whereas SZ is stable and

possesses a half-life of ~44 min (Figure 4E). These data indicate that the truncated NBD2 targets SZ* for rapid degradation.

2.3.2 SZ* is partially selected by ERAD

Since NBD2* on its own is degraded by the UPS pathway, I hypothesized that when tethered to the ER membrane, SZ*, would employ the ERAD-C pathway. Four lines of evidence support this conclusion: First, in yeast lacking the multi-drug pump Pdr5, SZ* was stabilized when the proteasome inhibitor MG132 was added (Figure 5A). In contrast, SZ was relatively stable regardless of MG132 treatment (Figure 5B). Second, degradation of SZ* was slowed upon incubation at the non-permissive temperature in the *cdc48-2* background (Figure 6A). Third, deleting the ERAD-C specific E3 ligase, Doa10, resulted in less efficient degradation of SZ* (Figure 6B). And fourth, mutations in either the cytosolic Hsp70, Ssa1, or Hsp40, Ydj1, reduced the rate of SZ* degradation (Figure 6C and 6D). In contrast, the ER lumenal Hsp70, Kar2, was dispensable for SZ* turnover (Figure 6E). The subcellular localization of SZ* was then determined by indirect immunofluorescence microscopy. In the *pdr5Δ* strain without treatment, SZ* co-localized with the ER-resident protein Kar2, which is consistent with the protein being targeted for ERAD (Figure 7A). Of note, SZ* was stabilized to a similar extent in each of the ERAD defective mutants, but was never completely stabilized. These data suggested that SZ* might be subject to another degradation pathway, such as post-ERQC, as well as ERAD.

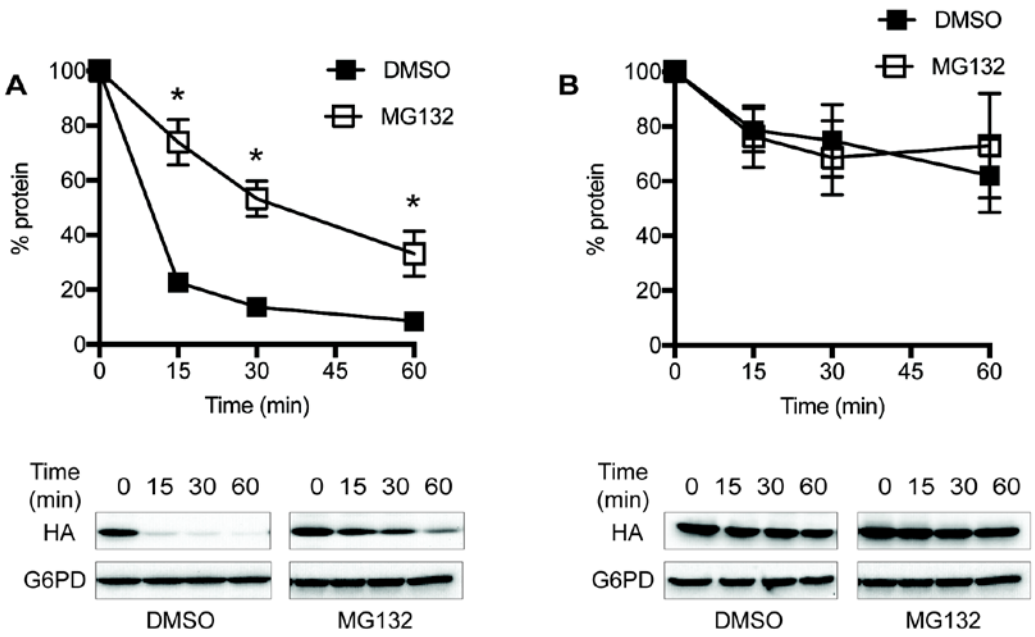

Figure 5 Proteasome dependence of SZ and SZ*

The stabilities of SZ* (A) and SZ* (B) in the *pdr5Δ* strain was measured by cycloheximide chase assay when proteasome was inhibited with 100μM MG132 Data represent the means ±SE of three independent experiments; * denotes $p<0.05$.

2.3.3 SZ* is sorted to the vacuole for degradation after Golgi transit

Considering the fact that SZ* is only partially degraded by ERAD and that SZ* shares a similar topology with canonical GQC substrate being a single-pass membrane protein, I next assayed whether the degradation of SZ* took place in the vacuole. To this end, I measured SZ* stability in a *pdr5Δ* mutant that also lacks Pep4, which eliminates ~90% of vacuolar protease activity (Ammerer et al., 1986). Even in the absence of MG132, SZ* was mostly stable, with about 70% remaining after 60 min (Figure 8A). The residual degradation of SZ* in the *pep4Δpdr5Δ* strain was inhibited by MG132 (Figure 8B). In line with this evidence, SZ* also

accumulated in the vacuolar lumen in *pep4Δpdr5Δ* yeast, as shown by indirect immunofluorescence microscopy (Figure 7B). Therefore, the majority of SZ* is delivered to the vacuole for degradation.

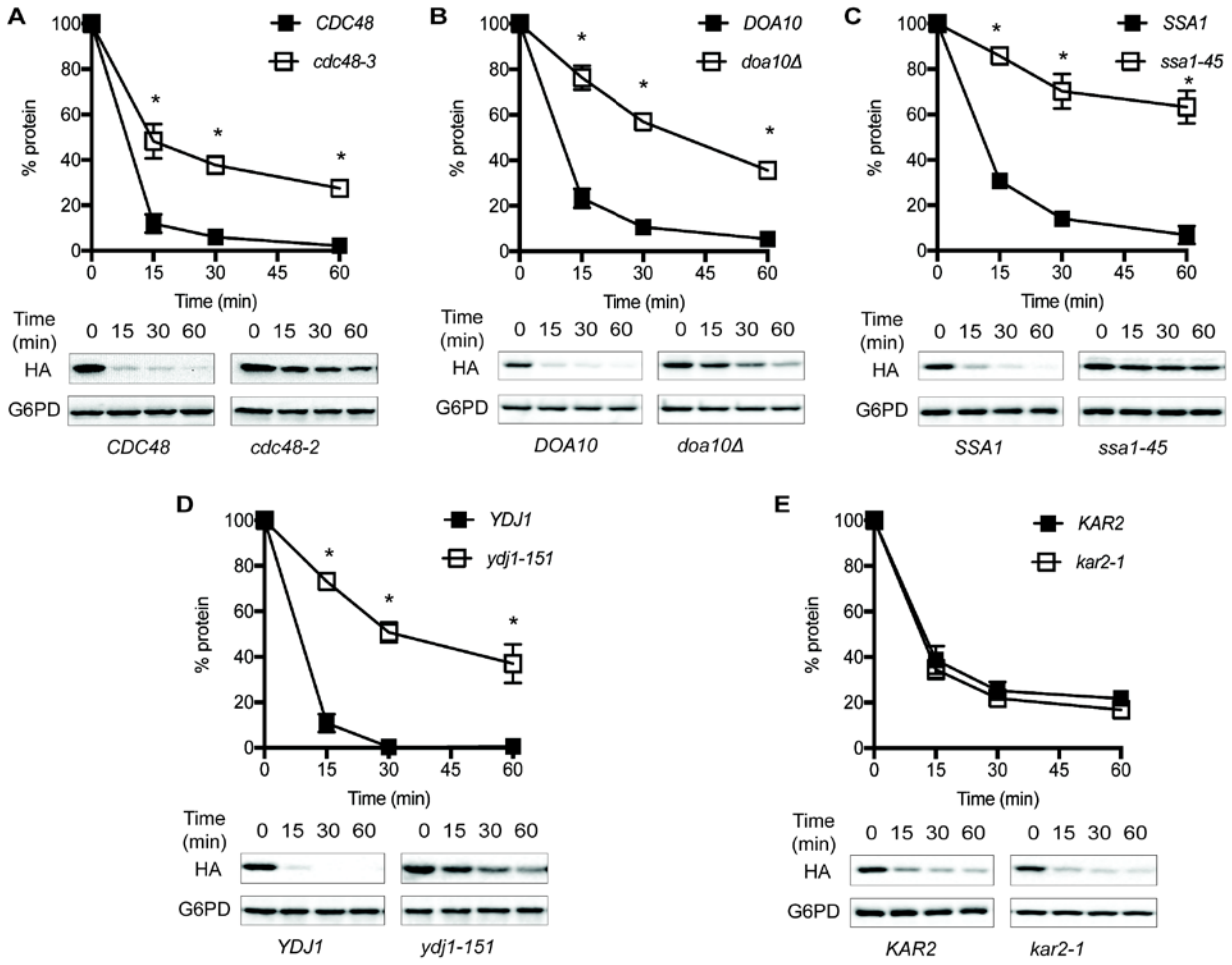

Figure 6 SZ* is partially degraded by ERAD pathway

The stabilities of SZ* were determined by cycloheximide chase analyses in the wild-type and indicated mutant strains including (A) temperature sensitive mutant of the AAA-ATPase Cdc48 (*cdc48-3)*, (B) deletion mutant of the ER-associated E3 ligase, Doa10, (C) (D) (E) temperature sensitive mutants of

cytosolic Hsp70, Ssa1(*ssa1-45*), Hsp40, Ydj1(*ydj1-151*), and ER lumenal Hsp70 Kar2 (*kar2-1*), respectively. Data represent means ±SE of three to six independent experiments; * denotes $p<0.05$.

Generally, the vacuolar delivery of misfolded membrane proteins happens through either the post-ERQC or ER-phagy pathways. To test if ER-phagy directs SZ* to the vacuole, I measured the stability of SZ* in multiple autophagy-deficient yeast strains (Lipatova and Segev, 2015). As shown in Figure 9, deletion of the selected autophagy core components did not affect the turnover of SZ*. Post-ERQC of SZ* was next investigated by measuring the steady-state level of SZ* in wild-type yeast and in strains defective for ER to Golgi transport (*sec23-1* and *ypt1-3*) and intra-Golgi transport (*sec7-4*). In contrast to the absence of an effect of autophagy on SZ* degradation, the steady-state level of SZ* at the non-permissive temperature increased from 2- to 4-fold in these mutants compared to the wild-type (Figure 10A). In a representative experiment, I measured the degradation kinetics of SZ* in the *sec23-1* background at the non-permissive temperature, and measured the half-lives in the wild-type versus *sec23-1* mutant strains as ~3.3 min and ~25 min, respectively (Figure 10B). Overall, these data suggest that SZ* is sorted into the vacuole for degradation after Golgi transit, and is therefore a substrate for both ERAD and post-ERQC.

2.3.4 SZ* transport to the vacuole requires the MVB pathway

The post-ERQC of membrane proteins, which includes GQC and plasma membrane QC, requires the MVB pathway for vacuolar delivery, during which ESCRT is indispensable for MVB biogenesis (Henne et al., 2013). Therefore, I next tested if the vacuolar delivery of SZ* was compromised when distinct ESCRT subunits were individually deleted. Due to concern that

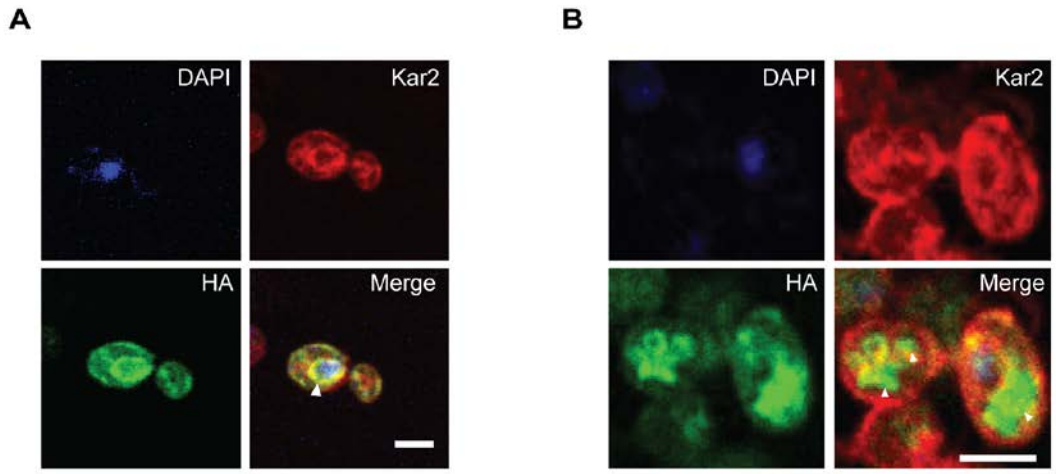

Figure 7 Subcellular localization of SZ* in *pdr5Δ* and *pep4Δpdr5Δ*

The subcellular localization of SZ* was determined in *pdr5Δ* (A) and *pep4Δpdr5Δ* (B) by indirect immunofluorescence microscopy. SZ*, ER, and the nucleus were detected with anti-HA antibody, anti-Kar2 antiserum, and DAPI, respectively. Arrowhead in (A) denotes the ER. Arrowheads in (B) denote the lobes of the vacuole and the whole vacuole. Scale bar: 5μm.

the lumenal HA epitope in SZ* would be degraded by vacuolar proteases, a GFP-tagged SZ* chimera was also constructed in which the vacuolar protease-resistant GFP moiety resides in the cytosol (Figure 11A). I first tested if GFP-tagged SZ* is degraded in a similar manner as HA-tagged SZ*. Cycloheximide chase data showed that GFP-tagged SZ* behaved similarly to the HA-tagged version in that both substrates remained susceptible to ERAD (specifically, the protein remained partially dependent on Doa10) and vacuolar degradation (Figure 12A). I next monitored GFP cleavage of SZ* in both wild-type and ESCRT several ESCRT mutants, including *vps27Δ* (ESCRT-0), *vps23Δ* (ESCRT-I), *vps36Δ* (ESCRT-II), *snf7Δ* (ESCRT-III), and *vps4Δ* (the AAA-ATPase required for ESCRT recycling). At steady state, cleavage of SZ* was evident in wild-type yeast but absent in the ESCRT mutants (Figure 11B). As expected, the steady-state level of the full length species of SZ* was higher in the ESCRT mutants than in

wild-type background. Furthermore, live cell imaging of GFP-tagged SZ* showed that instead of vacuolar lumenal localization in wild-type yeast, SZ* mislocalized in the pre-vacuolar compartment in *vps27Δ* cells (Figure 11C). Consequently, SZ* is sorted into the vacuole through the MVB pathway.

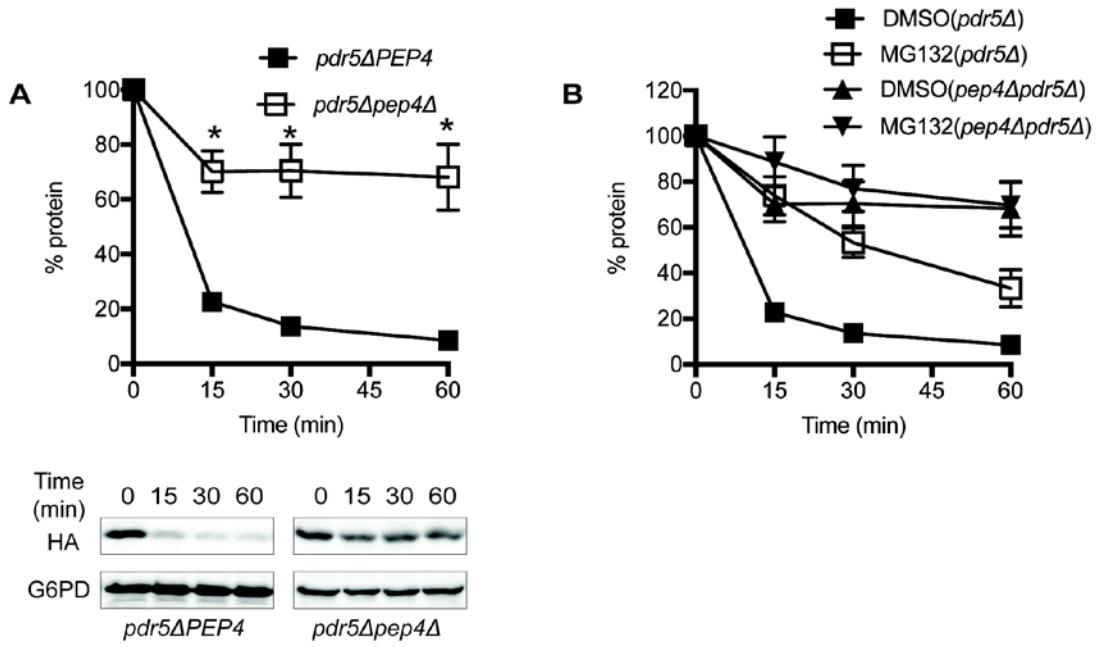

Figure 8 SZ* is mostly degraded in the vacuole

The stability of SZ* was determined by cycloheximide chase analysis in *PEP4pdr5Δ* and *pep4Δpdr5Δ* cells in the absence (A) and presence (B) of proteasome inhibition. Data represent means ±SE of three to six independent experiments; * denotes $p<0.05$.

Because plasma membrane localization of SZ* was undetectable by either indirect immunofluorescence or live cell fluorescence microscopy (Figure 7A, 7B and 11C), I hypothesized that SZ* is directed to the vacuole directly from the Golgi, but not after endocytosis from the plasma membrane. Because End3 coordinates assembly of the cortical actin

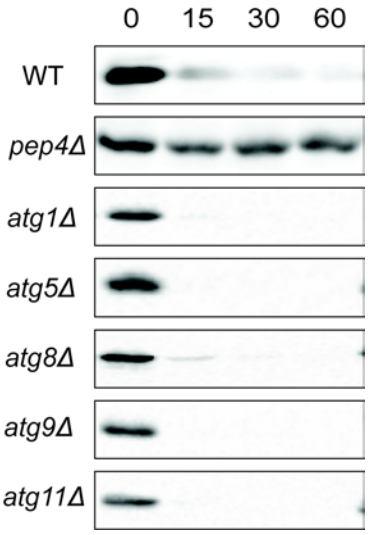

Figure 9 SZ* is not degraded though ER-phagy pathway

The stability of SZ* in wild-type and the indicated autophagy defective mutants was determined by cycloheximide chase analysis. Data represent means ±SE of three independent experiments.

cytoskeleton, and therefore the absence of this protein leads to defects in actin-dependent endocytosis (Benedetti et al., 1994), I assessed the degradation of SZ* in the *end3Δ* mutant strain after a temperature shift to 37°C. I found that deletion of *END3* had no effect on SZ* degradation (Figure 12B). Therefore, these data suggest that the population of SZ* that escapes ERAD is sorted directly from the Golgi to the vacuole through an MVB intermediate.

2.3.5 Heat stress increases ERAD targeting of SZ* by inducing its aggregation

Multiple protein degradation pathways within the cell including ERAD, GQC and ER-phagy are differentially affected by stress (Liu and Chang, 2008; Reggiori and Pelham, 2002; Schuck et al., 2014; Travers et al., 2000). To examine if SZ* targeting for either ERAD or vacuolar degradation is modified by exogenous stress, I first investigated whether a specific

stress would lead to the preferential degradation of SZ* via ERAD. Cells expressing SZ* were treated with a variety of stressors including ER stress, heat stress, heavy metal stress, oxidative stress, cell wall stress, and protein misfolding stress. Next, ERAD dependence was assayed after treating *pdr5*□ cells with either DMSO (the vehicle) or MG132. Strikingly, among these conditions, only heat-stress significantly increased the relative fold change of SZ* stabilized by MG132 compared to the control (Figure 13A and 13B). The effect of heat-stress on ERAD of SZ* was further tested by cycloheximide chase assay (Figure 13C). Upon MG132 treatment, SZ* half-life was prolonged from ~34 min at 26°C to >60 min at 37°C (Figure 13D).

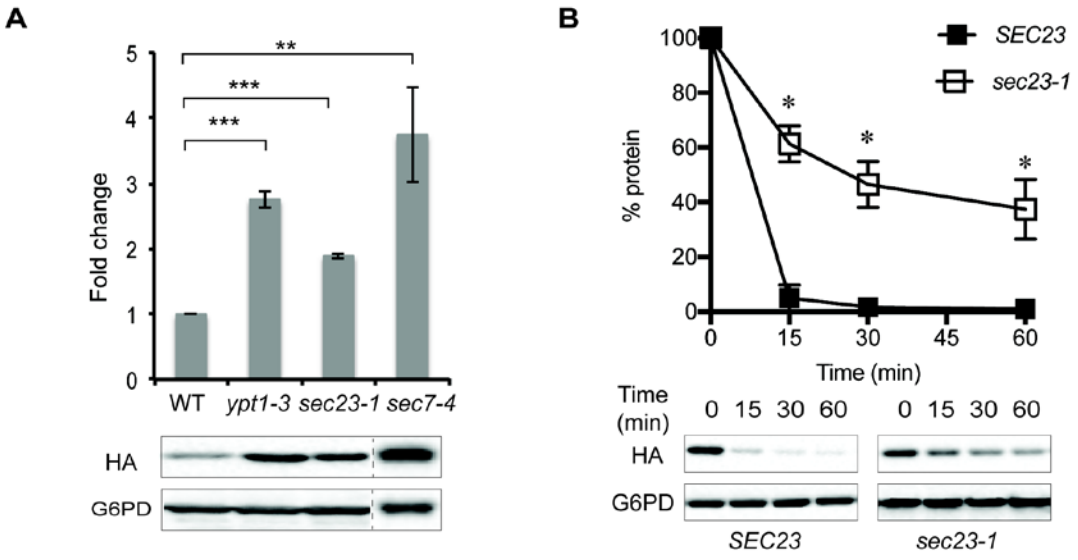

Figure 10 SZ* advances to the Golgi before vacuolar degradation

(A) The fold-change in steady-state levels of SZ* in wild-type and mutant yeast defective in ER-Golgi transport or intra-Golgi trafficking was examined by immunoblotting. (B) Cycloheximide chase analyses in *SEC23* and *sec23-1* cells were performed, and data represent three independent experiments; * denotes $p<0.05$, ** denotes $p<0.005$, *** denotes $p<0.0005$.

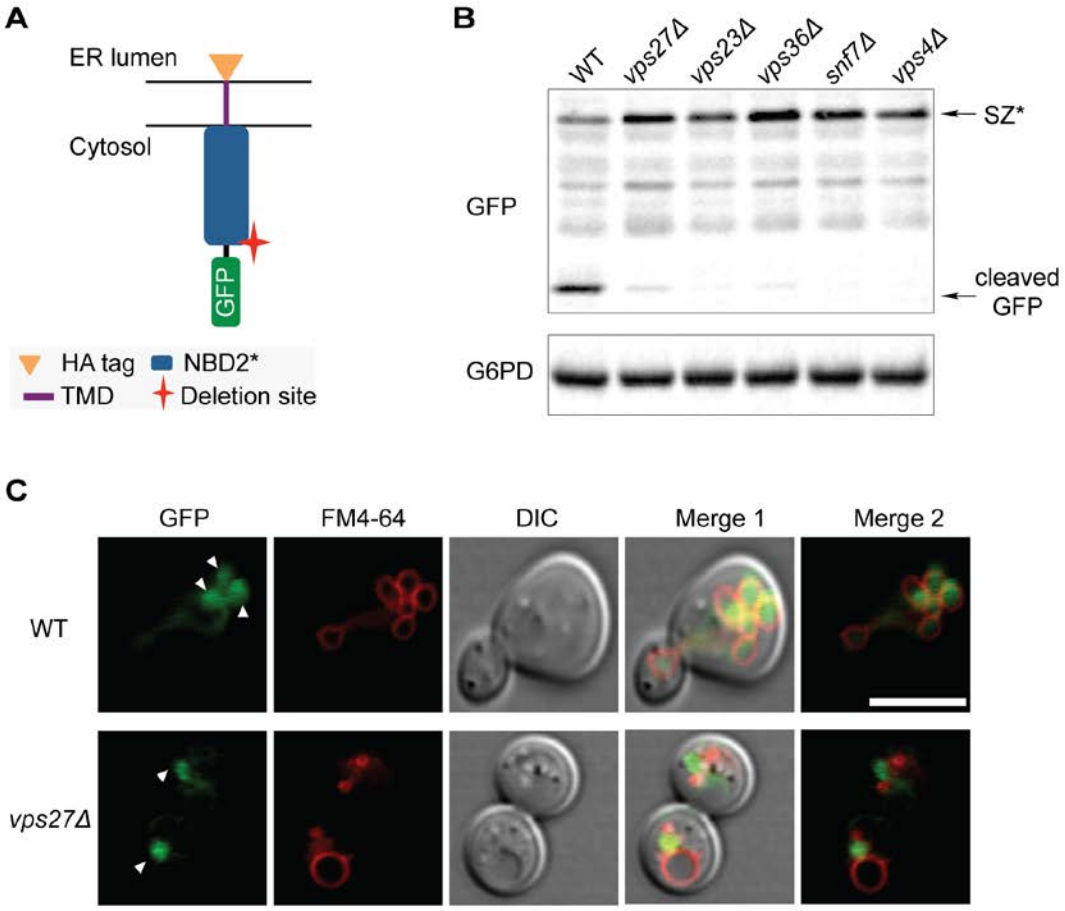

Figure 11 SZ* is delivered to the vacuole by way of MVB pathway

(A) Predicted topology of GFP-tagged SZ*. The cytosolic residence of GFP allows for analysis of MVB delivery to the vacuole. (B) GFP cleavage from GFP-SZ* in the wild-type and indicated mutant strains was determined by immunoblotting. G6PD serves as a loading control. (C) The cellular localization of SZ* in both wild-type and *vps27Δ* cells was determined by fluorescence microscopy. FM4-64 marks the vacuolar membrane. Arrowheads denote the lobes of the vacuole and the pre-vacuolar compartment (bottom). Scale bar: 5μm.

The effect of heat stress on SZ* degradation might have arisen from a general stress response, such as the heat-shock response (HSR), or from a temperature-dependent change in protein conformation. To examine whether HSR induction increased ERAD targeting of SZ*, I introduced a constitutively active heat shock factor 1 (Hsf1) mutant, Hsf1-R206S, into SZ*-expressing yeast (Sewell et al., 1995). The introduction of this mutant permits HSR activation in the absence of a temperature shift, thus uncoupling the HSR from a potential heat-induced protein conformational change. This allows us to differentiate whether the HSR versus a direct increase in temperature magnified SZ* targeting for ERAD. I first measured HSR induction in yeast expressing Hsf1-R206S at 26°C and found that the HSR was induced to an even greater extent than that produced by heat shock (Figure 14A). Nevertheless, Hsf1-R206S failed to enhance the ERAD of SZ*, as established in either a steady-state or cycloheximide chase assay (Figure 14B and 14C). This finding suggests that the temperature shift instead altered the conformation of SZ*.

Based on a homology model of NBD2, the truncation site in NBD2* resides between two beta sheets, which may lead to the generation of an aggregation-prone protein (Preston et al., 2018). Therefore, I surmised that heat stress induces SZ* aggregation, which in turn increases ERAD targeting. To test this hypothesis, I conducted detergent solubilization experiment and measured detergent solubility under different stress conditions. Briefly, SZ*-expressing yeast were used to prepare ER-derived microsomes, which were then pre-treated at either 26°C or 37°C before dodecyl maltoside (DDM) solubilization. Samples after DDM extraction were subject to centrifugation to separate the detergent soluble fraction. As shown in Figure 15A, the DDM solubility of SZ* was significantly reduced when microsomes were pre-treated at 37°C compared to the 26°C group. As a control, I tested whether Wsc1*, which is targeted for GQC,

was also subject to heat-induced aggregation *in vitro.* In contrast to SZ*, DDM solubility of Wsc1* remain unchanged at either treatment. Furthermore, Wsc1* was not directed for ERAD even after heat-stress but still retained its behavior as a post-ERQC substrate, which is consistent with the *in vitro* DDM solubilization result (Figure 15B and 15C). Therefore, it seems that incubation at an elevated temperature enhanced ERAD targeting of SZ* by decreasing detergent solubility.

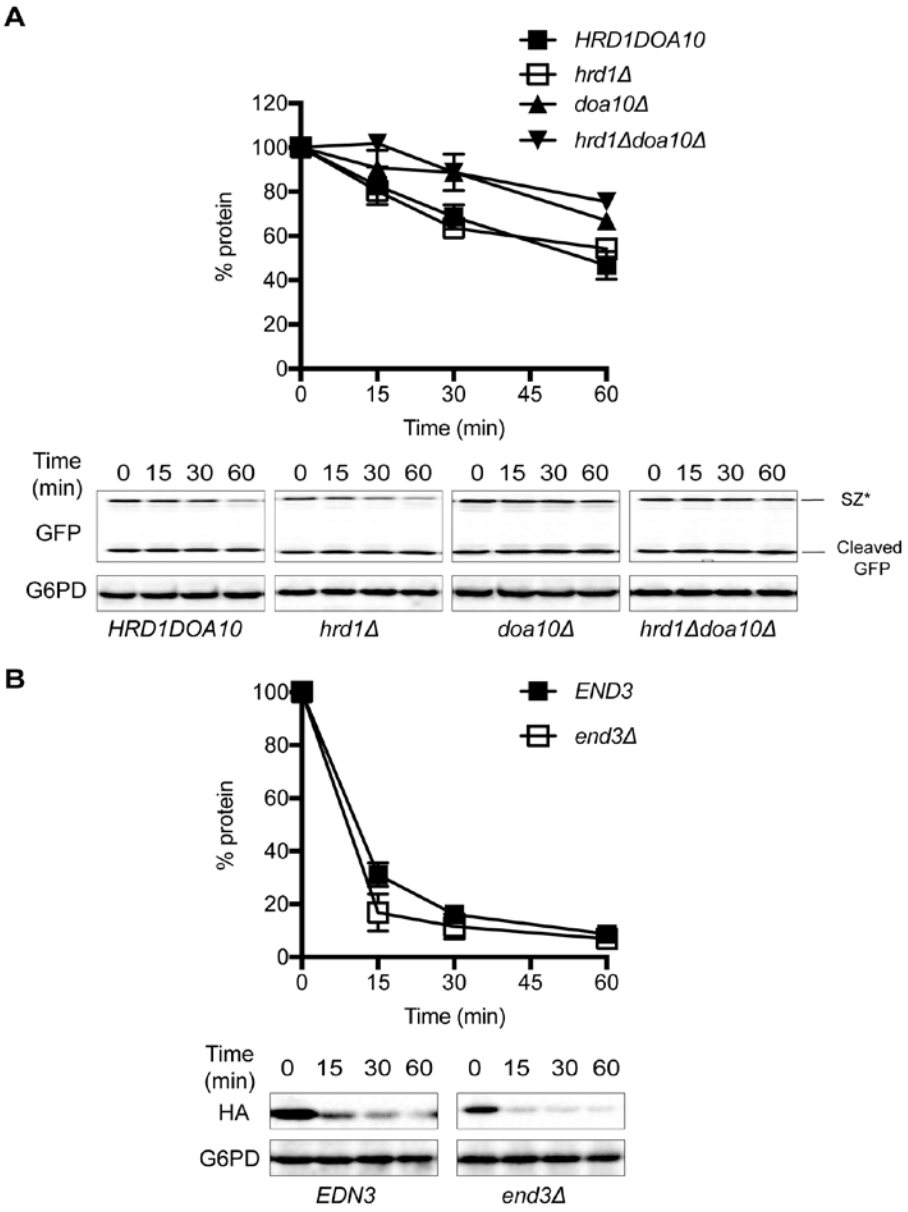

Figure 12 Endocytosis is not involved in vacuolar delivery of SZ*

(A) ERAD dependence of GFP tagged SZ* was assayed by cycloheximide chase in wild-type and mutant yeast lacking ER-resident E3 ligases *HRD1* and/or *DOA10*. Apparent differences in degradation rate between the strains were not statistically significant. (B) Stability of SZ* in wild-type and an endocytosis defective mutant was determined by cycloheximide chase analysis. Data represent means ±SE of three independent experiments.

To better establish a correlation between detergent solubility and ERAD targeting, I devised a mechanism to induce the aggregation of SZ* in the absence of a temperature shift. Given that protein aggregation is concentration-dependent, I next tested the effect of SZ* overexpression on its aggregation. A high copy number (2□□ plasmid under the control of a strong promoter (TEF promoter) was used to drive SZ* overexpression. As expected, SZ* overexpression led to a pronounced decrease in detergent solubility, even when the isolated microsomes were incubated at 26°C (Figure 15A). To further confirm that the decreased detergent solubility of SZ* resulted from the aggregation of its cytosolic domain, NBD2*, and not from another indirect effect from general protein overexpression, I tested if the aggregation of cytosolic NBD2* was concentration-dependent. A low and high (2□□ copy number NBD2* expression vector were introduced into yeast and cell lysates were prepared and incubated with sodium carbonate to liberate soluble fractions. While ~60% of NBD2* remained soluble when expressed at a relatively low level, overexpression of NBD2* was sufficient to reduce solubility by ~2-fold (Figure 15D). In line with these data, SZ*, which contains a single membrane span, when overexpressed was now exclusively targeted for ERAD (Figure 15E). Furthermore, overexpressed SZ* was retained in the ER in either the *PEP4* or *pep4Δ* background, which is in contrast to its significant accumulation in the vacuole in the *pep4Δ* mutant when expressed at low

levels (Figure 15F). Because SZ* degradation under low expression conditions showed a partial ERAD dependence (Figure 6A), these data are consistent with a model that aggregation propensity is a trigger for ER retention and thus ERAD substrate selection.

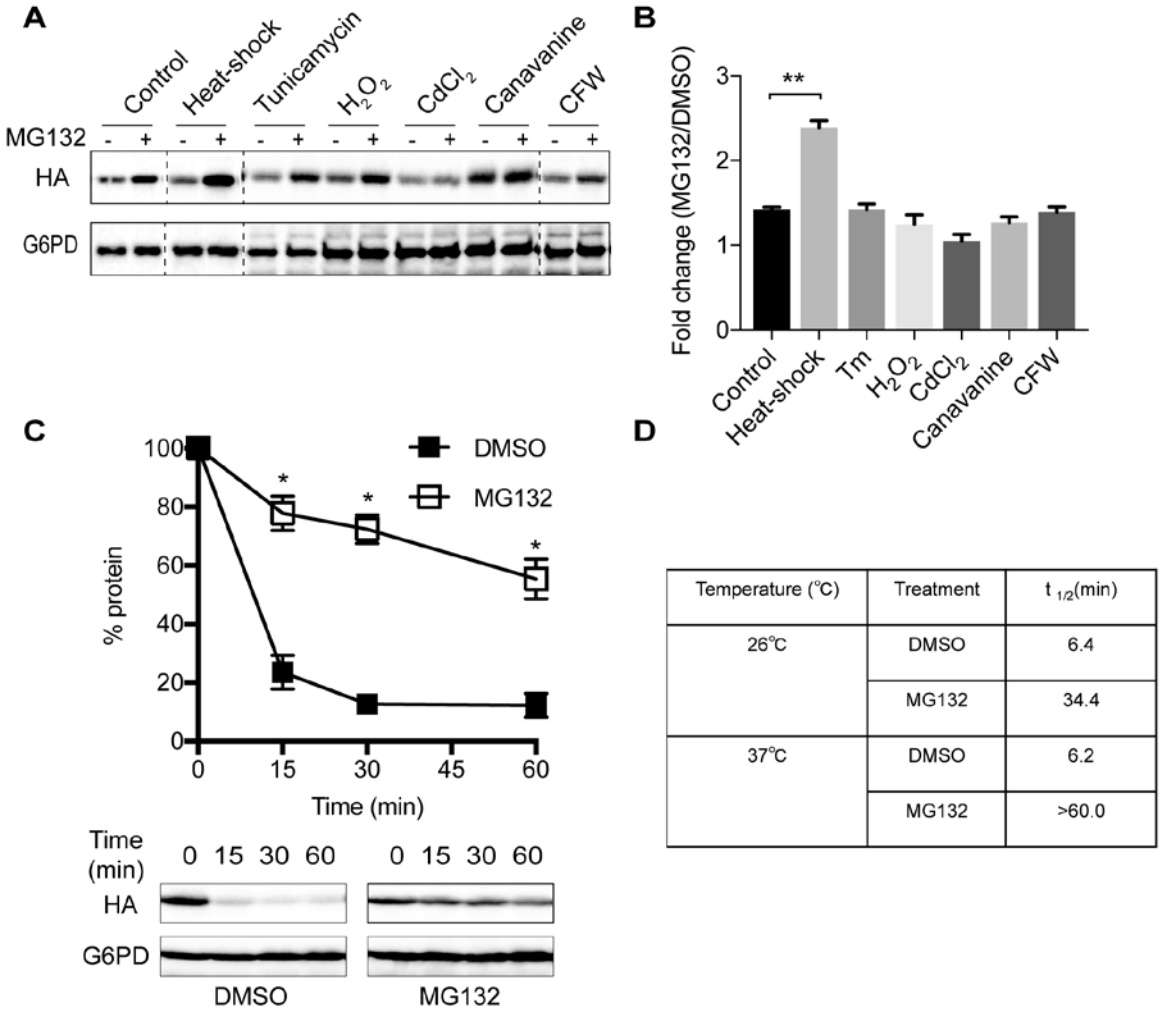

Temperature (°C)	Treatment	$t_{1/2}$(min)
26°C	DMSO	6.4
	MG132	34.4
37°C	DMSO	6.2
	MG132	>60.0

Figure 13 Heat stress increases the targeting of SZ* for ERAD

(A) A *pdr5Δ* mutant strain expressing SZ* was treated with the indicated stressors for 60 min prior to the addition of DMSO or 100μM MG132. The level of SZ* was visualized by immunoblotting. (B) ERAD dependence of SZ* was quantified by the relative fold change of SZ* level treated with MG132 versus DMSO as in (A), and normalized to the loading control G6PD. (C) ERAD dependence of SZ* was

assayed by cycloheximide chase at 37°C after treatment with the proteasome inhibitor MG132 or the vehicle DMSO. (D) The half-life of SZ* was calculated from cycloheximide chase data. Data represent the means ±SE of three independent experiments. * denotes $p<0.05$ and ** denotes $p<0.005$.

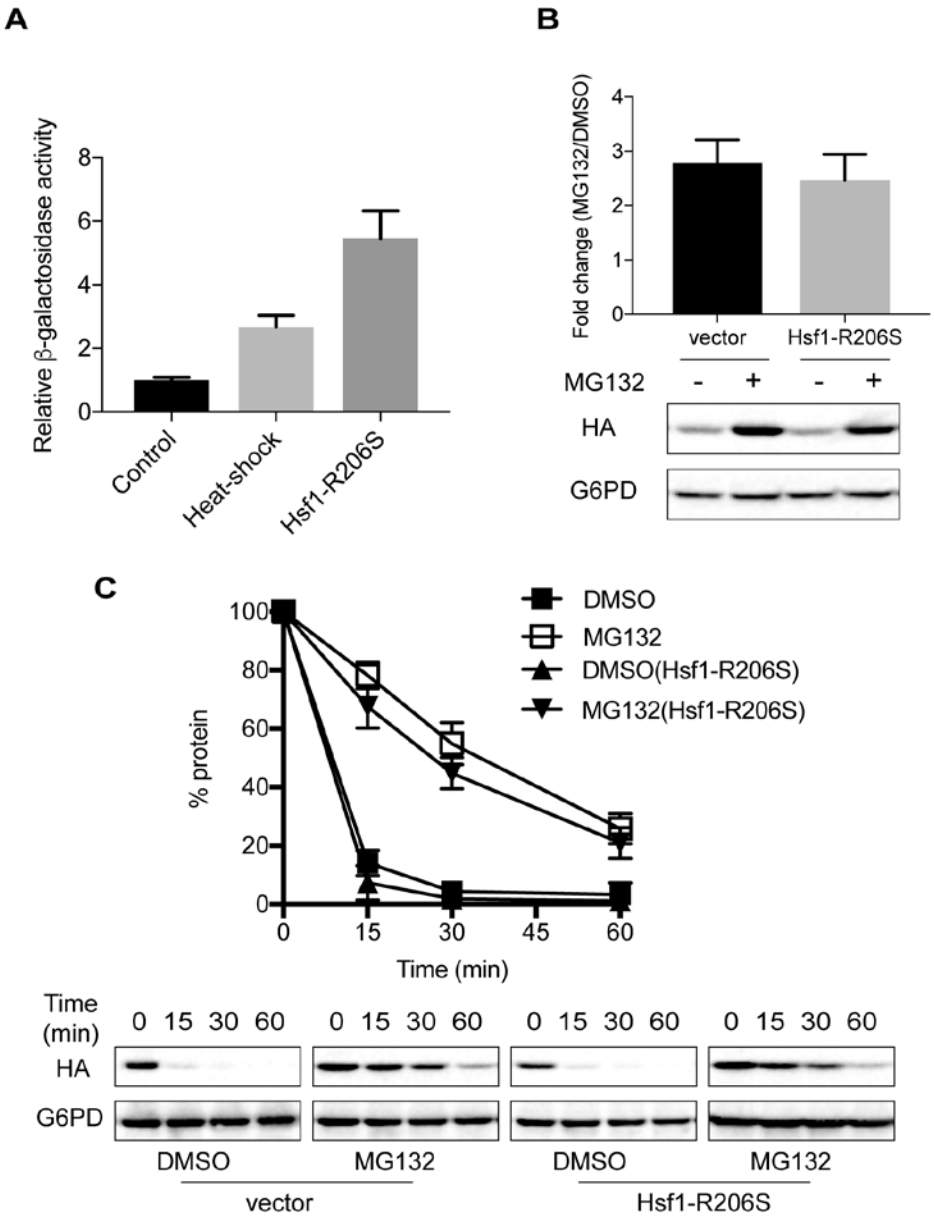

Figure 14 The enhanced ERAD targeting of SZ* is not caused by heat-shock response.

(A) Heat-shock induction was measured in a reporter assay that assesses beta-galactosidase activity. (B-C) The ERAD dependence of SZ* with constitutive HSR induction was assayed by measuring both (B)

steady-state levels and (C) by a cycloheximide chase assay. Data represent means ±SE of three independent experiments. ** denotes $p<0.005$

It is worth mentioning that overexpression of SZ* also makes it relatively stable, suggesting that the ERAD-C pathway may be saturated by its overexpression or that the overexpression of SZ* prevents the display of the degron, thus leading to inefficient degradation. To examine if the secretory pathway may be saturated or compromised upon SZ* overexpression, I measured the degradation of a post-ERQC substrates, Wsc1*, in conjunction with SZ* overexpression, because Wsc1* utilizes the same transport pathway from the ER to the vacuole as SZ* when expressed at low levels (Wang and Ng, 2010; Wang et al., 2011c). However, both the half-life and the Wsc1* Golgi glycosylation pattern were similar regardless of whether SZ* was present or absent (Figure 15G). This evidence suggests that the post-ERQC pathway does not become saturated upon SZ* overexpression. Instead, I propose that SZ* aggregation that is induced by overexpression, even in the absence of a temperature shift, results in ER-retention and increased ERAD targeting. This contrasts with the fate of an ERAD-L substrate, CPY*, whose overexpression still allows for ER exit and degradation in the vacuole, suggesting that a different ER retention mechanism exists for SZ* (Spear and Ng, 2003).

2.3.6 Fusion of an aggregation-prone domain targets a post-ERQC substrate for ERAD

To expand the significance of my findings, I next asked if the aggregation-prone NBD2* degron can act in a dominant manner to retain a post-ERQC substrate in the ER and induce degradation by the ERAD pathway. To answer this question, both NBD2* and the full length NBD2 domain were individually fused to Wsc1*, thereby generating W-N* and W-N,

respectively (Figure 16A). I first examined the detergent solubility of W-N* and W-N in isolated membranes. Considering the fact that substrates containing NBD2* (but not NBD2) are targeted for proteasome-dependent degradation, and that aggregation-propensity favors ERAD targeting (see above), W-N* was expected to be less soluble than W-N*. As hypothesized, the DDM solubility of W-N* was lower than that of W-N (Figure 16B). Next, I examined the trafficking of these proteins in the cell. Previous work suggested that the lumenal domain of Wsc1* is glycosylated in the Golgi, which serves as a read-out for ER exit as the Golgi species migrates somewhat slower than the ER population by SDS-PAGE (Wang and Ng, 2010). As expected, only W-N exits the ER as shown by the presence of the slightly higher molecular weight species (Figure 16C; Western blot, bottom panels). In contrast, W-N* was unable to exit the ER since Golgi-associated glycosylation was absent (Figure 16D; Western blot, bottom panels). Additionally, turnover of W-N* was proteasome-dependent (Figure 16D), whereas W-N was relatively stable and not degraded by the proteasome (Figure 16C). To confirm these results, I also performed pulse chase experiments, during which glycan maturation can be clearly detected. In accordance with the cycloheximide chase data, only W-N* exhibited partial proteasome-dependent degradation (Figure 17A and 17B). Consistent with proteasomal dependent degradation, the ERAD-C ubiquitin ligase Doa10 was required for efficient degradation of W-N* but not W-N (Figure 17C and 17D). Together, these data demonstrate that a misfolded and aggregation-prone domain, NBD2*, is sufficient to target a post-ERQC substrate for ERAD. Moreover, this aggregation-prone ERAD-C determinant is dominant over the selection of a substrate for post-ERQC.

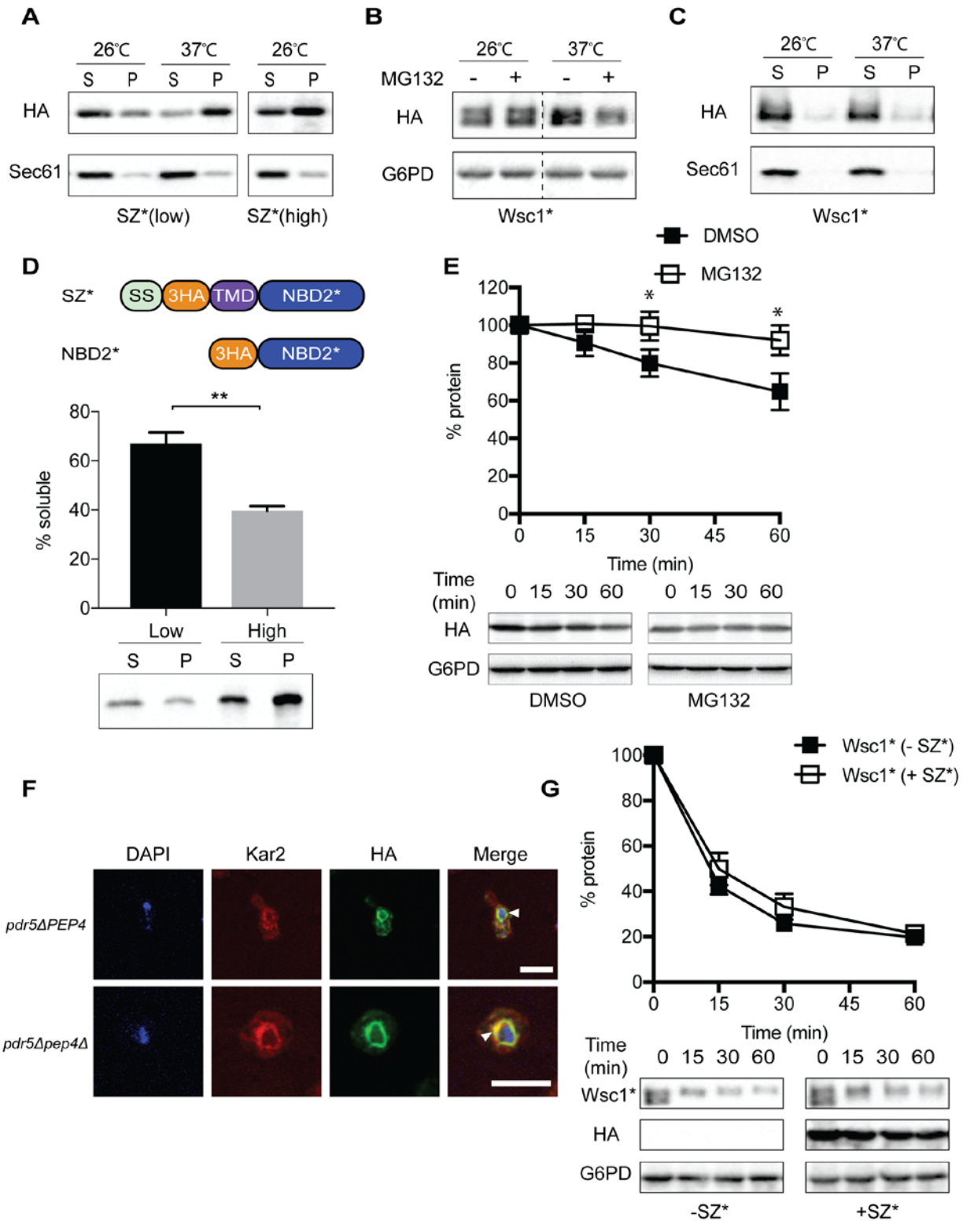
A
26°C
37°C
26°C
S P S P S P
HA
Sec61
SZ*(low)
SZ*(high)
B
26°C
37°C
MG132 - + - +
HA
G6PD
Wsc1*
C
26°C
37°C
S P S P
HA
Sec61
Wsc1*
D
SZ*
SS
3HA
TMD
NBD2*
NBD2*
3HA
NBD2*
**
% soluble
80
60
40
20
0
Low
High
S P S P
E
DMSO
MG132
120
100
80
60
40
20
0
% protein
*
*
0 15 30 45 60
Time (min)
Time (min)
0 15 30 60 0 15 30 60
HA
G6PD
DMSO
MG132
F
DAPI
Kar2
HA
Merge
pdr5ΔPEP4
pdr5Δpep4Δ
G
Wsc1* (- SZ*)
Wsc1* (+ SZ*)
100
80
60
40
20
0
% protein
0 15 30 45 60
Time (min)
Time (min)
0 15 30 60 0 15 30 60
Wsc1*
HA
G6PD
-SZ*
+SZ*

Figure 15 ERAD targeting of SZ* correlates with higher substrate aggretation propensity.

(A) Microsomes from wild-type yeast expressing SZ* under the control of the TEF promoter in either a *CEN* (low) or a 2μ (high) plasmid were treated at the indicated temperature and with 1% DDM. Protein residing in the supernatant (S) and pellet (P) fractions was analyzed after centrifugation at 18,000g for 30 min and immunoblotting. Sec61 was used as a control. (B) The proteasomal dependence of Wsc1* were assayed in steady-state levels after treatment with MG132 or DMSO at 26°C or 37°C. (C) The DDM solubility of Wsc1* was measured after incubation at the indicated temperature and centrifugation as in (A). (D) Wild-type yeast lysate containing a soluble version of SZ* that lacks a TMD ("NBD2*") was treated with 100mM Na_2CO_3, followed by centrifugation as in part (A) and immunoblotting. (E) ERAD dependence of SZ* at high expression was assayed by a cycloheximide chase at 26°C after treated with the proteasomal inhibitor MG132 or DMSO. (F) The cellular localization of SZ* expressed at high level, and the position of the nucleus and ER was determined in both *pdr5Δ* and *pep4Δ pdr5Δ* cells by indirect immunofluorescence microscopy in the absence of proteasome inhibition. Arrowheads denote the ER. Scale bar: 5μm. (G) Stability of Wsc1* was determined in the presence or absence of an SZ* high copy expression plasmid (p426TEF) by cycloheximide chase analysis. Data represent the means ±SE of three independent experiments; * denotes $p<0.05$, and ** denotes $p<0.005$

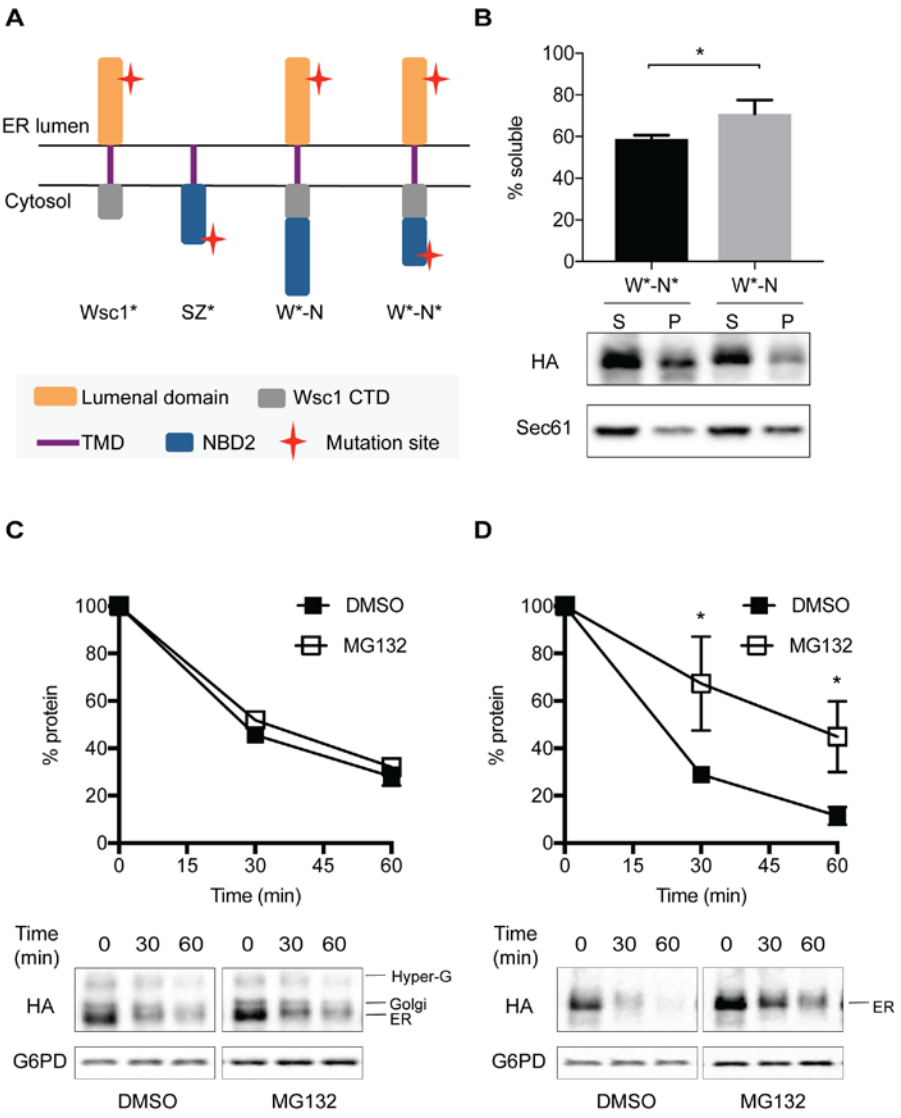

Figure 16 Fusion of the aggregation-prone NBD2* domain targets a post-ER quality control substrate, Wsc1*, for ERAD

(A) The predicted topologies of the chimeric proteins. (B) The DDM solubility of two chimeric proteins, W*-N and W*-N*, in ER-derived microsomes. ERAD dependence of (C) W*-N and (D) W*-N* was assayed by cycloheximide chase after treatment with the proteasomal inhibitor MG132 or the vehicle DMSO. Data represent means ±SE of three independent experiments; * denotes $p<0.05$.

2.4 DISCUSSION

Membrane proteins are subjected to multiple PQC checkpoints along the secretory pathway, including ERQC, GQC, and plasma membrane QC. During ERQC, the three branches of ERAD, ERAD-L, -C, and –M, monitor protein folding status in different locations relative to the ER membrane (i.e., the lumen, cytoplasm, and membrane, respectively). It has long been recognized that ERAD-C substrates seem to be statically retained in the ER for ERAD. Many ERAD-L substrates, however, do advance to the Golgi and are retrieved for ER degradation. In addition, one typical type of vacuole/lysosome-targeted GQC substrate is a single-pass membrane protein bearing folding lesions in the membrane domain, suggesting that ERAD-L may not efficiently detect folding lesions in the membrane span. A survey of vacuole-targeted GQC substrates showed that these substrates are mostly single-pass membrane proteins with folding lesions in either the lumenal or membrane domain. However, it remains unclear if membrane proteins with cytosolic folding lesions can be statically retained in the ER. To this end, I sought to investigate if membrane proteins with ERAD-C degrons are able to exit the ER and how ERAD-C machinery selects its substrates. This had never before been examined. Therefore, the first goal of this chapter was to characterize a new substrate and investigate how this protein was selected by ERAD-C. A novel substrate, SZ*, with well-characterized cytosolic degron NBD2* appended to the single-pass membrane domain of Wsc1 was constructed. Previous work on NBD2*, which is completely soluble, indicated that the nuclear ubiquitin ligase San1 targets it for proteasomal degradation (Guerriero et al., 2013; Prasad et al., 2012). Also, a somewhat similar construct (WS) created by the Ng lab suggested that the ER-resident E3 ligase Doa10 targets this protein for ERAD (Prasad et al., 2012). Here, I similarly found that SZ* is directed to the canonical ERAD-C pathway, as its turnover required ERAD-C-specific

components: Doa10 (Ubiquitin ligase), Ssa1 (cytosolic Hsp70), and Ydj1 (a cytosolic Hsp40 that associates with the ER). Therefore, my data first showed that the ERAD-C degron, which is shared with other well-characterized substrates such as Ste6* and Chimera A*, is sufficient to target SZ* for ERAD. My further characterization showed a surprising result: SZ* with a canonical ERAD-C degron also efficiently exited the ER and was directed for vacuolar degradation through the MVB pathway. This unexpected result not only expands the scope of misfolded membrane proteins that are able to escape ER retention and ERAD, but also suggests that misfolded membrane proteins, even with ERAD-C degrons, do have the potential of escaping ERAD and becoming a post-ERQC substrate.

There are several possible explanations underlying the ER exit of SZ*. First, two putative di-acidic ER exit signals exist in the cytosolic domain of SZ* (TLEVENN and QDEILEIEMYD), which may allow a substantial fraction of the substrate to be captured by the COPII machinery. In line with this hypothesis, a previous study showed that when CPY* was fused to a functional ER exit signal, it traffics from the ER and was degraded in the vacuole (Kincaid and Cooper, 2007). In contrast, the ER retention of another NBD2* bearing substrate, Ste6*, may result from the potential interactions between NBDs that may otherwise bury the ER exit signal on NBD2*. Second, the transmembrane domain of SZ*, which is derived from a plasma membrane protein, Wsc1, may contain a sorting signal for post-ER trafficking (Rayner and Pelham, 1997; Singh and Mittal, 2016). The requirement of the MVB pathway for sorting SZ* into the vacuole indicates the involvement of protein ubiquitination at a post-ER organelle, either the Golgi or at the plasma membrane. By testing protein stability in an endocytosis mutant (*end3Δ*), I confirmed that SZ* is a *bona fide* vacuole/ lysosome -targeted GQC substrates, which is sorted directly from the Golgi to the vacuole through the MVB pathway. The ubiquitin ligase

required for the post-ER ubiquitination of SZ*, however, remains unidentified. Given the topology and the cytosolic folding lesions in SZ*, Rsp5 may be a good candidate to test.

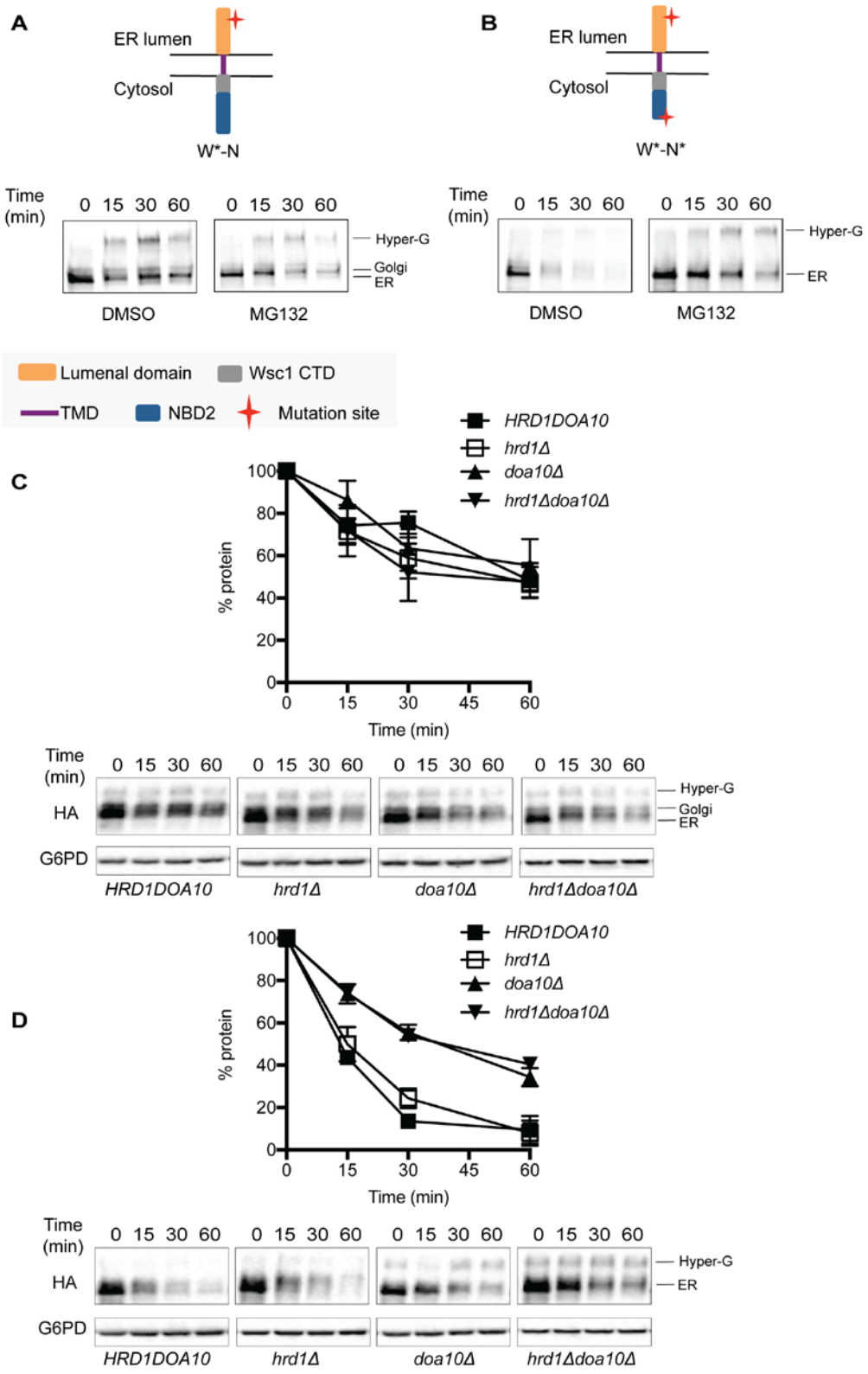

Figure 17 Charactering the ERAD-dependence of the Wsc1*-NBD2 and Wsc1*-NBD2*

Pulse chase analyses of chimeric proteins (A) W*-N and (B) W*-N* in the presence of the proteasomal inhibitor MG132 or the vehicle DMSO. Note the appearance of a Golgi modified species that was significantly more apparent in W*-N (A), and the different rates in the loss of the ER form of W*-N and W*-N* in the presence of MG132. ERAD dependence of (C) W*-N and (D) W*-N* was assayed by cycloheximide chase in wild-type and mutant yeast lacking the ER-resident E3 ligases *HRD1* and/or *DOA10*. Data represent means ±SE of three independent experiments. "Hyper-G" denotes hyperglycosylated species.

It remains elusive how ERAD cooperates with the post-ERQC machinery to safeguard protein homeostasis. One possibility is that ERAD retains and degrades substrates with ill-defined ERAD-specific degrons, which reside in substrates like CPY* and Ste6-166 (Loayza et al., 1998; Wolf and Schafer, 2005), whereas substrates lacking the degron, such as post-ERQC substrates Wsc1* and Pep12 (D) exit the ER for post-ERQC. Another view is that ER-associated chaperones—either lumenal (BiP and lectins) or cytosolic (Ssa1 and Ydj1)—act as gatekeepers for ER retention and ERAD after recognition. Those substrates that simply lack these recognition motifs will instead exit the ER. In fact, we previously reported that mutated forms of bovine pancreatic trypsin inhibitor (BPTI) that lack BiP binding sites escape ERAD and are targeted exclusively for vacuolar degradation (Coughlan et al., 2004). Similarly, the post-ERQC substrate Wsc1*, which is unable to bind BiP, was efficiently degraded in the vacuole. However, when attached to a BiP binding ERAD determinant, the C-terminal domain of CPY*, the chimeric protein was targeted for ERAD (Wang and Ng, 2010).

SZ* contains both an ERAD-C degron (NBD2*) and engages chaperones (Ssa1 and Ydj1), which complicates future attempts to define how this substrate is selected for ERAD.

However, my results indicate that aggregation propensity may be a new feature that dictates how ERAD substrates might be selected. Based on a homology model, NBD2* may be intrinsically aggregation-prone because the truncation site lies between two hydrophobic beta-sheets that are otherwise buried in the full-length domain (Preston et al., 2018). I propose that the exposed hydrophobic patches on NBD2* drive amorphous aggregation upon heat-shock and overexpression. Under those conditions, the ERAD machinery may outcompete the ER exit machinery (i.e., COPII) (Barlowe and Helenius, 2016). In this case, substrates aggregation may on the one hand enhance chaperone engagement, which leads to ER retention and ERAD, but on the other hand, substrate aggregation in the cytosolic domain may obscure the ER exit signal that is already weakly presented, hindering ER exit.

Compared to mammals, yeast possess only smaller COPII vesicles due to the lack of an enlargement mechanism that exists in mammals for large secretory cargo, like procollagen and chylomicrons (Jin et al., 2012). Therefore, SZ*, when aggregated under heat-stress or overexpression conditions, may also be too large to be incorporated into COPII vesicles. However, immunofluorescence imaging of overexpressed SZ* (Figure 15F) showed a diffusive ER pattern without any noticeable punctate, which doesn't seem to support this hypothesis. Instead, enhanced chaperone engagement and/or less efficient ER exit may explain why aggregated SZ* failed to exit the ER. (An alternate mechanism for ER retention is described in the next chapter.) Although the nature of a misfolded region that leads to the designation for one QC pathway over another remains unclear, my data indicate that aggregation propensity may be one such feature. Correlations between ER retention (which leads to the proteasome degradation) and protein aggregation are also supported by previous studies in both mammals and yeast. The relative localization of two aquaporin (AQP)-2 mutants in mammals, T126M (ER), and E258K

(Golgi), correlated with detergent solubility, with T126M being less soluble than E258K (Hirano et al., 2003; Tamarappoo et al., 1999). In yeast, the amino acid permeases (AAPs) require an ER membrane-localized chaperone Shr3 for proper folding and ER export (Kota et al., 2007). In the absence of Shr3, AAPs become aggregated and retained in the ER for efficient clearance by ERAD, which provide additional evidence on the negative correlation between protein aggregation and ER export.

In summary, the work in this chapter demonstrates for the first time that a single-pass membrane protein with an ERAD-C degron can be targeted for degradation by both ERAD and post-ERQC, and adds another substrate to the post-ERQC substrate toolbox (Figure 18). Furthermore, the aggregation state of SZ* determines the trafficking decision. Namely, substrate aggregation dictates degradation by ERAD over post-ERQC. In the future, it will be necessary to identify the machinery that leads to the selection of the substrate for degradation in the vacuole via the MVB pathway, and whether other substrates undergo a similar fate in the secretory pathway.

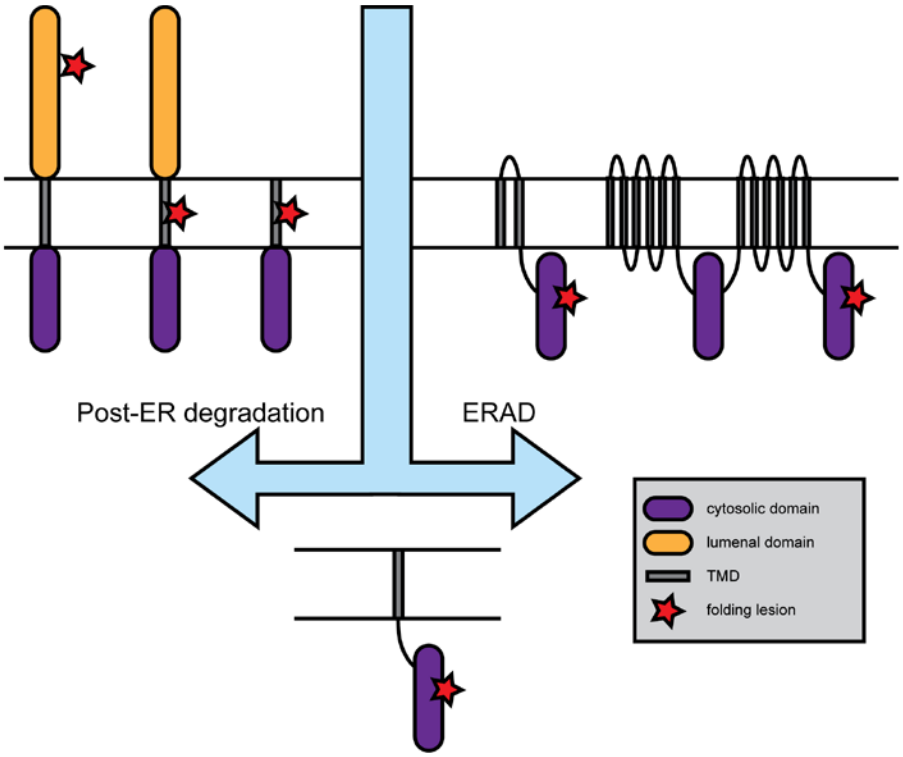

	A	B	C	D	E	F
Proteins	Wsc1*, CFS	Pep12(D)	CPS1, Phm5	SZ*	ChimeraA*	Ste6*
Functional position	PM/ UKN			UKN	UKN	PM
Proteolysis position	vacuole			vacuole/ proteasome	proteasome	
E3 ligase	Rsp5	Tul1		Doa10	Doa10	

Figure 18 Summary of the degradation fate of misfolded membrane proteins

3.0 SUBSTRATE UBIQUITINATION DICTATES THE ER RETENTION OF MISFOLDED PROTEINS

3.1 INTRODUCTION

Secretory or membrane proteins first begin their journey along the secretory pathway at the ER. After newly synthesized proteins reach their native conformation and assemble into multi-subunit complexes with defined stoichiometry, they concentrate in COPII vesicles for ER export (Barlowe and Helenius, 2016). During this process, cargo receptors for lumenal (e.g., Evr29) and membrane (e.g., Sec24) cargos recognize transport-competent proteins and recruit the outer layer Sec13/31 heterotetramer of the COPII coat. Polymerization of the COPII coat proteins forms a cage-like lattice which then drives ER cargo export (Stagg et al., 2006). COPII-mediated anterograde transport is vital for cellular homeostasis and survival as most genes involved in COPII transport are essential, and mutations in those genes have been found to cause human diseases such as Anderson disease, chylomicron retention disorder, and cranio-lenticulo-sutural-dysplasia (Khoriaty et al., 2012).

Due to genetic mutations, environmental stress such as heat shock, oxidative stress, heavy metal stress, and aging, protein misfolding becomes more common (Gidalevitz et al., 2011). Due to genetic mutations, a growing number of human diseases are also attributed to protein misfolding, especially those in the secretory pathway (Guerriero and Brodsky, 2012; Labbadia and Morimoto, 2015; Tao and Conn, 2014). To maintain protein homeostasis, multiple protein QC machineries along the secretory pathway are employed. The first QC checkpoint is ERAD. As described in detail in the previous chapters, ERAD employs the protein-ubiquitin

system to selectively eliminate proteins that are terminally misfolded, thereby preventing misfolded proteins from moving further along the secretory pathway. However, some proteins that are degraded by ERAD can also fold and function when cells are treated with folding "correctors", some of which are now FDA-approved (Rowe and Verkman, 2013). If the ERAD of those proteins is slowed, then the efficiency of these correctors is improved (Chung et al., 2016; Di et al., 2016; Penchala et al., 2013). Therefore, rescuing these proteins from ERAD and facilitating their ER exit can serve as a promising strategy for treatment of some human diseases.

The ability to rescue ERAD substrates is facilitated by the fact that many are poorly retained in the ER, which favors forward trafficking. In yeast, some ERAD-L substrates (such as CPY* and PrA*) exit the ER through COPII vesicle transport and are then retrieved for ER degradation (Caldwell et al., 2001; Taxis et al., 2002; Vashist et al., 2001). Subsequent studies showed that transport-defective CPY* is still efficiently eliminated by ERAD, suggesting that ER exit and ERAD are not sequential steps but competitive process (Kawaguchi et al., 2010; Spear and Ng, 2003). However, the molecular mechanism behind competition is unclear.

In this chapter, I aimed to understand how ERAD competes with the ER export machinery for substrates that display a functional ER exit signal. To this end, SZ*, which was described in the previous chapter, was used as a model. I first discovered that the cytosolic Hsp40, Ydj1, selectively recognizes and retains SZ* in the ER. Specifically, overexpression of Ydj1 leads to enhanced ERAD of SZ*, whereas deletion of *YDJ1* results in more efficient ER export. I then found that deletion of the gene encoding the ERAD-C ubiquitin ligase, Doa10, leads to more efficient ER export both *in vivo* and *in vitro*. This result strongly suggested that substrate ubiquitination may be a hallmark for ER retention and the prevention of ER export. To confirm this hypothesis, I fused SZ* with a four-tandem ubiquitin motif and assayed ER export

both *in vivo* and *in vitro*. As hoped, the ubiquitin-fused SZ* chimera was retained in the ER. Retention was evident even in a *doa10Δ* strain, which otherwise favored export of SZ*. Moreover, I found that Ydj1 was vital for SZ* ubiquitination, consistent with its role as a gatekeeper for a misfolded substrate. Overall, these data provide the first mechanistic evidence that ubiquitin can act as a hallmark for substrate retention in the ER, irrespective of the presence of a functional ER exit signal.

3.2 MATERIALS AND METHODS

Most of the materials and methods that used in this chapter remained the same as described in section 2.2. Therefore, only additional experimental methods that are specific to this chapter are listed.

3.2.1 Yeast growth conditions, strains, and plasmid construction

The *Saccharomyces cerevisiae* strains employed in this chapter are provided in Table 1. Yeast growth conditions and media remained the same as described in section 2.2.1.

To construct SZ*-Ub4, the BamHI restriction site on pSZ03 bearing SZ*-GFP was altered by site-directed mutagenesis (Quick-change site-directed mutagenesis kit, Agilent) using primers OSZ14 and OSZ15 (all primers used in this chapter was listed in Table 3). The SZ*-GFP insert was next PCR amplified using primers OSZ08 and OSZ16, and subcloned into the p416TEF vector at the XbaI/BamHI sites, generating pSZ09 (Mumberg et al., 1995). Next, a gene cassette encoding four ubiquitin moieties with K48, K63 and K29 mutated to R (plasmid

1677, kindly provided from the Ulrich lab, University of Mainz, Germany) was inserted into the C-terminus of SZ*-GFP (pSZ09) at the BamHI/HindIII sites, thus generating pSZ10 (Zhao and Ulrich, 2010).

The Ydj1-HPD mutant (pSZ12) was constructed by site-directed mutagenesis using template BPM390 (kindly provided by the Craig lab, University of Wisconsin) and primers OSZ17 and OSZ18. The DNA sequences of all constructs were confirmed by Genewiz.

3.2.2 Assays to measure protein ubiquitination

To measure the levels of protein ubiquitination in yeast, a 30ml culture of the indicated yeast strains expressing SZ*, SZ*-Ub4 or Wsc1* was grown to an A_{600} of ~1.0 in selective media at 26°C or 37°C (as indicated). Yeast cells were harvested by centrifugation at 3000rpm for 3 min in tabletop centrifuge at room temperature, and then washed with ice-cold buffer 88, and the cell pellets were frozen at -80°C. The cells were then thawed on ice, and resuspended in a microcentrifuge tube with 1ml of a detergent solution containing 20mM HEPES (pH=7.4), 50mM KOAc, 2mM EDTA, 0.1M sorbitol, 1% Triton X-100, 0.2% SDS, and protease inhibitors (1mM PMSF, 0.5μg/ml pepstatin A, and 1μg/ml leupeptin), and supplemented with 10mM N-ethylmaleimide. Next, the yeast cells were disrupted with small glass beads by agitation on a Vortex mixer (1 min for 6 times with 1 min on ice in between each agitation). Unbroken cells, cell debris, and insoluble material was removed using a tabletop centrifuge at 18,000g for 3 min at 4°C. Target proteins were immunoprecipitated overnight at 4°C with 30μl of anti-HA-conjugated beads (Roche Applied Science), and the next day HA beads were pelleted using a tabletop centrifugation for 1min at 700g at 4°C. The beads were then washed three times with the detergent solution, one time with 2M urea in the detergent solution, and one final wash with the

detergent solution. Precipitated proteins were eluted with 25µl TCA sample buffer for 30 min at 37°C, and then resolved on 10% SDS-PAGE followed by western blotting. Poly-ubiquitin was visualized using anti-ubiquitin antibody (P4D1 from Santa Cruz Biotechnology).

3.2.3 Assays to measure protein budding efficiency

An *in vitro* COPII budding assay was performed as previously described (Barlowe et al., 1994). Briefly, five components of the COPII complex, including Sar1, Sec23/24, and Sec13/31 were first purified using plasmid CBB205, yeast CBY1285, and yeast CBY120, respectively based on the protocol described previously (Barlowe et al., 1994). Plasmid CBB205, yeast CBY1285 and CBY120 are kind gifts from Dr. Charles Barlowe (Dartmouth College). The COPII proteins were then added to ER microsomes expressing SZ* from different yeast strains to the final indicated concentrations: microsomes (40µg/ml), Sar1 (5µg/ml), Sec23/24 (5µg/ml), and Sec13/31 (12µg/ml). The reaction was conducted in PCR tubes incubated at 25°C for 20 min in a mini PCR cycler. The budded vesicles were then separated from total ER membranes by centrifugation at 18,000g at 4°C in a tabletop centrifuge. The budded vesicles residing in the supernatant were then pelleted by a second centrifugation at 100,000g for 20 min at 4°C in a Beckman ultracentrifuge. The resulting budded and unbudded fractions were resuspended in 10µl TCA sample buffer and heated at 75°C. Samples were then resolved on 10% SDS-PAGE and immunoblotted for the indicated proteins.

3.3 RESULTS

3.3.1 The cytosolic Hsp40, Ydj1, recognizes and targets SZ* for ERAD

I demonstrated in the previous chapter that SZ*, which contains an ERAD-C degron, partially evades ERAD and becomes a vacuole/lysosome-targeted GQC substrate, and that substrate aggregation changed the balance between SZ* ERAD and post-ERQC (Sun and Brodsky, 2018). However, protein aggregation may not be a common feature of all ERAD-C substrates that are retained in the ER. Here, I sought to identify whether other features of this substrate designate ERAD over post-ERQC. Toward this goal, I first focused on identifying factors that selectively recognize and mediate the ERAD of SZ*.

The ERAD pathway takes place in four steps: substrate recognition, ubiquitination, retrotranslocation, and proteasome degradation (Needham et al., 2019). During the recognition step, ERAD substrates with an exposed signal or folding lesion are captured and bound by molecular chaperones, which then deliver substrates to the ubiquitination machinery (Berner et al., 2018; Christianson and Ye, 2014; Ruggiano et al., 2014). In the previous chapter, the cytosolic Hsp40, Ydj1, was shown to facilitate the ERAD of SZ*. In contrast to a temperature sensitive mutant form of Ydj1, *ydj1-151*, which was used in the previous chapter, a *YDJ1* null mutant was employed to avoid artifacts associated with heat stress-induced aggregation (Sun and Brodsky, 2018). Consistent with data generated in *ydj1-151*, SZ* was also stabilized in a *ydj1Δ* strain (Figure 19A). During the degradation of other ERAD-C substrates, Ydj1 has been shown to play an important role in mediating substrate ubiquitination (Lee et al., 1996; Prasad et al., 2018). To test whether Ydj1 was also required for SZ* ubiquitination, the protein was immunoprecipitated under denaturing conditions in wild-type and *ydj1Δ* yeast. I found that SZ*

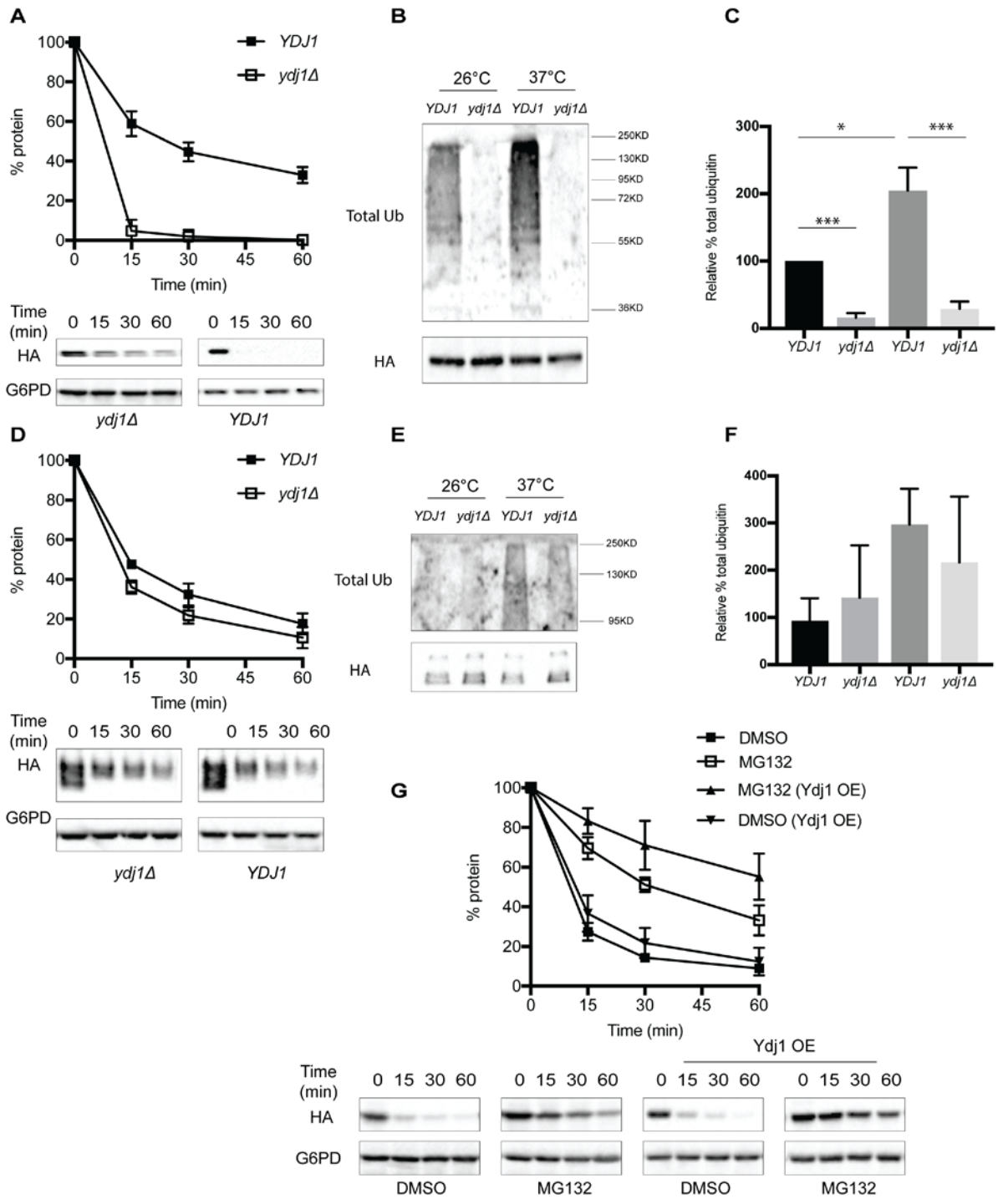

Figure 19 The cytosolic Hsp40, Ydj1, mediates the ubiquitination of SZ* and targets it for ERAD

(A) The stability of SZ* in wild-type and *ydj1Δ* mutant was determined by a cycloheximide chase assay at 26°C. (B) SZ* ubiquitination was detected in wild-type and *ydj1Δ* yeast grown at 26°C to the log phase and then shifted to 37°C or 26°C for 30 min. Cells were lysed and SZ* was immunoprecipitated using anti-HA-conjugated agarose beads. Total ubiquitin and SZ* were detected using anti-ubiquitin antibody (P4D1 from Santa Cruz Biotechnology) and HA antibody (Roche), respectively. (C) Quantification of the data shown in part (B). (D) The stability of a post-ERQC substrate, Wsc1*, in wild-type and *ydj1Δ* was determined by a cycloheximide chase assay in cells grown at 26°C. (E) The ubiquitination of Wsc1* was detected as described in (B). (F) Quantification of the data shown in part (E). (G) Proteasome dependent degradation was measured by cycloheximide chase assay in *pdr5Δ* yeast containing either a vector control or a vector engineered for the expression of Ydj1 (Ydj1OE). Cells were incubated at 26°C and 100μM MG132 or DMSO was added for 30 min before cycloheximide addition. Data represent the means ± SE of three independent experiments; * $p<0.05$, ** $P<0.005$, *** $P<0.0005$.

was poly-ubiquitinated in the wild-type strain, whereas the ubiquitination on SZ* was essentially abolished upon *YDJ1* deletion in cells grown at 26°C (Figure 19B). Furthermore, enhanced ERAD targeting of SZ* after cells were shifted to 37°C (Figure 13C) correlated with a higher level of SZ* ubiquitination, which was also dependent on Ydj1. As a control for these studies, I tested whether a post-ERQC substrate, Wsc1*, was also subject to Ydj1-mediated ubiquitination and degradation. In contrast to data with SZ*, Ydj1 was dispensable for Wsc1* ubiquitination or degradation (Figure 19D and 19E). Based on these results, I next reasoned that overexpression of Ydj1 may increase SZ* ERAD. As hypothesized, the degree of SZ* stabilization in the presence of the proteasome inhibitor MG132 was even higher after Ydj1 overexpression, consistent with Ydj1-mediated targeting of SZ* ERAD (Figure 19G). These data indicate that Ydj1 is required for SZ* ubiquitination and subsequent ERAD.

3.3.2 Loss of Ydj1 facilitates the ER export of SZ*

Because SZ* can also be targeted for post-ERQC (Sun and Brodsky, 2018), I next tested if the loss of Ydj1 affected ER exit. The ER export of SZ* can be monitored by the generation of a free, stable GFP moiety that results from vacuolar delivery of SZ*-GFP. As shown in Figure 20A, loss of *YDJ1* resulted in a higher level of the cleaved GFP moiety, indicating that the population that exited the ER and was sorted into the vacuole rose when this chaperone was absent. To determine whether only Ydj1 affected SZ* degradation and trafficking, I tested another ER-associated Hsp40, Hlj1, which is dispensable for SZ* ERAD. Consistent with the lack of an effect of Hlj1 on the ERAD of SZ*, Hlj1 had no effect on SZ* trafficking, as indicated by the similar amount of cleaved GFP in *hlj1Δ* and wild-type strains (Figure 20A). Because Ydj1 recruits Rsp5 through a PPXY motif to clear heat stress damaged proteins (Fang et al., 2014). I examined if the PPXY motif in Ydj1 is required to retain SZ* in the ER, even though these studies were conducted at 26°C. Therefore, Ydj1*, with a PPXY motif mutated to GGXY, was then introduced into the *ydj1Δ* strain (Fang et al., 2014). Similar to what was found in the wild-type strain, GFP cleavage was low, so the PPXY motif is dispensable for Ydj1 function during ER retention (Figure 20B). To determine if Ydj1 acts as an ERAD gatekeeper, GFP cleavage of SZ* was tested upon Ydj1 overexpression. In line with the cycloheximide chase data (Figure 19G), Ydj1 overexpression enhanced SZ* ER retention as shown by less GFP cleavage compared to wild-type yeast (Figure 20C).

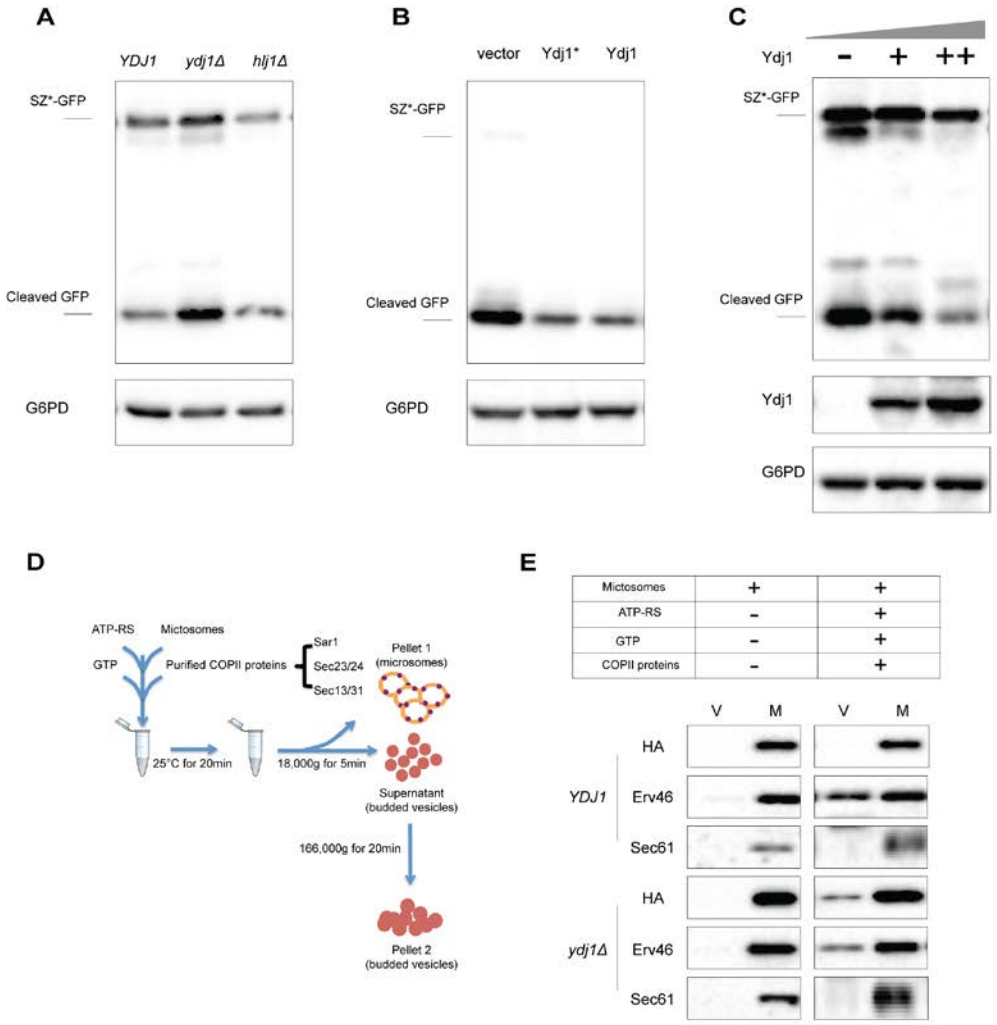

Figure 20 Loss of Ydj1 facilitates the ER exit of SZ*

(A) GFP cleavage from SZ*-GFP was assayed in a yeast strain lacking Ydj1 or another ER-associated Hsp40 and Hlj1. Cells expressing SZ*-GFP were grown to log phase at 22°C and 1OD of cells were collected and proteins were precipitated to detect both the full-length SZ* and cleaved GFP. (B) GFP cleavage from SZ*-GFP was assayed in yeast deleted for *YDJ1* but that contained a vector control, or vectors engineered for the expression of Ydj1 or Ydj1*, which contained a mutation in the PPXY motif in the C-terminal tail. (C) Decreased levels of GFP cleavage from SZ*-GFP are evident in yeast expressing elevated level of Ydj1. Cells expressing SZ*-GFP but deleted for (-), expressing normal levels (+), or expressing elevated levels (++) of Ydj1 were grown to log phase at 26°C and 1OD of cells were collected

and proteins were precipitated to detect both the full-length SZ* and cleaved GFP. (D) A schematic of the *in vitro* ER exit/budding assay, which was used to measure COPII-mediated export of SZ* from the ER. (E) An *in vitro* COPII budding assay was performed with microsomes prepared from wild-type and *ydj1Δ* yeast expressing SZ*. In the experimental group, microsomes, enriched COPII proteins, GTP and an ATP-regenerating system (ATP-RS) were incubated in buffer for 25 min at 25°C. The control experiment was conducted in the absence of COPII proteins and energy. Unbudded membranes (M) reside in the pellet after centrifugation at 18,000. The budded vesicles (V) in the supernatant were collected after ultracentrifugation. Data are representative of three independent experiments.

To confirm the hypothesis that Ydj1 helps retain SZ* in the ER, I next conducted an *in vitro* budding assay using purified COPII components and ER-enriched microsomes from *YDJ1* and *ydj1Δ* yeast expressing SZ*-GFP (Figure 20D). Briefly, microsomes were prepared as described in the previous chapter, and the purified COPII components, including Sar1, Sec23/24, and Sec13/31, were isolated as published (Barlowe et al., 1994). These reagents were then mixed in the presence or absence of ATP/GTP or in the presence or absence of COPII (Figure 20E). In this assay, proteins that exit the ER in COPII vesicles will reside in the budded vesicles, which are separated from unbudded ER membranes by centrifugation. In line with the GFP cleavage experiment in Figure 19, loss of Ydj1 promoted ER export of SZ. Of note, because the *in vitro* budding efficiency is low, the amount of exported SZ* is barely detectable in the wild-type background (Barlowe et al., 1994). These data suggest that other auxiliary factors that may be excluded in the *in vitro* system support ER export of SZ*. Regardless, both my *in vivo* and *in vitro* data indicate that Ydj1 helps retain an ERAD substrate in the ER.

3.3.3 Defects in SZ* ubiquitination facilitate ER exit

As an Hsp40 co-chaperone for Hsp70 and other chaperones, Ydj1 plays two roles during ERAD: maintaining substrate solubility and mediating substrate ubiquitination (Lee et al., 1996; Nishikawa et al., 2005; Prasad et al., 2018). Because SZ* is aggregation-prone, particularly at elevated temperatures, I measured SZ* solubility in DDM in the presence or absence of Ydj1 (Sun and Brodsky, 2018). As shown in Figure 21A, SZ* became less soluble in detergent-treated lysates from *ydj1Δ* cells. Because substrate aggregation can favor the selection of membrane proteins for ERAD, the loss of the Ydj1 could instead favor—not prevent (via facilitated ER exit)—ERAD (Preston et al., 2018; Sun and Brodsky, 2018). These dual functions of Ydj1 during ERAD seem contradictory. To better explore how Ydj1 retains SZ* in the ER, and supports substrate ubiquitination and degradation, I explored whether Hsp70 interaction was required for these functions. The HPD motif on Ydj1 is required to activate the ATPase activity of Hsp70, which together are required to prevent substrate aggregation (Mayer and Bukau, 2005; Nishikawa et al., 2005; Tsai and Douglas, 1996). Therefore, I tested whether mutating the HPD motif would block substrate ubiquitination, which may phenocopy the loss of Ydj1 during ERAD. To this end, I first measured the stability of SZ* in a *ydj1Δ* strain containing either a vector, wild-type Ydj1, or the Ydj1-HPD mutant, respectively. As shown in Figure 21B, cells expressing the HPD mutant stabilized SZ* to a similar extent as those containing the vector control, suggesting that the HPD motif—and by definition, Hsp70 (Ssa1) interaction—is required to efficiently degrade SZ*. As expected, cells expressing the Ydj1-HPD mutant also exhibited compromised SZ* ubiquitination, which was similar to the effects observed in Ydj1 null mutants (Figure 21C and 21D). Moreover, in line with evidence presented above, ER export of SZ* was more efficient in the Ydj1-HPD mutant than in wild-type cells, as evidenced by

increased GFP cleavage (Figure 21E). Therefore, cells expressing the Ydj1-HPD mutant protein, which is defective for substrate ubiquitination, also display increased ER exit of SZ*, similar to the Ydj1 null mutant. Next, the DDM solubility of SZ* was measured in cells expressing the Ydj1-HPD mutant. The solubility of SZ* was also decreased in this strain to a similar extent as in the Ydj1 null mutant. These results suggest that Ydj1 maintenance of substrate solubility and substrate ubiquitination are coupled, as shown for the effects of other chaperone during ERAD (Nishikawa et al., 2001).

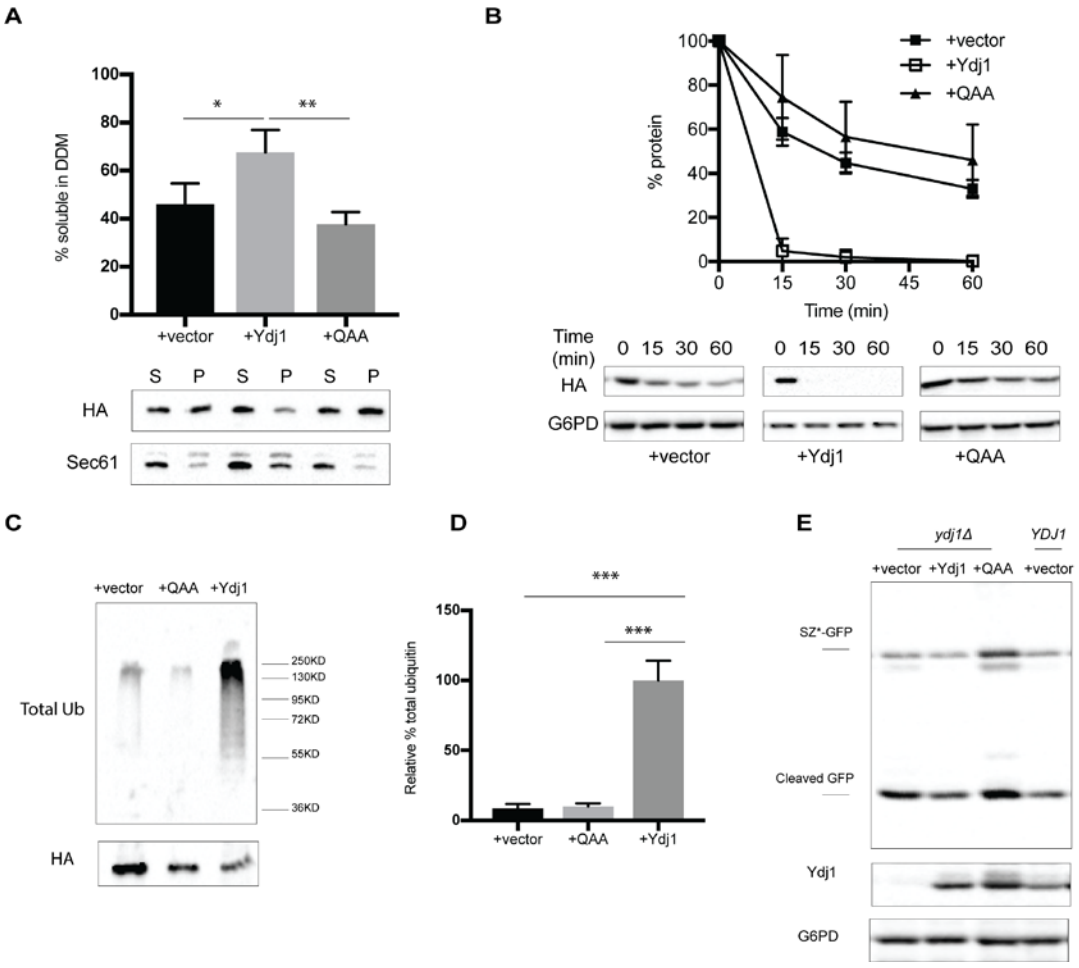

Figure 21 Defects in SZ*ubiquitination by mutating HPD motif of Ydj1 facilitate ER exit

(A) Microsomes from *ydj1Δ* expressing SZ* and containing a vector or expressing Ydj1 or the QAA (HPD) mutant were treated with 1% dodecyl maltoside (DDM). Protein residing in the supernatant (S) and pellet (P) fractions was analyzed after centrifugation at 18,000g for 30 min. (B) The stability of SZ* was determined by cycloheximide chase assay in *ydj1Δ* yeast containing a vector control (+vector) or a vector engineered for the expression of wild-type Ydj1 (+Ydj1) or the Ydj1-HPD mutant (+QAA). (C) SZ* ubiquitination was detected in *ydj1Δ* yeast containing a vector control (+vector) or a vector engineered for the expression of wild-type Ydj1 (+Ydj1) or the Ydj1-HPD mutant (+QAA). Cells were grown at 26°C to log phase and lysed, and SZ* was immunoprecipitated using anti-HA-conjugated agarose beads. Total ubiquitin and SZ* were detected using anti-ubiquitin antibody (P4D1 from Santa Cruz Biotechnology) and HA antibody (Roche), respectively. (D) Quantification of (C). (E) GFP cleavage from SZ*-GFP was assayed in *ydj1Δ* yeast containing a vector control (+vector) or a vector engineered for the expression of wild-type Ydj1 (+Ydj1) or the Ydj1-HPD mutant (+QAA). As a control, GFP cleavage from SZ*-GFP was also tested in wild-type yeast containing a vector. Data represents means ± SE of three independent experiments; * $p<0.05$, ** $P<0.005$, *** $P<0.0005$.

3.3.4 Defects in SZ* ubiquitination by deletion of an E3 ligase also promote ER export

Based on the data presented above, I propose that ER retention of SZ* is determined either by substrate ubiquitination alone, which is facilitated by Ydj1, or by the maintenance of solubility and ubiquitination. To distinguish between these two possibilities, I next focused on the action of the ubiquitination ligase, Doa10, which functions downstream of Ydj1 during SZ* ERAD.

Doa10 was shown in the previous chapter to facilitate SZ* degradation (Figure 6B). To directly measure if Doa10 is required for substrate ubiquitination, I measured SZ* ubiquitination in the presence and absence of Doa10. In this experiment, SZ* was expressed in both wild-type and *doa10Δ* yeast at 26°C. After cell lysis, SZ* was immunoprecipitated under denaturing conditions, and the ubiquitination of SZ* was detected by western blot (Figure 22A and 22B). As predicted, ubiquitination of SZ* was reduced in the *doa10Δ* strain. Therefore, by examining the ER exit and solubility of SZ* in the presence or absence of Doa10, one could establish if ubiquitination is required for ER retention. I measured the cleavage and stability of GFP from SZ*-GFP in the *DOA10* and *doa10Δ* strains. As shown in Figure 22C, higher levels of cleaved GFP accumulated in the *doa10Δ* strain, indicating that more SZ* exited the ER. In parallel, cleaved GFP accumulated in the vacuole (indicating the population of SZ* that had exited the ER), as suggested by immunofluorescence microscopy (Figure 22D and 22E). Consistent with GFP cleavage data, imaging quantification showed higher level of vacuolar GFP signal in both *doa10Δ* and *ydj1Δ* yeast compared to the wild-type strain. Next, to measure the kinetics of GFP cleavage, I performed a pulse-chase assay. As shown in Figure 22F, cleaved GFP was generated at a much higher rate in the *doa10Δ* strain within the 60 min chase period. These data demonstrate that the loss of the E3 ligase, Doa10, also promotes ER export of SZ*.

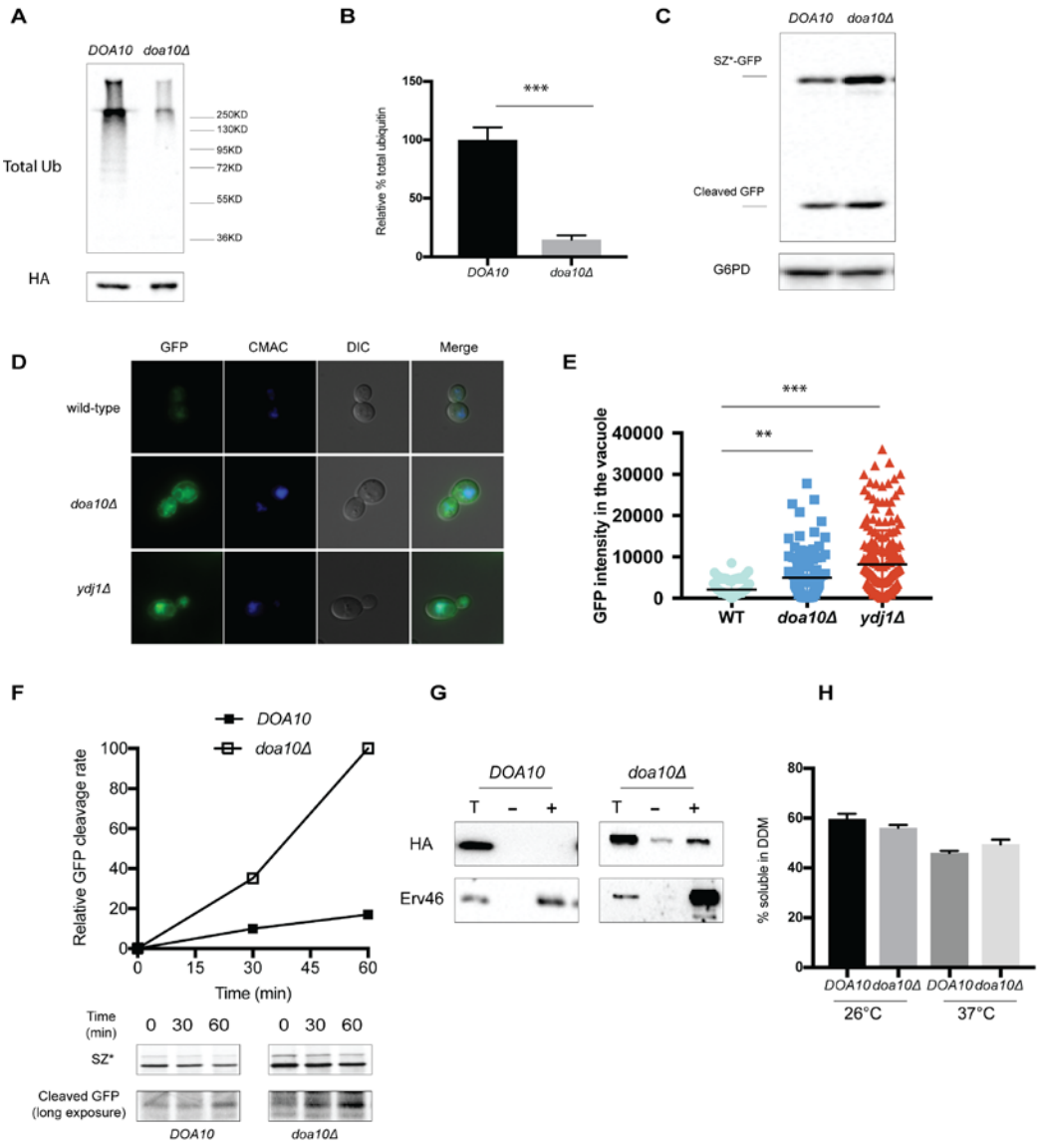

Figure 22 Decreased ubiquitination of SZ* by deleting *DOA10* facilitate ER exit

(A) Wild-type and *doa10Δ* cells expressing SZ* were grown at 26°C to log phase, the ubiquitination of SZ* was detected after cell lysis by denaturing immunoprecipitation.. (B) Quantification of (A). (C) GFP cleavage from SZ*-GFP was assayed in wild-type and *doa10Δ* yeast as described in Figure 20. (D) Wild-type, *doa10Δ*, and *ydj1Δ* yeast expressing SZ*-GFP were examined by fluorescent microscopy. Both the full length species and the cleaved GFP are shown; CMAC staining marks the vacuole and DIC is shown. (E) Quantification of GFP intensity in the vacuole in part (D) was determined from >100 cells in each

strain; Statistical significance was determined with a one-way ANOVA and Dunn's multiple comparison tests. ** $p<0.005$, *** $p<0.0005$. (F) The GFP cleavage rate of SZ*-GFP was measured in a pulse chase assay in wild-type and *doa10Δ* yeast. The cleavage rate was determined by normalizing cleaved GFP to full-length SZ*-GFP at 0 min, and the relative GFP cleavage rate in *doa10Δ* yeast at 60 min was standardized to 100%. (G) An *in vitro* budding assay was performed with microsomes prepared from wild-type and *doa10Δ* yeast expressing SZ*. T: 10% total protein; -: budded proteins in a reaction without COPII proteins; +: budded proteins in a reaction with COPII proteins. (H) Microsomes from wild-type and *doa10Δ* expressing SZ* were incubated at 26°C or 37°C for 30 min, and treated with 1% dodecyl maltoside (DDM) for 30 min on ice. Protein residing in the supernatant (S) and pellet (P) fractions was analyzed after centrifugation at 18,000g for 30 min. Data represents means ± SE of three independent experiments.

To confirm this result, I next performed an *in vitro* budding assay to directly measure the efficiency of SZ* ER export. Consistent with the *in vivo* data shown above, deleting *DOA10* resulted in a higher SZ* budding efficiency when microsomes from wild-type and *doa10* cells were examined (Figure 22G). Finally, to assess if substrate aggregation also contributed to ER retention, the DDM solubility of SZ* was tested in lysates prepared form these strain backgrounds. As shown in Figure 22H, DDM solubility was unchanged, regardless of whether Doa10 was present. Therefore, the loss of Doa10 has no effect on SZ* solubility yet still affects ER retention. Overall, these data demonstrated that ubiquitination, but not necessarily aggregation, can act as a hallmark for ER retention.

3.3.5 The addition of four tandem ubiquitins prevents SZ* exit from the ER

To confirm my hypothesis that ubiquitin is sufficient to retain an ERAD substrate in the ER, I surmised that attachment of a poly-ubiquitin tag to SZ* will be sufficient to prevent ER export. To this end, I first constructed a chimeric substrate, SZ*-Ub4, with four tandem ubiquitins attached to the C-terminus of SZ*-GFP (Figure 23A). In these constructs, the K48 and K63 positions in the appended ubiquitin moieties were mutated to R to minimize the formation of a poly-ubiquitin chain on the ubiquitin tag. Furthermore, these four ubiquitins were constructed in a head-to-tail fashion, which lead to poor targeting of a cytosolic protein to the ubiquitin-proteasome pathway (Zhao and Ulrich, 2010).

I first tested if attachment of four ubiquitins changed the degradation pathway. Similar to SZ*, SZ*-Ub4 was also sorted into the vacuole for degradation through the MVB pathway (Figure 23B; note the cleaved GFP signal, top panel in wild-type and *vps36Δ* yeast). Moreover, the amount of cleaved GFP from SZ*-Ub4 was much lower than the amount of cleaved GFP form SZ*-GFP (compare lane 1 and 5). These results strongly suggest that the ubiquitin motif prevents ER exit. Since the ubiquitin motif was attached to the C-terminus of GFP, the epitope in GFP in the full-length protein (but not the cleaved GFP) was obscured by ubiquitin, as the full-length band signal enhanced by boiling the nitrocellulose membrane (data not shown). To confirm these results, cells expressing SZ*-Ub4 were examined by fluorescence microscopy. Consistent with measurements of GFP cleavage by immunoblot (Figure 23B), imaging data showed decreased vacuolar GFP intensity (i.e., the population that exited the ER) of SZ*-Ub4 compared to SZ*-GFP (Figure 23C and 23D). The level of GFP cleavage from SZ*-Ub4 also remained similar regardless whether Doa10 was present (Figure 23B and 23D). To confirm that the presence of a poly-ubiquitin motif was sufficient to prevent ER exit, I then performed an *in*

vitro budding assay to test the efficiency of SZ*-Ub4 exit from the ER. In contrast to the efficient budding of SZ*-GFP in the microsomes prepared from the *doa10Δ* strain, SZ*-Ub4 failed to exit the ER, even in the absence of Doa10 (Figure 23E) (compare lane 6 and 12). These data demonstrate both *in vivo* and *in vitro* that a four-tandem ubiquitin motif prevents ER export of a misfolded protein that is targeted for both ERAD and post-ERQC.

A K11 poly-ubiquitin linkage was found to be enriched in ERAD substrates (Locke et al., 2014). Because K11 is still present in the four-tandem ubiquitin tag—and therefore could have acquired a poly-ubiquitin linkage—I next tested if the tag induces poly-ubiquitination on SZ*-Ub4. However, poly-ubiquitination could not be detected on SZ*-Ub4 in either *DOA10* or *doa10Δ* cells (Figure 23F). In contrast, SZ*-GFP was poly-ubiquitinated in *DOA10* cells, as anticipated (Figure 23G). These data preclude the possibility that the four-tandem ubiquitin conjugated species had become poly-ubiquitinated, thus obscuring the ER exit signal on SZ*.

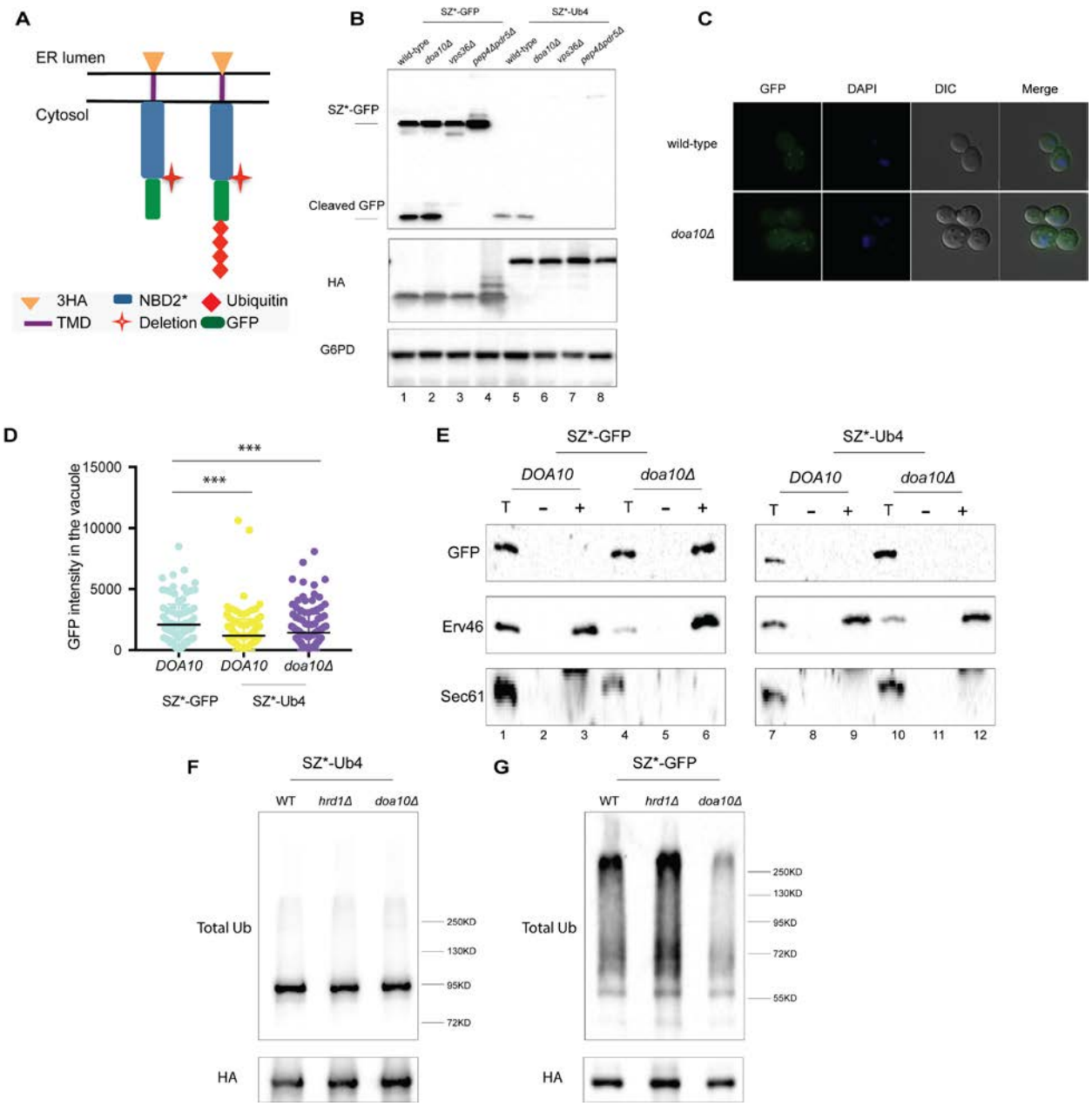

Figure 23 Four tandem ubiquitin prevent SZ* from entering COPII vesicles

(A) Predicted topology of GFP-tagged SZ* and SZ*-Ub4. (B) GFP cleavage of SZ*-GFP and SZ*-Ub4 in the wild-type and indicated mutant strains was determined when cell lysates were examined with anti-GFP (to detect the cleaved GFP) and anti-HA (to detect the full length species) by immunoblotting. (C) Wild-type and *doa10Δ* yeast expressing SZ*-Ub4 were examined by fluorescent microscopy. Both the full length species and the cleaved GFP are shown; CMAC staining marks the vacuole and DIC is shown.

(D) Quantification of GFP intensity in the vacuole in part (C). More than 100 cells in each strain were counted; Statistical significance was determined with a one-way ANOVA and Dunn's multiple comparison tests. *** $p<0.0005$. (E) *In vitro* budding efficiency was measured in a budding assay using microsomes prepared from wild-type and *doa10Δ* cells expressing SZ*-GFP or SZ*-Ub4. T: 10% total protein; -: budded proteins in a reaction without COPII proteins; +: budded proteins in a reaction with COPII proteins. (F) The ubiquitination of SZ*-Ub4 was detected in cell lysates after by denaturing immunoprecipitation in wild-type, *hrd1Δ* and *doa10Δ* yeast. (G) The ubiquitination of SZ*-GFP was similarly detected as in (F) in wild-type, *hrd1Δ* and *doa10Δ* cells.

3.4 DISCUSSION

Most proteins transported to post-ER compartments are concentrated in COPII vesicles by interacting with cargo receptors, such as members of the Erv complex and Sec24 family members (Gomez-Navarro and Miller, 2016). In order to be recognized by COPII cargo receptors, many transport competent proteins have to present an ER exit signal. In many cases, the presentation of a functional ER exit signal seems to be tightly coupled with protein folding, as misfolded proteins are mostly excluded from COPII vesicles and retained in the ER for proteasome degradation (Ma et al., 2017). However, this view has been challenged by a growing number of misfolded proteins that exit the ER through COPII-mediated anterograde trafficking and are targeted either for vacuolar degradation or for proteasome degradation after retrieval from later compartments. Nevertheless, other misfolded proteins may still present an ER exit signal, but due to the robust nature of the ERAD pathway, these substrates are prevented from leaving the ER. In this chapter, I sought to understand how a misfolded protein, SZ*, that

contains both an ERAD-C degron as well as an ER exit signal, can be retained in the ER and destroyed by the ERAD pathway.

My earlier work established that the aggregation of SZ* contributed to ER retention and directed the substrate to the ERAD pathway versus ER exit (Sun and Brodsky, 2018). However, aggregation is most likely not a common feature for ER retention, indicating that ERAD employs other mechanisms to compete with the COPII machinery to retain substrates. To this end, I first examined which step in the ERAD pathway regulates ER export. During this effort, factors required for substrate recognition and ubiquitination were tested.

Ydj1 is a type I Hsp40 that regulates the function of Hsp70 (Kampinga and Craig, 2010). It directly captures its substrate and delivers them to Hsp70 for refolding or ubiquitination (Cyr et al., 1992; Kampinga and Craig, 2010; Lu and Cyr, 1998; Nakatsukasa et al., 2008). I first inhibited the substrate recognition step of SZ* ERAD by deleting *YDJ1*. Surprisingly, SZ* was more efficiently routed for vacuolar degradation upon *YDJ1* deletion. This provided the first evidence suggesting that loss of Ydj1 promotes ER export of an ERAD substrate. With the robust ER exit of SZ* *in vivo* as shown by the cycloheximide chase data and imaging data, an efficient *in vitro* budding efficiency was expected. However, the *in vitro* budding of SZ* in wild-type yeast could not be detected compared to the positive control Erv46. As shown in chapter 2 and chapter 3, SZ* is subject to both ERAD and COPII-mediated ER export, which together determines the fate of SZ*: ERAD versus post-ER degradation. However, the *in vitro* budding assay contains only the minimum components required for less efficient COPII budding but all the ER retention factors in the microsomes, thereby shifting the competition more for ER retention. Even for ERAD-L substrate, CPY*, which undergoes constant ER export before ERAD, the *in vitro* budding efficiency is as low as 1% (Vashist et al., 2001). Considering the

difference between ERAD-C and ERAD-L branches and the competition between ERAD and ER export of SZ*, the undetectable ER budding *in vitro* is not surprising.

Thus far, Ydj1 has only been shown to slow the degradation of ER-retained misfolded proteins (Guerriero et al., 2017; Huyer et al., 2004b; Sun and Brodsky, 2018; Youker et al., 2004). As might be expected, the loss of Ydj1 also decreased SZ* detergent solubility, which at first might seem to contradict the fact that the loss of Ydj facilitates its ER export. However, it is worth mentioning that substrate aggregation induced by either heat-stress or overexpression, as described in the previous chapter, has no effect on substrate ubiquitination. Also, substrate aggregation induced by the deletion of *YDJ1* may be less severe than that induced by heat-stress or overexpression. More pertinent, however, the loss of Ydj1 obviated substrate ubiquitination.

To more definitively parse the contributions of aggregation and ubiquitination, I next focused on the ERAD-C-specific E3 ubiquitin ligase, Doa10. Deletion of *DOA10* enhanced ER export of SZ*. This observation is reminiscent of a previous study reporting that inactivation of ERAD by deleting ERAD-L E3 ligase, Hrd1, promoted ER exit of an ERAD-L substrate, CPY* (Kincaid and Cooper, 2007). Most importantly, the detergent solubility of SZ* remains unchanged regardless of whether Doa10 was present. This experiment allowed me to uncouple the dual effects caused by *YDJ1* knockout: increased substrate insolubility and decreased substrate ubiquitination. Therefore, inhibiting substrate ubiquitination by either directly deleting the E3 ligase or indirectly via the loss of a chaperone promotes ER export of ERAD substrate. Together, poly-ubiquitin can act as a hallmark for ER retention. To definitively support this conclusion, SZ* was fused to four-tandem ubiquitin tag at its C-terminus. A four-tandem ubiquitin motif was previously shown to be sufficient for targeting cytosolic proteins for proteasome degradation, albeit with a poor efficiency (Zhao and Ulrich, 2010). With its head-to-

tail conformation, which resembles the K63 ubiquitin linkage (Komander et al., 2009), the four tandem ubiquitin fusion may not target SZ* for efficient ERAD since K63 is not a favorable ERAD signal (Grice and Nathan, 2016; Locke et al., 2014). However, this provides an advantage as this motif confers ER retention but inefficient degradation (Zhao and Ulrich, 2010). As predicted, SZ*-Ub4 was retained in the ER and less was directed to the vacuole compared to SZ*-GFP. Also, SZ*-GFP was more stable when fused to Ub4. Of note, SZ*-Ub4 forms puncta in the ER, which is reminiscent of the pattern seen when other misfolded proteins formed ER-associated compartments (ERACs) (Huyer et al., 2004a; Kakoi et al., 2013). One of these substrates is CFTR, which when expressed in yeast forms ERACs that co-localize with COPII components, including Sar1, Sec13 and Sec23. Considering that SZ*-GFP can enter COPII for ER export, it is very likely that the puncta formed by SZ*-Ub4 resulted from ERAC formation. In the future, this can be studied by co-localization experiments with SZ*-Ub4 and COPII components.

To better accommodate the rate-limiting step of retrotranslocation, ERAD needs to efficiently and rapidly recognize and ubiquitinate substrates, which once ubiquitinated are then retained in the ER and retrotranslocated. The mechanism of ER retention of ubiquitinated substrates may result from both active retention by multiple ubiquitin-binding proteins in the ER, such as the Cdc48 cofactors Ufd1 and Npl4, or by passive retention by excluding poly-ubiquitinated substrates that either have their ER exit signals obscured by poly-ubiquitination or are simply too large to enter the COPII vesicles. The identification of putative ER-retention ubiquitin-binding factors in the ER will also be investigated in the near future.

In summary, by inhibiting a pre-ubiquitination step in the ERAD pathway, i.e., substrate recognition or ubiquitination, I demonstrated that substrate ubiquitination can dictate ER

retention. Furthermore, I identified the ER-associated Hsp40, Ydj1, as a gatekeeper for ERAD substrates as its deletion allows a misfolded protein to escape the ER and its overexpression enhanced ERAD. I also provide the first evidence that a four tandem-ubiquitin motif is sufficient to retain a substrate in the ER despite the presence of a functional ER exit signal.

4.0 CONCLUSIONS AND FUTURE DIRECTIONS

In this chapter, I will summarize my work and describe how they advance the scientific understanding of ERAD in terms of substrate selection. Both short-term and long-term experiments are proposed to provide some intellectual insights to future directions.

4.1 CONCLUSIONS

My project began with a simple question: why do some misfolded proteins exit the ER before being degraded while others are statically retained in the ER? To address this question, I set out to understand the features in a misfolded substrate that dictates its fate for ERAD versus post-ER degradation.

The scrutiny of misfolded proteins that exit the ER before degradation revealed that these substrates bear folding lesions in either the lumenal domain or in the transmembrane domain. Therefore, I first sought to investigate if a substrate with a ERAD-C degron has the potential to be exported from the ER. Before my study, no known substrates bearing cytosolic folding lesions were shown to leave the ER. I thus designed a novel substrate, SZ*, that stems from a post-ERQC substrate, Wsc1*, but with its wild-type cytosolic domain replaced with a canonical cytosolic degron (NBD2*) (Wang and Ng, 2010). To simplify the substrate and minimize the potential for ER retention mediated by ERAD-L factors, the lumenal domain of Wsc1* was also replaced with a triple-HA tag, which allowed for protein detection. As predicted, the cytosolic degron, NBD2*, drove SZ* to the conventional ERAD-C pathway, which requires Hsp40

(Ydj1), Hsp70 (Ssa1), an E3 ligase (Doa10), Cdc48, which extracts proteins from the ER, and the proteasome (Sun and Brodsky, 2018). Surprisingly, inhibiting ERAD by inactivating these factors only partially stabilized SZ*, with more than half still being degraded. This indicated the involvement of another degradation pathway during clearance of SZ*: transport to the vacuole. Given the multiple routes that direct proteins from the ER to the vacuole, I first tested if ER-phagy is responsible for sorting SZ* to the vacuole. By testing the degradation of SZ* in multiple mutants defective in autophagy, the ER-phagy pathway was ruled out as none of those mutants stabilized SZ*. These results suggested that SZ* was degraded in the vacuole via the post-ERQC pathway. Dissection of the post-ER degradation requirements for SZ* demonstrated that SZ* advances to the Golgi through COPII-mediated forward trafficking and is then directly sorted to the vacuole by way of the MVB pathway.

To date, most substrates are exclusively eliminated by only one PQC machinery. Vacuole/lysosome -targeted GQC substrates such as Wsc1* and Pep12(D) lack an ERAD determinant, which makes them ERAD resistant. In contrast, most canonical ERAD substrates, due to a dominant ERAD signal that overrides an ER exit signal if otherwise exposed, are efficiently degraded by ERAD under normal conditions (Spear and Ng, 2003; Wolf and Schafer, 2005). SZ* thus serves as the first substrate that can be selected for degradation by both the ERAD and post-ERQC pathways, which also provided a powerful tool for studying the competition between ERAD and post-ERQC. In addition, my data demonstrated that substrates with cytosolic folding lesions still have the potential for ER export, which argues against the idea that ERAD-C substrates are all retained in the ER (Vashist et al., 2001).

Protein aggregation has been implicated as the cause for multiple human diseases, such as Huntington’s disease, Alzheimer’s disease, and Parkinson’s disease (Aguzzi and O'Connor,

2010; Ross and Poirier, 2004; Valastyan and Lindquist, 2014). Hydrophobic motifs that may lead to protein aggregation if improperly positioned were previously shown to be an ERAD signal for a cytosolic protein, serum- and glucocorticoid-induced kinase 1 (Sgk1) (Arteaga et al., 2006). It is worth mentioning that Sgk1 associates tightly with ER membrane so that it employs the ERAD machinery for its degradation. Deletion or reduction of hydrophobicity redistributed Sgk1 to the nucleus and cytosol. These studies indicated that protein aggregation may acts as an ERAD targeting signal. To test this hypothesis, I applied a variety of stressors to yeast cells expressing SZ*, and its ERAD dependence was assayed. Based on those data, I demonstrated that protein aggregation induced by heat-stress enhanced ERAD targeting of SZ*. Next, I sought to induce the aggregation of SZ* without a temperature shift. The homology model of the degron in NBD2* suggested that this truncation makes the domain aggregation prone (Preston et al., 2018). Therefore, I overexpressed SZ* to drive aggregation. As expected, SZ* became less soluble in detergent when overexpressed, thereby increasing ERAD targeting. Together with the data described above, I was able to demonstrate that substrate aggregation dictates the fate of SZ* for ERAD over post-ER degradation (Sun and Brodsky, 2018). Meanwhile, a similar construct, ChiA*, which bears two transmembrane segment but with the same cytosolic degron, NBD2*, was constructed by Dr. Chris Guerriero (Guerriero et al., 2017). Although ChiA* was targeted exclusively for ERAD, results with multiple truncation variants of ChiA* revealed a positive correlation between ERAD degradation rate and substrate aggregation propensity, suggesting that ERAD favors aggregation prone substrates (Preston et al., 2018).

My conclusions could be explained by the following mechanisms: (1) Substrate aggregation may induce rapid ERAD of SZ* by more efficient recognition by the ERAD machinery, and degradation occurred so rapidly there was no time for ER export; (2) Substrate

aggregation may obscure the ER exit signal, which makes this poorly exported substrate an even lower efficient post-ERQC substrate; (3) Substrate aggregation may make the protein physically too large to enter COPII vesicles. In line with my conclusion, our lab recently reported that protein aggregation can direct a substrate for the ERAD pathway. In this parallel study, detergent insolubility of a series of ERAD substrates appeared to be negatively correlated with protein half-life (Preston et al., 2018). Therefore, my data provided the first evidence showing that substrate aggregation may assist ERAD to win the battle against post-ERQC.

My next question was, "how might ERAD substrates be rescued for ER export?" To answer this question, I decided to investigate the ER export of SZ* by inhibiting individual steps during ERAD. Previous studies have shown that disabling ERAD by deleting an ERAD-specific E3 ligase could result in enhanced ER export of some ERAD substrates that display a functional ER exit signal (Kincaid and Cooper, 2007). This, nevertheless, raises more questions than answers for the mechanism behind this phenomenon remained unclear and only one step in the ERAD pathway (Hrd1-medited ubiquitination) was inhibited.

I first demonstrated that inhibiting the ERAD recognition step by deleting Hsp40 *YDJ1* resulted in more efficient ER export of SZ*. Ydj1 was also shown as a gatekeeper for ERAD as its overexpression lead to increased ER retention of SZ*, and deletion increased ER exit. By constructing an Ydj1-HPD mutant that is defective for substrate ubiquitination, I was able to show that its ability to retain SZ* in the ER was mediated by substrate ubiquitination and potentially aggregation, and that Hsp70 function was also required for this process. I next inactivated the ERAD-C-specific E3 ligase *DOA10*. Similar to the *YDJ1* deletion, SZ* more efficiently exited the ER both *in vivo* and *in vitro* upon loss of Doa10. These data suggested further that substrate ubiquitination is necessary for ER retention, particularly because substrate

aggregation was unaffected in the *doa10Δ* strain. To test if ubiquitin was sufficient to mediate substrate ER retention independent of the ubiquitination machinery, four-tandem ubiquitins were attached covalently to the C-terminus of SZ*. Surprisingly, the ER exit of SZ*-Ub4, as indicated by the presence of cleaved GFP after vacuolar delivery, was negligible compared to SZ*. Even in the absence of Doa10, SZ*-Ub4 remained mostly in the ER with little being delivered to the vacuole, suggesting that ubiquitin is sufficient for retaining SZ*. These studies showed for the first time that ubiquitin acts as a hallmark that is necessary and sufficient for ER retention, thereby providing insights into how to rescue membrane proteins from ERAD by targeting the steps prior to substrate ubiquitination. This could serve as a promising therapeutic strategy for some human diseases such as lysosomal storage diseases. Lysosomal storage diseases are caused by mutations in lysosomal enzymes that result in protein misfolding and the subsequent degradation by ERAD (Platt et al., 2018). Some mutations disturb protein stability but still maintain partial function if rescued for lysosomal transport (Grace et al., 1994; Hruska et al., 2008). ER export rescue by inhibiting substrate ubiquitination may thus be beneficial in facilitating lysosomal transport of these misfolded enzymes especially glucocerebrosidase. In terms of the mutant plasma membrane proteins such as CFTR, ER export rescue may not be sufficient to protect proteins en route to the plasma membrane. Therefore, a combination of ERAD inhibition and other pharmacologic correctors are both required to correct mutant CFTR (Brodsky and Frizzell, 2015; Chung et al., 2016).

In summary, my work in this thesis sought to address two questions: (1) Are misfolded proteins with ERAD-C degrons able to exit the ER for post-ER degradation? (2) What features of misfolded proteins dictate their fate for ERAD versus post-ER degradation? By rational alteration of a post-ERQC substrate with a canonical ERAD-C degron, Wsc1*, I designed a

novel model substrate, SZ*, that is degraded by both ERAD and post-ER degradation. My further investigation with SZ* provided the first mechanistic evidence that substrate aggregation and ubiquitination can favor ERAD over post-ER degradation.

4.2 FUTURE DIRECTIONS

In light of my discoveries, it is important to highlight several limitations as well. Such considerations will further guide future work toward pursuing a detailed mechanism of substrate ER retention and ERAD.

First, does inhibition of post-ubiquitination steps of ERAD, including Cdc48-mediated retrotranslocation and proteasomal degradation, promote ER export of SZ*? My work only focused on substrate recognition and ubiquitination. For example, in mammalian cells, inhibiting a post-ubiquitination step of ERAD, such as retrotranslocation, promotes ER export of misfolded lysosomal glucocerebrosidase (GC), which is linked to lysosomal storage disorders (Wang et al., 2011a). It is worth noting that inhibition of retrotranslocation with the small molecule eeyarestatin I (Eer I) caused significant induction of the UPR and apoptosis, suggesting that the increased ER export of GC probably resulted from an indirect effect of the UPR, which promotes both protein folding and ER export (Travers et al., 2000; Wang et al., 2011a). In contrast, only treatment with kifunensine, which inhibits ER mannosidase I during the ERAD recognition step, rescued ER export of mutant GC without inducing the UPR and apoptosis. Additional studies are thus needed to determine if inhibiting a post-ubiquitination step during ERAD directly rescues substrate ER export. To this end, a temperature sensitive Cdc48 mutant, *cdc48-3*, will be used to inhibit retrotranslocation without causing significant ER stress compared to EerI treatment.

Pulse-chase assays will be conducted to monitor SZ*-GFP cleaved in both the *CDC48* and *cdc48-3* background when Cdc48 is functional or non-functional, respectively. Concurrently, the ER exit of SZ* will be directly measured in an *in vitro* budding assay using SZ*-containing microsomes from both *CDC48* and *cdc48-3* strains. Next, the proteasomal degradation step of ERAD will be inhibited by treatment of yeast lacking the multidrug pump, Pdr5, with the proteasome inhibitor MG132. Both the pulse-chase assay and *in vitro* budding assay will again be performed upon addition of MG132 or the vehicle, DMSO. I hypothesize that inhibiting a post-ubiquitination step of ERAD (by either inactivating Cdc48 or adding the proteasome inhibitor) will fail to rescue ER export of SZ*. Together with my current study, I will be able to provide the first evidence that pre-ubiquitination steps are key targets for promoting the ER exit of misfolded proteins.

Second, how do four tandem ubiquitins drive SZ* puncta formation? Are the puncta formed by SZ*-Ub4 ERAC? Appending four tandem ubiquitins dramatically changed the localization of SZ* from a mostly vacuolar location to puncta that seem to reside at the ER (Figure 22D and Figure 23C). However, further characterization of the puncta formed by SZ*-Ub4 is needed. These puncta are reminiscent of ERAC structures formed by CFTR (expressed in yeast) and other misfolded membrane proteins like Ste6-L1239X (Huyer et al., 2004a; Kakoi et al., 2013). CFTR, when expressed in yeast, sequesters in ERACs that co-localize with COPII components, including Sar1 and Sec23 (Kakoi et al., 2013). Since SZ* still bears a functional ER exit signal that can efficiently drive more than half of SZ* for ER exit, I hypothesize that four tandem ubiquitins target SZ* for sequestration into ERACs that co-localize with COPII components. To this end, an ER-localized fluorescent protein, Sec63-mCherry, will be used to confirm the ER localization of SZ*-Ub4. The co-localization between SZ*-Ub4 and COPII

components, including Sar1, Sec23, and Sec24, will be then tested. A previous study has shown that ERAC formation of CFTR requires the Hsp40s, Ydj1 and Hlj1, although their functions during this process remain unknown. Based on my hypothesis that ubiquitin drives SZ* to enter ERACs, the four-tandem ubiquitin attachment should bypass the requirement for Hsp40 (Ydj1 in this case) during ERAC formation by SZ*. To test this hypothesis, the localization pattern of SZ*-Ub4 will be imaged in both wild-type and *ydj1Δ* strains. To further expand the significance of my work, other wild-type proteins that efficiently exit the ER such, as the plasma membrane protein Yor1, will be used to test if four-tandem ubiquitins is sufficient to drive ERAC formation. Yor1 is the yeast ortholog of CFTR, and also has been modeled at a site (ΔF670) orthologous to the most common cystic fibrosis causing mutant ΔF508 (Katzmann et al., 1999; Louie et al., 2012). Therefore, Yor1 will be a valuable substrate to test my hypothesis, since the results may be applicable to CFTR due to the overall homology between Yor1 and CFTR. These experiments will advance our understanding of how ERACs are formed, I propose that ubiquitin may act as the driving force to sequester substrates into ERACs.

Third, what factors in the ER mediate ER retention of a ubiquitinated substrate? ER-localized ubiquitin binding proteins are the main candidates because ubiquitin binding domains (UBDs) on those proteins can selectively bind ubiquitin (Hicke and Dunn, 2003; Husnjak and Dikic, 2012). There are about 80 proteins in yeast that contain UBDs, many of which are associated with the ER (Tsuchiya et al., 2017). In the long term, a fluorescent imaging-based screen could be used to identify specific UBD-containing proteins that mediate ER retention of SZ*-Ub4. In this screen, ERAC formation of SZ*-Ub4 will be imaged in yeast lacking individual genes that encode UBD-containing proteins. The loss of ERAC formation of SZ*-Ub4, and its accumulation in the vacuole, will implicate a specific UBD-containing protein. Because the four-

tandem ubiquitin motif is not an ERAD-favored ubiquitin linkage, one can also perform the *in vitro* budding assay with SZ*-Ub4 and then titrate potential ubiquitin binding proteins away with increasing concentrations of purified K48 linked tetra-ubiquitin. Based on my hypothesis, the *in vitro* addition of K48 tetra-ubiquitin may outcompete the linear ubiquitin on SZ* for binding to a UBD-containing protein that mediates ER retention, which will be indicated by increased packaging of SZ*-Ub4 into COPII vesicles *in vitro*.

Fourth, can de-ubiquitination rescue the ER export of misfolded substrate when ERAD is functional? ERAD activity is tightly modulated in cells, because both hyperactive and hypoactive ERAD can wreak havoc on protein homeostasis and even cause cell death (Guerriero and Brodsky, 2012; Hebert and Molinari, 2007). My study mostly spotlighted how ERAD modulation affects ER export of misfolded proteins. With the discovery that substrate ubiquitination acts as an ER retention signal, it will be intriguing to investigate in the future if de-ubiquitination of the substrate rescues ER export. This will shed light on the targeted rescue of misfolded protein without modulating ERAD activity. To this end, SZ* will be fused to the catalytic domain of a non-specific DUB from herpes virus that has been shown to render the protein to which it is attached non-ubiquitinable (Stringer and Piper, 2011). The strong de-ubiquitination function of DUB is further evidenced by a recent study where a DUB confers dominant-negative effects even to a ubiquitin ligase when fused to the enzyme (MacDonald et al., 2017). As a control, a catalytically dead mutant of DUB will be fused to the protein of interest. Both the *in vivo* GFP cleavage assay and an *in vitro* budding assay will be performed to test ER export efficiency in the presence of active or inactive DUB. Based on my discovery, I hypothesize that the appended DUB will facilitate ER export of SZ*.

To further expand the significance of my study, it is necessary to test how ubiquitination and de-ubiquitination affect ER export of native yeast proteins that localize in a post-ER compartment, such as the plasma membrane. Yor1 seems to be a good candidate because: (1) It is a plasma membrane protein that requires ER export; (2) The levels of Yor1 that reach the plasma membrane can be tested by oligomycin resistance on a yeast spot assay; (3) The Yor1ΔF670 mutant is mostly trapped in the ER and is eliminated by ERAD; (4) Yor1 is a CFTR homolog that is natively expressed in yeast. Therefore, the DUB will be fused to both wild-type Yor1 and Yor1ΔF670 mutant. The catalytically inactive DUB will be used as a control. Besides the GFP cleavage and *in vitro* budding assay used above, the oligomycin resistant spot assay will be conducted to investigate the physiological relevance of my findings. If the DUB fusion enhances ER export and oligomycin resistance of Yor1 and the mutant, these experiments will shed light on the significance of rescuing the ER export of misfolded proteins by modulating substrate ubiquitination.

APPENDIX

YEAST STRAINS, PLASMIDS, AND PRIMERS USED IN THIS STUDY

Table 1 Yeast strains used in this study

Strain	Genotype	Reference
BY4742	*MATα, his3Δ1, leu2Δ0, lys2Δ0 ura3Δ3*	(Winzeler et al., 1999)
pdr5Δ	*MATα, his3Δ1, leu2Δ0, ura3Δ3 pdr5Δ::KanMX*	(Winzeler et al., 1999)
pdr5Δ pep4Δ	*MATα, met15Δ0, his3Δ1, leu2Δ0, ura3Δ3 pdr5Δ::KanMX, pep4Δ::KanMX*	This lab
vps4Δ	MATα, his3Δ1, leu2Δ0, ura3Δ3 vps4Δ::KanMX	(Winzeler et al., 1999)
vps23Δ	MATα, his3Δ1, leu2Δ0, ura3Δ3 vps23Δ::KanMX	(Winzeler et al., 1999)
vps36Δ	MATα, his3Δ1, leu2Δ0, ura3Δ3 vps36Δ::KanMX	(Winzeler et al., 1999)
vps27Δ	MATα, his3Δ1, leu2Δ0, ura3Δ3 vps27Δ::KanMX	(Winzeler et al., 1999)
snf7Δ	MATα, his3Δ1, leu2Δ0, ura3Δ3 snf7Δ::KanMX	(Winzeler et al., 1999)
atg1Δ	*MATα, his3Δ1, leu2Δ0, ura3Δ3 atg1Δ::KanMX*	(Winzeler et al., 1999)
atg5Δ	*MATα, his3Δ1, leu2Δ0, ura3Δ3 atg5Δ::KanMX*	(Winzeler et al., 1999)
atg8Δ	*MATα, his3Δ1, leu2Δ0, ura3Δ3 atg8Δ::KanMX*	(Winzeler et al., 1999)
atg9Δ	*MATα, his3Δ1, leu2Δ0, ura3Δ3atg9Δ::KanMX*	(Winzeler et al., 1999)
atg11Δ	*MATα, his3Δ1, leu2Δ0, ura3Δ3 atg11Δ::KanMX*	(Winzeler et al., 1999)
SSA1	*MATα, his3-11,15, leu2-3,112, ura3-52. trp1-Δ1, lys2, ssa2- 1(LEU2), ssa3-1(TRP1), ssa4-2(LYS2)*	(Becker et al., 1996)
ssa1-45	*MATα, his3-11,15, leu2-3,112, ura3-52. trp1-Δ1, lys2, ssa1-45, ssa2-1(LEU2), ssa3-1(TRP1), ssa4-2(LYS2)*	(Becker et al., 1996)
KAR2	*MATa ura3-52, leu2-3,112, ade2-101*	(Sanders et al., 1992)
kar2-1	*MATa, kar2-1, ura3-52, leu2-3,112, ade2-101*	(Brodsky et al., 1999)
HLJ1 YDJ1	*MATα, ade2, his3, leu2, ura3, trp1*	(Youker et al., 2004)
ydj1-151	*MATα, ade2, his3, leu2 ,ura3, trp1, can1-100, ydj1-2::HIS3 ydj1-151::LEU2*	(Youker et al., 2004)
DOA10 HRD1	*MATa, his3-Δ200, leu2-3,112, ura3-52, lys2-801, trp1-1, gal2*	(Huyer et al., 2004b)
doa10Δ	*MATa, his3-Δ200, leu2-3,112, ura3-52, lys2-801, trp1-1, gal2, doa10Δ::HIS3*	(Huyer et al., 2004b)
hrd1Δ	*MATa, his3-Δ200, leu2-3,112, ura3-52, lys2-801, trp1-1, gal2, hrd1Δ::LEU2*	(Huyer et al., 2004b)
doa10Δ	*MATa, his3-Δ200, leu2-3,112, ura3-52, lys2-801, trp1-*	(Huyer et al., 2004b)

hrd1Δ	*1, gal2 doa10Δ::HIS3, hrd1Δ::LEU2*	
cdc48-2	Back-crossed 3X to BY4742	(Moir et al., 1982)
W303-1A	*MATa, ura3-1, his-3-11,15, ade2-1, trp1-1, leu2-3,112 and can1-100*	(Wallis et al., 1989)
RSY300	*MATa his3-11,15 leu2-3,112 ura3-1 se7-4*	(Lupashin et al., 1996)
CBY616	*MATa his3Δ200 ura3-52 leu2Δ1 trp1Δ63*	Charles Barlowe lab
CBY829	*MATa his3Δ200 ura3-52 leu2Δ1 trp1Δ63 ypt1-3*	(Otte et al., 2001)
CBY1060	*MATa his3Δ200 ura3-52 leu2Δ1 trp1Δ63 sec23-1*	Charles Barlowe lab
CBY1703	*MATa his3Δ1 leu2Δ0 lys2Δ0 ura3Δ0 sec18-1 isogenic to BY4742*	Charles Barlowe lab
ydj1Δ	*MATα, his3Δ1, leu2Δ0, ura3Δ3 ydj1Δ::KanMX*	(Winzeler et al., 1999)
hlj1Δ	*MATα, his3Δ1, leu2Δ0, ura3Δ3 hlj1Δ::KanMX*	(Winzeler et al., 1999)
CBY1285	Used for Sec23/Sec24 purification	Charles Barlowe lab
CBY120	Used for Sec13/Sec31 purification	Charles Barlowe lab

Table 2 Yeast plasmids used in this study

Plasmids	Description	Reference
pSZ01	*CEN* URA3 P-TEF SZ*	This study
pSZ02	*CEN* URA3 P-TEF SZ	This study
pSZ03	*CEN* URA3 P-TEF SZ*-GFP	This study
pSZ04	*CEN* URA3 P-TEF W-N	This study
pSZ05	*CEN* URA3 P-TEF W-N*	This study
pSZ06	*CEN* URA3 P-TEF 3HA-NBD2*	This study
pSZ07	*2μ* URA3 P-TEF 3HA-NBD2*	This study
pSZ08	*2μ* URA3 P-TEF SZ*	This study
pSW148	CEN LEU2 P-GAS Wsc1*	(Prasad et al., 2012)
pRP12	CEN HIS3 P-TDH3 Wsc1*	(Prasad et al., 2012)
pFA6a-link-yoSuperfolderGFP-CaURA3	*CEN* URA3 P-TEF sfGFP	(Lee et al., 2013)
pHSE-lacZ	*2μ* URA3 P-SSA3 LacZ	(Santoro et al., 1998)
pYEP96	2μ TRP1 hsf1-R206S	(Sewell et al., 1995)
pCG01	2μ URA3 ste6–166NBD2	(Guerriero et al., 2013)
pSZ09	*CEN* URA3 P-TEF SZ*-GFP with BamHI site between GGGGS linker and GFP mutated and subcloned with XbaI/BamHI sites	This study
pSZ10	*CEN* URA3 P-TEF SZ*-GFP-Ub4	This study
pSZ11	*CEN* LEU2 P-Ydj1 Ydj1	Elizabeth Craig lab
pSZ12	*CEN* URA3 P-Ydj1 Ydj1-QAA	This study

Ydj1* (BPM569)	*CEN* URA3 P-Ydj1 CEN URA3 P-Ydj1 Ydj1-PY/GG	(Fang et al., 2014)
CBB205	Used for Sar1 purification	(Barlowe et al., 1994)

Table 3 Primers used in this study

Primer	Sequence (5'-3')	Reference
OSZ01	gtacactagtatgtttttcaacagactaagcgct	This study
OSZ02	gttagaggtgccgatgattacccatacgatgttcctgactatgcgggctatccctatgacgtcccggactatgcaggatcctatccatatgacgttccagattacgctgctcagtgcaagaaagccaatgtaggg	This study
OSZ03	aagaaagccaatgtaggggc	This study
OSZ04	agtactcgagttattcactatgcgttataaccattgttag	This study
OSZ05	gcaaaaacctttattattcaatggaaccatcag	This study
OSZ06	gttatctctgatggttccattgaataat	This study
OSZ07	agtactcgagttaactgctttggttggaaacaatttg	This study
OSZ08	gtactctagaatgtttttcaacagactaag	This study
OSZ09	gtacggatcctgagccacctcctcctgagcctccaccaccagatccacccccccctctgacaatcaacaagatataaagagcaatg	This study
OSZ10	gtcaatccagacgaagctgatgccatggcctacccatacgatgttcctgactatgcgggc	This study
OSZ11	gcccgcatagtcaggaacatcgtatgggtaggccatggcatcagcttcgtctggattgac	This study
OSZ12	gtcaactagtatgagaccgaacaaaacaag	This study
OSZ13	gtacactagtatgtacccatacgatgttcctg	This study
OSZ14	gcctttagacatggagcctgagccacctcct	This study
OSZ15	aggaggtggctcaggctccatgtctaaaggc	This study
OSZ16	gtcaggatccctttgtacaattcgtccattc	This study
OSZ17	agcttcctcacttggattcttagctgcttggtattttaaggcgcattttc	This study
OSZ18	gaaaatgcgccttaaaataccaagcagctaagaatccaagtgaggaagct	This study

.

BIBLIOGRAPHY

Adle, D.J., W. Wei, N. Smith, J.J. Bies, and J. Lee. 2009. Cadmium-mediated rescue from ER associated degradation induces expression of its exporter. *Proc Natl Acad Sci U S A*. 106:10189-10194.

Aguzzi, A., and T. O'Connor. 2010. Protein aggregation diseases: pathogenicity and therapeutic perspectives. *Nat Rev Drug Discov*. 9:237-248.

Ahner, A., K. Nakatsukasa, H. Zhang, R.A. Frizzell, and J.L. Brodsky. 2007. Small heat-shock proteins select deltaF508-CFTR for endoplasmic reticulum-associated degradation. *Mol Biol Cell*. 18:806-814.

Amengual, J., L. Guo, A. Strong, J. Madrigal-Matute, H. Wang, S. Kaushik, J.L. Brodsky, D.J. Rader, A.M. Cuervo, and E.A. Fisher. 2018. Autophagy Is Required for Sortilin-Mediated Degradation of Apolipoprotein B100. *Circ Res*. 122:568-582.

Ammerer, G., C.P. Hunter, J.H. Rothman, G.C. Saari, L.A. Valls, and T.H. Stevens. 1986. PEP4 gene of Saccharomyces cerevisiae encodes proteinase A, a vacuolar enzyme required for processing of vacuolar precursors. *Mol Cell Biol*. 6:2490-2499.

Arteaga, M.F., L. Wang, T. Ravid, M. Hochstrasser, and C.M. Canessa. 2006. An amphipathic helix targets serum and glucocorticoid-induced kinase 1 to the endoplasmic reticulum-associated ubiquitin-conjugation machinery. *Proc Natl Acad Sci U S A*. 103:11178-11183.

Arvan, P., X. Zhao, J. Ramos-Castaneda, and A. Chang. 2002. Secretory pathway quality control operating in Golgi, plasmalemmal, and endosomal systems. *Traffic*. 3:771-780.

Avci, D., S. Fuchs, B. Schrul, A. Fukumori, M. Breker, I. Frumkin, C.Y. Chen, M.L. Biniossek, E. Kremmer, O. Schilling, H. Steiner, M. Schuldiner, and M.K. Lemberg. 2014. The yeast ER-intramembrane protease Ypf1 refines nutrient sensing by regulating transporter abundance. *Mol Cell*. 56:630-640.

B'Chir, W., A.C. Maurin, V. Carraro, J. Averous, C. Jousse, Y. Muranishi, L. Parry, G. Stepien, P. Fafournoux, and A. Bruhat. 2013. The eIF2alpha/ATF4 pathway is essential for stress-induced autophagy gene expression. *Nucleic Acids Res*. 41:7683-7699.

Balchin, D., M. Hayer-Hartl, and F.U. Hartl. 2016. In vivo aspects of protein folding and quality control. *Science*. 353:aac4354.

Baldridge, R.D., and T.A. Rapoport. 2016. Autoubiquitination of the Hrd1 Ligase Triggers Protein Retrotranslocation in ERAD. *Cell*. 166:394-407.

Barlowe, C., and A. Helenius. 2016. Cargo Capture and Bulk Flow in the Early Secretory Pathway. *Annu Rev Cell Dev Biol*. 32:197-222.

Barlowe, C., L. Orci, T. Yeung, M. Hosobuchi, S. Hamamoto, N. Salama, M.F. Rexach, M. Ravazzola, M. Amherdt, and R. Schekman. 1994. COPII: a membrane coat formed by Sec proteins that drive vesicle budding from the endoplasmic reticulum. *Cell*. 77:895-907.

Becker, J., W. Walter, W. Yan, and E.A. Craig. 1996. Functional interaction of cytosolic hsp70 and a DnaJ-related protein, Ydj1p, in protein translocation in vivo. *Mol Cell Biol*. 16:4378-4386.

Belgareh-Touze, N., S. Leon, Z. Erpapazoglou, M. Stawiecka-Mirota, D. Urban-Grimal, and R. Haguenauer-Tsapis. 2008. Versatile role of the yeast ubiquitin ligase Rsp5p in intracellular trafficking. *Biochem Soc Trans*. 36:791-796.

Benedetti, H., S. Raths, F. Crausaz, and H. Riezman. 1994. The END3 gene encodes a protein that is required for the internalization step of endocytosis and for actin cytoskeleton organization in yeast. *Mol Biol Cell*. 5:1023-1037.

Bernales, S., K.L. McDonald, and P. Walter. 2006. Autophagy counterbalances endoplasmic reticulum expansion during the unfolded protein response. *PLoS Biol*. 4:e423.

Bernales, S., S. Schuck, and P. Walter. 2007. ER-phagy: selective autophagy of the endoplasmic reticulum. *Autophagy*. 3:285-287.

Berner, N., K.R. Reutter, and D.H. Wolf. 2018. Protein Quality Control of the Endoplasmic Reticulum and Ubiquitin-Proteasome-Triggered Degradation of Aberrant Proteins: Yeast Pioneers the Path. *Annu Rev Biochem*. 87:751-782.

Bienkowski, R.S., S.F. Curran, and R.A. Berg. 1986. Kinetics of intracellular degradation of newly synthesized collagen. *Biochemistry*. 25:2455-2459.

Blythe, E.E., K.C. Olson, V. Chau, and R.J. Deshaies. 2017. Ubiquitin- and ATP-dependent unfoldase activity of P97/VCP*NPLOC4*UFD1L is enhanced by a mutation that causes multisystem proteinopathy. *Proc Natl Acad Sci U S A*. 114:E4380-E4388.

Bodnar, N.O., and T.A. Rapoport. 2017. Molecular Mechanism of Substrate Processing by the Cdc48 ATPase Complex. *Cell*. 169:722-735 e729.

Bowers, K., and T.H. Stevens. 2005. Protein transport from the late Golgi to the vacuole in the yeast Saccharomyces cerevisiae. *Biochim Biophys Acta*. 1744:438-454.

Braakman, I., and N.J. Bulleid. 2011. Protein folding and modification in the mammalian endoplasmic reticulum. *Annu Rev Biochem*. 80:71-99.

Braakman, I., and D.N. Hebert. 2013. Protein folding in the endoplasmic reticulum. *Cold Spring Harb Perspect Biol*. 5:a013201.

Braun, S., K. Matuschewski, M. Rape, S. Thoms, and S. Jentsch. 2002. Role of the ubiquitin-selective CDC48(UFD1/NPL4)chaperone (segregase) in ERAD of OLE1 and other substrates. *EMBO J*. 21:615-621.

Briant, K., N. Johnson, and E. Swanton. 2017. Transmembrane domain quality control systems operate at the endoplasmic reticulum and Golgi apparatus. *PLoS One*. 12:e0173924.

Brodsky, J.L., and R.A. Frizzell. 2015. A combination therapy for cystic fibrosis. *Cell*. 163:17.

Brodsky, J.L., E.D. Werner, M.E. Dubas, J.L. Goeckeler, K.B. Kruse, and A.A. McCracken. 1999. The requirement for molecular chaperones during endoplasmic reticulum-associated protein degradation demonstrates that protein export and import are mechanistically distinct. *J Biol Chem*. 274:3453-3460.

Caldwell, S.R., K.J. Hill, and A.A. Cooper. 2001. Degradation of endoplasmic reticulum (ER) quality control substrates requires transport between the ER and Golgi. *J Biol Chem*. 276:23296-23303.

Camirand, A., A. Heysen, B. Grondin, and A. Herscovics. 1991. Glycoprotein biosynthesis in Saccharomyces cerevisiae. Isolation and characterization of the gene encoding a specific processing alpha-mannosidase. *J Biol Chem*. 266:15120-15127.

Carvalho, P., V. Goder, and T.A. Rapoport. 2006. Distinct ubiquitin-ligase complexes define convergent pathways for the degradation of ER proteins. *Cell*. 126:361-373.

Carvalho, P., A.M. Stanley, and T.A. Rapoport. 2010. Retrotranslocation of a misfolded luminal ER protein by the ubiquitin-ligase Hrd1p. *Cell*. 143:579-591.

Chang, A., and G.R. Fink. 1995. Targeting of the yeast plasma membrane [H+]ATPase: a novel gene AST1 prevents mislocalization of mutant ATPase to the vacuole. *J Cell Biol*. 128:39-49.

Chen, B., M. Retzlaff, T. Roos, and J. Frydman. 2011. Cellular strategies of protein quality control. *Cold Spring Harb Perspect Biol*. 3:a004374.

Christ, L., C. Raiborg, E.M. Wenzel, C. Campsteijn, and H. Stenmark. 2017. Cellular Functions and Molecular Mechanisms of the ESCRT Membrane-Scission Machinery. *Trends Biochem Sci*. 42:42-56.

Christianson, J.C., and Y. Ye. 2014. Cleaning up in the endoplasmic reticulum: ubiquitin in charge. *Nat Struct Mol Biol*. 21:325-335.

Chung, W.J., J.L. Goeckeler-Fried, V. Havasi, A. Chiang, S.M. Rowe, Z.E. Plyler, J.S. Hong, M. Mazur, G.A. Piazza, A.B. Keeton, E.L. White, L. Rasmussen, A.M. Weissman, R.A. Denny, J.L. Brodsky, and E.J. Sorscher. 2016. Increasing the Endoplasmic Reticulum Pool of the F508del Allele of the Cystic Fibrosis Transmembrane Conductance Regulator Leads to Greater Folding Correction by Small Molecule Therapeutics. *PLoS One*. 11:e0163615.

Cooper, A.A., and T.H. Stevens. 1996. Vps10p cycles between the late-Golgi and prevacuolar compartments in its function as the sorting receptor for multiple yeast vacuolar hydrolases. *J Cell Biol*. 133:529-541.

Coughlan, C.M., J.L. Walker, J.C. Cochran, K.D. Wittrup, and J.L. Brodsky. 2004. Degradation of mutated bovine pancreatic trypsin inhibitor in the yeast vacuole suggests post-endoplasmic reticulum protein quality control. *J Biol Chem*. 279:15289-15297.

Cyr, D.M., X. Lu, and M.G. Douglas. 1992. Regulation of Hsp70 function by a eukaryotic DnaJ homolog. *J Biol Chem*. 267:20927-20931.

De Craene, J.O., O. Soetens, and B. Andre. 2001. The Npr1 kinase controls biosynthetic and endocytic sorting of the yeast Gap1 permease. *J Biol Chem*. 276:43939-43948.

Deloche, O., B.G. Yeung, G.S. Payne, and R. Schekman. 2001. Vps10p transport from the trans-Golgi network to the endosome is mediated by clathrin-coated vesicles. *Mol Biol Cell*. 12:475-485.

Denic, V., E.M. Quan, and J.S. Weissman. 2006. A luminal surveillance complex that selects misfolded glycoproteins for ER-associated degradation. *Cell*. 126:349-359.

Di, X.J., Y.J. Wang, D.Y. Han, Y.L. Fu, A.S. Duerfeldt, B.S. Blagg, and T.W. Mu. 2016. Grp94 Protein Delivers gamma-Aminobutyric Acid Type A (GABAA) Receptors to Hrd1 Protein-mediated Endoplasmic Reticulum-associated Degradation. *J Biol Chem*. 291:9526-9539.

Dikic, I. 2018. Open questions: why should we care about ER-phagy and ER remodelling? *BMC Biol*. 16:131.

Dobzinski, N., S.G. Chuartzman, R. Kama, M. Schuldiner, and J.E. Gerst. 2015. Starvation-Dependent Regulation of Golgi Quality Control Links the TOR Signaling and Vacuolar Protein Sorting Pathways. *Cell Rep*. 12:1876-1886.

Doonan, L.M., E.A. Fisher, and J.L. Brodsky. 2018. Can modulators of apolipoproteinB biogenesis serve as an alternate target for cholesterol-lowering drugs? *Biochim Biophys Acta Mol Cell Biol Lipids*. 1863:762-771.

Dubouloz, F., O. Deloche, V. Wanke, E. Cameroni, and C. De Virgilio. 2005. The TOR and EGO protein complexes orchestrate microautophagy in yeast. *Mol Cell*. 19:15-26.

Dusseljee, S., R. Wubbolts, D. Verwoerd, A. Tulp, H. Janssen, J. Calafat, and J. Neefjes. 1998. Removal and degradation of the free MHC class II beta chain in the endoplasmic reticulum requires proteasomes and is accelerated by BFA. *J Cell Sci*. 111 (Pt 15):2217-2226.

Duttler, S., S. Pechmann, and J. Frydman. 2013. Principles of cotranslational ubiquitination and quality control at the ribosome. *Mol Cell*. 50:379-393.

Eisele, Y.S., C. Monteiro, C. Fearns, S.E. Encalada, R.L. Wiseman, E.T. Powers, and J.W. Kelly. 2015. Targeting protein aggregation for the treatment of degenerative diseases. *Nat Rev Drug Discov*. 14:759-780.

Fang, N.N., G.T. Chan, M. Zhu, S.A. Comyn, A. Persaud, R.J. Deshaies, D. Rotin, J. Gsponer, and T. Mayor. 2014. Rsp5/Nedd4 is the main ubiquitin ligase that targets cytosolic misfolded proteins following heat stress. *Nat Cell Biol*. 16:1227-1237.

Feige, M.J., and L.M. Hendershot. 2013. Quality control of integral membrane proteins by assembly-dependent membrane integration. *Mol Cell*. 51:297-309.

Foresti, O., V. Rodriguez-Vaello, C. Funaya, and P. Carvalho. 2014. Quality control of inner nuclear membrane proteins by the Asi complex. *Science*. 346:751-755.

Forrester, A., C. De Leonibus, P. Grumati, E. Fasana, M. Piemontese, L. Staiano, I. Fregno, A. Raimondi, A. Marazza, G. Bruno, M. Iavazzo, D. Intartaglia, M. Seczynska, E. van Anken, I. Conte, M.A. De Matteis, I. Dikic, M. Molinari, and C. Settembre. 2019. A selective ER-phagy exerts procollagen quality control via a Calnexin-FAM134B complex. *EMBO J*. 38.

Fotia, A.B., J. Ekberg, D.J. Adams, D.I. Cook, P. Poronnik, and S. Kumar. 2004. Regulation of neuronal voltage-gated sodium channels by the ubiquitin-protein ligases Nedd4 and Nedd4-2. *J Biol Chem*. 279:28930-28935.

Fregno, I., E. Fasana, T.J. Bergmann, A. Raimondi, M. Loi, T. Solda, C. Galli, R. D'Antuono, D. Morone, A. Danieli, P. Paganetti, E. van Anken, and M. Molinari. 2018. ER-to-lysosome-

associated degradation of proteasome-resistant ATZ polymers occurs via receptor-mediated vesicular transport. *EMBO J*. 37.

Froissard, M., N. Belgareh-Touze, M. Dias, N. Buisson, J.M. Camadro, R. Haguenauer-Tsapis, and E. Lesuisse. 2007. Trafficking of siderophore transporters in Saccharomyces cerevisiae and intracellular fate of ferrioxamine B conjugates. *Traffic*. 8:1601-1616.

Fujita, E., Y. Kouroku, A. Isoai, H. Kumagai, A. Misutani, C. Matsuda, Y.K. Hayashi, and T. Momoi. 2007. Two endoplasmic reticulum-associated degradation (ERAD) systems for the novel variant of the mutant dysferlin: ubiquitin/proteasome ERAD(I) and autophagy/lysosome ERAD(II). *Hum Mol Genet*. 16:618-629.

Fujita, K., S. Omura, and J. Silver. 1997. Rapid degradation of CD4 in cells expressing human immunodeficiency virus type 1 Env and Vpu is blocked by proteasome inhibitors. *J Gen Virol*. 78 (Pt 3):619-625.

Fumagalli, F., J. Noack, T.J. Bergmann, E. Cebollero, G.B. Pisoni, E. Fasana, I. Fregno, C. Galli, M. Loi, T. Solda, R. D'Antuono, A. Raimondi, M. Jung, A. Melnyk, S. Schorr, A. Schreiber, L. Simonelli, L. Varani, C. Wilson-Zbinden, O. Zerbe, K. Hofmann, M. Peter, M. Quadroni, R. Zimmermann, and M. Molinari. 2016. Translocon component Sec62 acts in endoplasmic reticulum turnover during stress recovery. *Nat Cell Biol*. 18:1173-1184.

Gates, S.N., A.L. Yokom, J. Lin, M.E. Jackrel, A.N. Rizo, N.M. Kendsersky, C.E. Buell, E.A. Sweeny, K.L. Mack, E. Chuang, M.P. Torrente, M. Su, J. Shorter, and D.R. Southworth. 2017. Ratchet-like polypeptide translocation mechanism of the AAA+ disaggregase Hsp104. *Science*. 357:273-279.

Gauss, R., K. Kanehara, P. Carvalho, D.T. Ng, and M. Aebi. 2011. A complex of Pdi1p and the mannosidase Htm1p initiates clearance of unfolded glycoproteins from the endoplasmic reticulum. *Mol Cell*. 42:782-793.

Gelsthorpe, M.E., N. Baumann, E. Millard, S.E. Gale, S.J. Langmade, J.E. Schaffer, and D.S. Ory. 2008. Niemann-Pick type C1 I1061T mutant encodes a functional protein that is selected for endoplasmic reticulum-associated degradation due to protein misfolding. *J Biol Chem*. 283:8229-8236.

Ghavidel, A., K. Baxi, V. Ignatchenko, M. Prusinkiewicz, T.G. Arnason, T. Kislinger, C.E. Carvalho, and T.A. Harkness. 2015. A Genome Scale Screen for Mutants with Delayed Exit from Mitosis: Ire1-Independent Induction of Autophagy Integrates ER Homeostasis into Mitotic Lifespan. *PLoS Genet*. 11:e1005429.

Gidalevitz, T., V. Prahlad, and R.I. Morimoto. 2011. The stress of protein misfolding: from single cells to multicellular organisms. *Cold Spring Harb Perspect Biol*. 3.

Gnann, A., J.R. Riordan, and D.H. Wolf. 2004. Cystic fibrosis transmembrane conductance regulator degradation depends on the lectins Htm1p/EDEM and the Cdc48 protein complex in yeast. *Mol Biol Cell*. 15:4125-4135.

Gomez-Navarro, N., and E. Miller. 2016. Protein sorting at the ER-Golgi interface. *J Cell Biol*. 215:769-778.

Grace, M.E., K.M. Newman, V. Scheinker, A. Berg-Fussman, and G.A. Grabowski. 1994. Analysis of human acid beta-glucosidase by site-directed mutagenesis and heterologous expression. *J Biol Chem*. 269:2283-2291.

Grice, G.L., and J.A. Nathan. 2016. The recognition of ubiquitinated proteins by the proteasome. *Cell Mol Life Sci*. 73:3497-3506.

Grumati, P., I. Dikic, and A. Stolz. 2018. ER-phagy at a glance. *J Cell Sci*. 131.

Grumati, P., G. Morozzi, S. Holper, M. Mari, M.I. Harwardt, R. Yan, S. Muller, F. Reggiori, M. Heilemann, and I. Dikic. 2017. Full length RTN3 regulates turnover of tubular endoplasmic reticulum via selective autophagy. *Elife*. 6.

Guerriero, C.J., and J.L. Brodsky. 2012. The delicate balance between secreted protein folding and endoplasmic reticulum-associated degradation in human physiology. *Physiol Rev*. 92:537-576.

Guerriero, C.J., K.R. Reutter, A.A. Augustine, G.M. Preston, K.F. Weiberth, T.D. Mackie, H.C. Cleveland-Rubeor, N.P. Bethel, K.M. Callenberg, K. Nakatsukasa, M. Grabe, and J.L. Brodsky. 2017. Transmembrane helix hydrophobicity is an energetic barrier during the retrotranslocation of integral membrane ERAD substrates. *Mol Biol Cell*. 28:2076-2090.

Guerriero, C.J., K.F. Weiberth, and J.L. Brodsky. 2013. Hsp70 targets a cytoplasmic quality control substrate to the San1p ubiquitin ligase. *J Biol Chem*. 288:18506-18520.

Habeck, G., F.A. Ebner, H. Shimada-Kreft, and S.G. Kreft. 2015. The yeast ERAD-C ubiquitin ligase Doa10 recognizes an intramembrane degron. *J Cell Biol*. 209:261-273.

Hammond, C., and A. Helenius. 1994. Quality control in the secretory pathway: retention of a misfolded viral membrane glycoprotein involves cycling between the ER, intermediate compartment, and Golgi apparatus. *J Cell Biol*. 126:41-52.

Hampton, R.Y., R.G. Gardner, and J. Rine. 1996. Role of 26S proteasome and HRD genes in the degradation of 3-hydroxy-3-methylglutaryl-CoA reductase, an integral endoplasmic reticulum membrane protein. *Mol Biol Cell*. 7:2029-2044.

Han, S., Y. Liu, and A. Chang. 2007. Cytoplasmic Hsp70 promotes ubiquitination for endoplasmic reticulum-associated degradation of a misfolded mutant of the yeast plasma membrane ATPase, PMA1. *J Biol Chem*. 282:26140-26149.

Hartl, F.U. 2017. Protein Misfolding Diseases. *Annu Rev Biochem*. 86:21-26.

Haynes, C.M., S. Caldwell, and A.A. Cooper. 2002. An HRD/DER-independent ER quality control mechanism involves Rsp5p-dependent ubiquitination and ER-Golgi transport. *J Cell Biol*. 158:91-101.

Hebert, D.N., and M. Molinari. 2007. In and out of the ER: protein folding, quality control, degradation, and related human diseases. *Physiol Rev*. 87:1377-1408.

Helenius, A., and M. Aebi. 2004. Roles of N-linked glycans in the endoplasmic reticulum. *Annu Rev Biochem*. 73:1019-1049.

Henne, W.M., N.J. Buchkovich, and S.D. Emr. 2011. The ESCRT pathway. *Dev Cell*. 21:77-91.

Henne, W.M., H. Stenmark, and S.D. Emr. 2013. Molecular mechanisms of the membrane sculpting ESCRT pathway. *Cold Spring Harb Perspect Biol*. 5.

Hicke, L., and R. Dunn. 2003. Regulation of membrane protein transport by ubiquitin and ubiquitin-binding proteins. *Annu Rev Cell Dev Biol*. 19:141-172.

Hidvegi, T., M. Ewing, P. Hale, C. Dippold, C. Beckett, C. Kemp, N. Maurice, A. Mukherjee, C. Goldbach, S. Watkins, G. Michalopoulos, and D.H. Perlmutter. 2010. An autophagy-enhancing drug promotes degradation of mutant alpha1-antitrypsin Z and reduces hepatic fibrosis. *Science*. 329:229-232.

Hiller, M.M., A. Finger, M. Schweiger, and D.H. Wolf. 1996. ER degradation of a misfolded luminal protein by the cytosolic ubiquitin-proteasome pathway. *Science*. 273:1725-1728.

Hirano, K., C. Zuber, J. Roth, and M. Ziak. 2003. The proteasome is involved in the degradation of different aquaporin-2 mutants causing nephrogenic diabetes insipidus. *Am J Pathol*. 163:111-120.

Hitt, R., and D.H. Wolf. 2004. DER7, encoding alpha-glucosidase I is essential for degradation of malfolded glycoproteins of the endoplasmic reticulum. *FEMS Yeast Res*. 4:815-820.

Holkeri, H., and M. Makarow. 1998. Different degradation pathways for heterologous glycoproteins in yeast. *FEBS Lett*. 429:162-166.

Hong, E., A.R. Davidson, and C.A. Kaiser. 1996. A pathway for targeting soluble misfolded proteins to the yeast vacuole. *J Cell Biol*. 135:623-633.

Horn, S.C., J. Hanna, C. Hirsch, C. Volkwein, A. Schutz, U. Heinemann, T. Sommer, and E. Jarosch. 2009. Usa1 functions as a scaffold of the HRD-ubiquitin ligase. *Mol Cell*. 36:782-793.

Houck, S.A., and D.M. Cyr. 2012. Mechanisms for quality control of misfolded transmembrane proteins. *Biochim Biophys Acta*. 1818:1108-1114.

Houck, S.A., H.Y. Ren, V.J. Madden, J.N. Bonner, M.P. Conlin, J.A. Janovick, P.M. Conn, and D.M. Cyr. 2014. Quality control autophagy degrades soluble ERAD-resistant conformers of the misfolded membrane protein GnRHR. *Mol Cell*. 54:166-179.

Hrizo, S.L., V. Gusarova, D.M. Habiel, J.L. Goeckeler, E.A. Fisher, and J.L. Brodsky. 2007. The Hsp110 molecular chaperone stabilizes apolipoprotein B from endoplasmic reticulum-associated degradation (ERAD). *J Biol Chem*. 282:32665-32675.

Hruska, K.S., M.E. LaMarca, C.R. Scott, and E. Sidransky. 2008. Gaucher disease: mutation and polymorphism spectrum in the glucocerebrosidase gene (GBA). *Hum Mutat*. 29:567-583.

Hsu, V.W., L.C. Yuan, J.G. Nuchtern, J. Lippincott-Schwartz, G.J. Hammerling, and R.D. Klausner. 1991. A recycling pathway between the endoplasmic reticulum and the Golgi apparatus for retention of unassembled MHC class I molecules. *Nature*. 352:441-444.

Hughes, E.A., C. Hammond, and P. Cresswell. 1997. Misfolded major histocompatibility complex class I heavy chains are translocated into the cytoplasm and degraded by the proteasome. *Proc Natl Acad Sci U S A*. 94:1896-1901.

Husnjak, K., and I. Dikic. 2012. Ubiquitin-binding proteins: decoders of ubiquitin-mediated cellular functions. *Annu Rev Biochem*. 81:291-322.

Huyer, G., G.L. Longsworth, D.L. Mason, M.P. Mallampalli, J.M. McCaffery, R.L. Wright, and S. Michaelis. 2004a. A striking quality control subcompartment in Saccharomyces cerevisiae: the endoplasmic reticulum-associated compartment. *Mol Biol Cell*. 15:908-921.

Huyer, G., W.F. Piluek, Z. Fansler, S.G. Kreft, M. Hochstrasser, J.L. Brodsky, and S. Michaelis. 2004b. Distinct machinery is required in Saccharomyces cerevisiae for the endoplasmic reticulum-associated degradation of a multispanning membrane protein and a soluble luminal protein. *J Biol Chem*. 279:38369-38378.

Hwang, J., and L. Qi. 2018. Quality Control in the Endoplasmic Reticulum: Crosstalk between ERAD and UPR pathways. *Trends Biochem Sci*. 43:593-605.

Ishida, Y., H. Kubota, A. Yamamoto, A. Kitamura, H.P. Bachinger, and K. Nagata. 2006. Type I collagen in Hsp47-null cells is aggregated in endoplasmic reticulum and deficient in N-propeptide processing and fibrillogenesis. *Mol Biol Cell*. 17:2346-2355.

Ishida, Y., A. Yamamoto, A. Kitamura, S.R. Lamande, T. Yoshimori, J.F. Bateman, H. Kubota, and K. Nagata. 2009. Autophagic elimination of misfolded procollagen aggregates in the endoplasmic reticulum as a means of cell protection. *Mol Biol Cell*. 20:2744-2754.

Ito, H., Y. Fukuda, K. Murata, and A. Kimura. 1983. Transformation of intact yeast cells treated with alkali cations. *J Bacteriol*. 153:163-168.

Ito, M., N. Amizuka, H. Ozawa, and K. Oda. 2002. Retention at the cis-Golgi and delayed degradation of tissue-non-specific alkaline phosphatase with an Asn153-->Asp substitution, a cause of perinatal hypophosphatasia. *Biochem J*. 361:473-480.

Jakob, C.A., P. Burda, J. Roth, and M. Aebi. 1998. Degradation of misfolded endoplasmic reticulum glycoproteins in Saccharomyces cerevisiae is determined by a specific oligosaccharide structure. *J Cell Biol*. 142:1223-1233.

Jarosch, E., C. Taxis, C. Volkwein, J. Bordallo, D. Finley, D.H. Wolf, and T. Sommer. 2002. Protein dislocation from the ER requires polyubiquitination and the AAA-ATPase Cdc48. *Nat Cell Biol*. 4:134-139.

Jensen, T.J., M.A. Loo, S. Pind, D.B. Williams, A.L. Goldberg, and J.R. Riordan. 1995. Multiple proteolytic systems, including the proteasome, contribute to CFTR processing. *Cell*. 83:129-135.

Jin, L., K.B. Pahuja, K.E. Wickliffe, A. Gorur, C. Baumgartel, R. Schekman, and M. Rape. 2012. Ubiquitin-dependent regulation of COPII coat size and function. *Nature*. 482:495-500.

Jorgensen, M.U., S.D. Emr, and J.R. Winther. 1999. Ligand recognition and domain structure of Vps10p, a vacuolar protein sorting receptor in Saccharomyces cerevisiae. *Eur J Biochem*. 260:461-469.

Kakoi, S., T. Yorimitsu, and K. Sato. 2013. COPII machinery cooperates with ER-localized Hsp40 to sequester misfolded membrane proteins into ER-associated compartments. *Mol Biol Cell*. 24:633-642.

Kalies, K.U., S. Allan, T. Sergeyenko, H. Kroger, and K. Romisch. 2005. The protein translocation channel binds proteasomes to the endoplasmic reticulum membrane. *EMBO J*. 24:2284-2293.

Kampinga, H.H., and E.A. Craig. 2010. The HSP70 chaperone machinery: J proteins as drivers of functional specificity. *Nat Rev Mol Cell Biol*. 11:579-592.

Karagoz, G.E., D. Acosta-Alvear, and P. Walter. 2019. The Unfolded Protein Response: Detecting and Responding to Fluctuations in the Protein-Folding Capacity of the Endoplasmic Reticulum. *Cold Spring Harb Perspect Biol*.

Katzmann, D.J., E.A. Epping, and W.S. Moye-Rowley. 1999. Mutational disruption of plasma membrane trafficking of Saccharomyces cerevisiae Yor1p, a homologue of mammalian multidrug resistance protein. *Mol Cell Biol*. 19:2998-3009.

Kawaguchi, S., C.L. Hsu, and D.T. Ng. 2010. Interplay of substrate retention and export signals in endoplasmic reticulum quality control. *PLoS One*. 5:e15532.

Khaminets, A., T. Heinrich, M. Mari, P. Grumati, A.K. Huebner, M. Akutsu, L. Liebmann, A. Stolz, S. Nietzsche, N. Koch, M. Mauthe, I. Katona, B. Qualmann, J. Weis, F. Reggiori, I. Kurth, C.A. Hubner, and I. Dikic. 2015. Regulation of endoplasmic reticulum turnover by selective autophagy. *Nature*. 522:354-358.

Khmelinskii, A., E. Blaszczak, M. Pantazopoulou, B. Fischer, D.J. Omnus, G. Le Dez, A. Brossard, A. Gunnarsson, J.D. Barry, M. Meurer, D. Kirrmaier, C. Boone, W. Huber, G.

Rabut, P.O. Ljungdahl, and M. Knop. 2014. Protein quality control at the inner nuclear membrane. *Nature*. 516:410-413.

Khoriaty, R., M.P. Vasievich, and D. Ginsburg. 2012. The COPII pathway and hematologic disease. *Blood*. 120:31-38.

Kim, I., K. Mi, and H. Rao. 2004. Multiple interactions of rad23 suggest a mechanism for ubiquitylated substrate delivery important in proteolysis. *Mol Biol Cell*. 15:3357-3365.

Kincaid, M.M., and A.A. Cooper. 2007. Misfolded proteins traffic from the endoplasmic reticulum (ER) due to ER export signals. *Mol Biol Cell*. 18:455-463.

Knop, M., A. Finger, T. Braun, K. Hellmuth, and D.H. Wolf. 1996. Der1, a novel protein specifically required for endoplasmic reticulum degradation in yeast. *EMBO J*. 15:753-763.

Koegl, M., T. Hoppe, S. Schlenker, H.D. Ulrich, T.U. Mayer, and S. Jentsch. 1999. A novel ubiquitination factor, E4, is involved in multiubiquitin chain assembly. *Cell*. 96:635-644.

Kolb, A.R., P.G. Needham, C. Rothenberg, C.J. Guerriero, P.A. Welling, and J.L. Brodsky. 2014. ESCRT regulates surface expression of the Kir2.1 potassium channel. *Mol Biol Cell*. 25:276-289.

Komander, D., F. Reyes-Turcu, J.D. Licchesi, P. Odenwaelder, K.D. Wilkinson, and D. Barford. 2009. Molecular discrimination of structurally equivalent Lys 63-linked and linear polyubiquitin chains. *EMBO Rep*. 10:466-473.

Kota, J., C.F. Gilstring, and P.O. Ljungdahl. 2007. Membrane chaperone Shr3 assists in folding amino acid permeases preventing precocious ERAD. *J Cell Biol*. 176:617-628.

Kothe, M., Y. Ye, J.S. Wagner, H.E. De Luca, E. Kern, T.A. Rapoport, and W.I. Lencer. 2005. Role of p97 AAA-ATPase in the retrotranslocation of the cholera toxin A1 chain, a non-ubiquitinated substrate. *J Biol Chem*. 280:28127-28132.

Kruse, K.B., J.L. Brodsky, and A.A. McCracken. 2006. Characterization of an ERAD gene as VPS30/ATG6 reveals two alternative and functionally distinct protein quality control pathways: one for soluble Z variant of human alpha-1 proteinase inhibitor (A1PiZ) and another for aggregates of A1PiZ. *Mol Biol Cell*. 17:203-212.

Labbadia, J., and R.I. Morimoto. 2015. The biology of proteostasis in aging and disease. *Annu Rev Biochem*. 84:435-464.

Lee, D.H., M.Y. Sherman, and A.L. Goldberg. 1996. Involvement of the molecular chaperone Ydj1 in the ubiquitin-dependent degradation of short-lived and abnormal proteins in Saccharomyces cerevisiae. *Mol Cell Biol*. 16:4773-4781.

Lee, M.C., E.A. Miller, J. Goldberg, L. Orci, and R. Schekman. 2004. Bi-directional protein transport between the ER and Golgi. *Annu Rev Cell Dev Biol*. 20:87-123.

Lee, S., W.A. Lim, and K.S. Thorn. 2013. Improved blue, green, and red fluorescent protein tagging vectors for S. cerevisiae. *PLoS One*. 8:e67902.

Lefrancois, S., J. Zeng, A.J. Hassan, M. Canuel, and C.R. Morales. 2003. The lysosomal trafficking of sphingolipid activator proteins (SAPs) is mediated by sortilin. *EMBO J*. 22:6430-6437.

Letourneur, F., and P. Cosson. 1998. Targeting to the endoplasmic reticulum in yeast cells by determinants present in transmembrane domains. *J Biol Chem*. 273:33273-33278.

Li, G., G. Zhao, X. Zhou, H. Schindelin, and W.J. Lennarz. 2006. The AAA ATPase p97 links peptide N-glycanase to the endoplasmic reticulum-associated E3 ligase autocrine motility factor receptor. *Proc Natl Acad Sci U S A*. 103:8348-8353.

Li, J., J. Labbadia, and R.I. Morimoto. 2017. Rethinking HSF1 in Stress, Development, and Organismal Health. *Trends Cell Biol*. 27:895-905.

Li, M., T. Koshi, and S.D. Emr. 2015. Membrane-anchored ubiquitin ligase complex is required for the turnover of lysosomal membrane proteins. *J Cell Biol*. 211:639-652.

Lipatova, Z., and N. Segev. 2015. A Role for Macro-ER-Phagy in ER Quality Control. *PLoS Genet*. 11:e1005390.

Liu, Y., and A. Chang. 2008. Heat shock response relieves ER stress. *EMBO J*. 27:1049-1059.

Loayza, D., A. Tam, W.K. Schmidt, and S. Michaelis. 1998. Ste6p mutants defective in exit from the endoplasmic reticulum (ER) reveal aspects of an ER quality control pathway in Saccharomyces cerevisiae. *Mol Biol Cell*. 9:2767-2784.

Locke, M., J.I. Toth, and M.D. Petroski. 2014. Lys11- and Lys48-linked ubiquitin chains interact with p97 during endoplasmic-reticulum-associated degradation. *Biochem J*. 459:205-216.

Loi, M., I. Fregno, C. Guerra, and M. Molinari. 2018. Eat it right: ER-phagy and recovER-phagy. *Biochem Soc Trans*. 46:699-706.

Louie, R.J., J. Guo, J.W. Rodgers, R. White, N. Shah, S. Pagant, P. Kim, M. Livstone, K. Dolinski, B.A. McKinney, J. Hong, E.J. Sorscher, J. Bryan, E.A. Miller, and J.L.t. Hartman. 2012. A yeast phenomic model for the gene interaction network modulating CFTR-DeltaF508 protein biogenesis. *Genome Med*. 4:103.

Loureiro, J., B.N. Lilley, E. Spooner, V. Noriega, D. Tortorella, and H.L. Ploegh. 2006. Signal peptide peptidase is required for dislocation from the endoplasmic reticulum. *Nature*. 441:894-897.

Lu, Z., and D.M. Cyr. 1998. The conserved carboxyl terminus and zinc finger-like domain of the co-chaperone Ydj1 assist Hsp70 in protein folding. *J Biol Chem*. 273:5970-5978.

Lukacs, G.L., and A.S. Verkman. 2012. CFTR: folding, misfolding and correcting the DeltaF508 conformational defect. *Trends Mol Med*. 18:81-91.

Luo, W., and A. Chang. 1997. Novel genes involved in endosomal traffic in yeast revealed by suppression of a targeting-defective plasma membrane ATPase mutant. *J Cell Biol*. 138:731-746.

Lupashin, V.V., S. Hamamoto, and R.W. Schekman. 1996. Biochemical requirements for the targeting and fusion of ER-derived transport vesicles with purified yeast Golgi membranes. *J Cell Biol*. 132:277-289.

Ma, W., E. Goldberg, and J. Goldberg. 2017. ER retention is imposed by COPII protein sorting and attenuated by 4-phenylbutyrate. *Elife*. 6.

MacDonald, C., S. Winistorfer, R.M. Pope, M.E. Wright, and R.C. Piper. 2017. Enzyme reversal to explore the function of yeast E3 ubiquitin-ligases. *Traffic*. 18:465-484.

MacGurn, J.A., P.C. Hsu, and S.D. Emr. 2012. Ubiquitin and membrane protein turnover: from cradle to grave. *Annu Rev Biochem*. 81:231-259.

Mackie, T.D., B.Y. Kim, A.R. Subramanya, D.J. Bain, A.F. O'Donnell, P.A. Welling, and J.L. Brodsky. 2018. The endosomal trafficking factors CORVET and ESCRT suppress plasma membrane residence of the renal outer medullary potassium channel (ROMK). *J Biol Chem*. 293:3201-3217.

Marcusson, E.G., B.F. Horazdovsky, J.L. Cereghino, E. Gharakhanian, and S.D. Emr. 1994. The sorting receptor for yeast vacuolar carboxypeptidase Y is encoded by the VPS10 gene. *Cell*. 77:579-586.

Marini, J.C., A. Forlino, W.A. Cabral, A.M. Barnes, J.D. San Antonio, S. Milgrom, J.C. Hyland, J. Korkko, D.J. Prockop, A. De Paepe, P. Coucke, S. Symoens, F.H. Glorieux, P.J. Roughley, A.M. Lund, K. Kuurila-Svahn, H. Hartikka, D.H. Cohn, D. Krakow, M. Mottes, U. Schwarze, D. Chen, K. Yang, C. Kuslich, J. Troendle, R. Dalgleish, and P.H. Byers. 2007. Consortium for osteogenesis imperfecta mutations in the helical domain of type I collagen: regions rich in lethal mutations align with collagen binding sites for integrins and proteoglycans. *Hum Mutat*. 28:209-221.

Marshall, R.S., Z. Hua, S. Mali, F. McLoughlin, and R.D. Vierstra. 2019. ATG8-Binding UIM Proteins Define a New Class of Autophagy Adaptors and Receptors. *Cell*. 177:766-781 e724.

Marshall, R.S., F. Li, D.C. Gemperline, A.J. Book, and R.D. Vierstra. 2015. Autophagic Degradation of the 26S Proteasome Is Mediated by the Dual ATG8/Ubiquitin Receptor RPN10 in Arabidopsis. *Mol Cell*. 58:1053-1066.

Mayer, M.P., and B. Bukau. 2005. Hsp70 chaperones: cellular functions and molecular mechanism. *Cell Mol Life Sci*. 62:670-684.

McCaughey, J., N.L. Stevenson, S. Cross, and D.J. Stephens. 2019. ER-to-Golgi trafficking of procollagen in the absence of large carriers. *J Cell Biol*. 218:929-948.

McCracken, A.A., and J.L. Brodsky. 1996. Assembly of ER-associated protein degradation in vitro: dependence on cytosol, calnexin, and ATP. *J Cell Biol*. 132:291-298.

Medicherla, B., Z. Kostova, A. Schaefer, and D.H. Wolf. 2004. A genomic screen identifies Dsk2p and Rad23p as essential components of ER-associated degradation. *EMBO Rep*. 5:692-697.

Mehnert, M., T. Sommer, and E. Jarosch. 2014. Der1 promotes movement of misfolded proteins through the endoplasmic reticulum membrane. *Nat Cell Biol*. 16:77-86.

Meusser, B., C. Hirsch, E. Jarosch, and T. Sommer. 2005. ERAD: the long road to destruction. *Nat Cell Biol*. 7:766-772.

Michaelis, S., and I. Herskowitz. 1988. The a-factor pheromone of Saccharomyces cerevisiae is essential for mating. *Mol Cell Biol*. 8:1309-1318.

Mitchell, D.M., M. Zhou, R. Pariyarath, H. Wang, J.D. Aitchison, H.N. Ginsberg, and E.A. Fisher. 1998. Apoprotein B100 has a prolonged interaction with the translocon during which its lipidation and translocation change from dependence on the microsomal triglyceride transfer protein to independence. *Proc Natl Acad Sci U S A*. 95:14733-14738.

Mochida, K., Y. Oikawa, Y. Kimura, H. Kirisako, H. Hirano, Y. Ohsumi, and H. Nakatogawa. 2015. Receptor-mediated selective autophagy degrades the endoplasmic reticulum and the nucleus. *Nature*. 522:359-362.

Mogk, A., E. Kummer, and B. Bukau. 2015. Cooperation of Hsp70 and Hsp100 chaperone machines in protein disaggregation. *Front Mol Biosci*. 2:22.

Moir, D., S.E. Stewart, B.C. Osmond, and D. Botstein. 1982. Cold-sensitive cell-division-cycle mutants of yeast: isolation, properties, and pseudoreversion studies. *Genetics*. 100:547-563.

Mumberg, D., R. Muller, and M. Funk. 1995. Yeast vectors for the controlled expression of heterologous proteins in different genetic backgrounds. *Gene*. 156:119-122.

Nakatsukasa, K., G. Huyer, S. Michaelis, and J.L. Brodsky. 2008. Dissecting the ER-associated degradation of a misfolded polytopic membrane protein. *Cell*. 132:101-112.

Needham, P.G., and J.L. Brodsky. 2013. How early studies on secreted and membrane protein quality control gave rise to the ER associated degradation (ERAD) pathway: the early history of ERAD. *Biochim Biophys Acta*. 1833:2447-2457.

Needham, P.G., C.J. Guerriero, and J.L. Brodsky. 2019. Chaperoning Endoplasmic Reticulum-Associated Degradation (ERAD) and Protein Conformational Diseases. *Cold Spring Harb Perspect Biol.*

Neuber, O., E. Jarosch, C. Volkwein, J. Walter, and T. Sommer. 2005. Ubx2 links the Cdc48 complex to ER-associated protein degradation. *Nat Cell Biol*. 7:993-998.

Nielsen, M.S., C. Jacobsen, G. Olivecrona, J. Gliemann, and C.M. Petersen. 1999. Sortilin/neurotensin receptor-3 binds and mediates degradation of lipoprotein lipase. *J Biol Chem*. 274:8832-8836.

Nielsen, M.S., P. Madsen, E.I. Christensen, A. Nykjaer, J. Gliemann, D. Kasper, R. Pohlmann, and C.M. Petersen. 2001. The sortilin cytoplasmic tail conveys Golgi-endosome transport and binds the VHS domain of the GGA2 sorting protein. *EMBO J*. 20:2180-2190.

Nishikawa, S., J.L. Brodsky, and K. Nakatsukasa. 2005. Roles of molecular chaperones in endoplasmic reticulum (ER) quality control and ER-associated degradation (ERAD). *J Biochem*. 137:551-555.

Nishikawa, S.I., S.W. Fewell, Y. Kato, J.L. Brodsky, and T. Endo. 2001. Molecular chaperones in the yeast endoplasmic reticulum maintain the solubility of proteins for retrotranslocation and degradation. *J Cell Biol*. 153:1061-1070.

Oh, E., D. Akopian, and M. Rape. 2018. Principles of Ubiquitin-Dependent Signaling. *Annu Rev Cell Dev Biol*. 34:137-162.

Okamoto, K. 2014. Organellophagy: eliminating cellular building blocks via selective autophagy. *J Cell Biol*. 205:435-445.

Okiyoneda, T., P.M. Apaja, and G.L. Lukacs. 2011. Protein quality control at the plasma membrane. *Curr Opin Cell Biol*. 23:483-491.

Otte, S., W.J. Belden, M. Heidtman, J. Liu, O.N. Jensen, and C. Barlowe. 2001. Erv41p and Erv46p: new components of COPII vesicles involved in transport between the ER and Golgi complex. *J Cell Biol*. 152:503-518.

Park, S.H., N. Bolender, F. Eisele, Z. Kostova, J. Takeuchi, P. Coffino, and D.H. Wolf. 2007. The cytoplasmic Hsp70 chaperone machinery subjects misfolded and endoplasmic reticulum import-incompetent proteins to degradation via the ubiquitin-proteasome system. *Mol Biol Cell*. 18:153-165.

Penchala, S.C., S. Connelly, Y. Wang, M.S. Park, L. Zhao, A. Baranczak, I. Rappley, H. Vogel, M. Liedtke, R.M. Witteles, E.T. Powers, N. Reixach, W.K. Chan, I.A. Wilson, J.W. Kelly, I.A. Graef, and M.M. Alhamadsheh. 2013. AG10 inhibits amyloidogenesis and cellular toxicity of the familial amyloid cardiomyopathy-associated V122I transthyretin. *Proc Natl Acad Sci U S A*. 110:9992-9997.

Perlmutter, D.H. 2011. Alpha-1-antitrypsin deficiency: importance of proteasomal and autophagic degradative pathways in disposal of liver disease-associated protein aggregates. *Annu Rev Med*. 62:333-345.

Piper, R.C., and D.J. Katzmann. 2007. Biogenesis and function of multivesicular bodies. *Annu Rev Cell Dev Biol*. 23:519-547.

Pizzirusso, M., and A. Chang. 2004. Ubiquitin-mediated targeting of a mutant plasma membrane ATPase, Pma1-7, to the endosomal/vacuolar system in yeast. *Mol Biol Cell*. 15:2401-2409.

Platt, F.M., A. d'Azzo, B.L. Davidson, E.F. Neufeld, and C.J. Tifft. 2018. Lysosomal storage diseases. *Nat Rev Dis Primers*. 4:27.

Plemper, R.K., J. Bordallo, P.M. Deak, C. Taxis, R. Hitt, and D.H. Wolf. 1999. Genetic interactions of Hrd3p and Der3p/Hrd1p with Sec61p suggest a retro-translocation complex mediating protein transport for ER degradation. *J Cell Sci*. 112 (Pt 22):4123-4134.

Potelle, S., A. Klein, and F. Foulquier. 2015. Golgi post-translational modifications and associated diseases. *J Inherit Metab Dis*. 38:741-751.

Prasad, R., S. Kawaguchi, and D.T. Ng. 2012. Biosynthetic mode can determine the mechanism of protein quality control. *Biochem Biophys Res Commun*. 425:689-695.

Prasad, R., C. Xu, and D.T.W. Ng. 2018. Hsp40/70/110 chaperones adapt nuclear protein quality control to serve cytosolic clients. *J Cell Biol*. 217:2019-2032.

Preissler, S., and D. Ron. 2018. Early Events in the Endoplasmic Reticulum Unfolded Protein Response. *Cold Spring Harb Perspect Biol*.

Preston, G.M., and J.L. Brodsky. 2017. The evolving role of ubiquitin modification in endoplasmic reticulum-associated degradation. *Biochem J*. 474:445-469.

Preston, G.M., C.J. Guerriero, M.B. Metzger, S. Michaelis, and J.L. Brodsky. 2018. Substrate Insolubility Dictates Hsp104-Dependent Endoplasmic-Reticulum-Associated Degradation. *Mol Cell*. 70:242-253 e246.

Raote, I., and V. Malhotra. 2019. Protein transport by vesicles and tunnels. *J Cell Biol*. 218:737-739.

Raote, I., M. Ortega-Bellido, A.J. Santos, O. Foresti, C. Zhang, M.F. Garcia-Parajo, F. Campelo, and V. Malhotra. 2018. TANGO1 builds a machine for collagen export by recruiting and spatially organizing COPII, tethers and membranes. *Elife*. 7.

Rapoport, T.A., L. Li, and E. Park. 2017. Structural and Mechanistic Insights into Protein Translocation. *Annu Rev Cell Dev Biol*. 33:369-390.

Rayner, J.C., and H.R. Pelham. 1997. Transmembrane domain-dependent sorting of proteins to the ER and plasma membrane in yeast. *EMBO J*. 16:1832-1841.

Reggiori, F., and H.R. Pelham. 2002. A transmembrane ubiquitin ligase required to sort membrane proteins into multivesicular bodies. *Nat Cell Biol*. 4:117-123.

Ross, C.A., and M.A. Poirier. 2004. Protein aggregation and neurodegenerative disease. *Nat Med*. 10 Suppl:S10-17.

Roth, F.P., J.D. Hughes, P.W. Estep, and G.M. Church. 1998. Finding DNA regulatory motifs within unaligned noncoding sequences clustered by whole-genome mRNA quantitation. *Nat Biotechnol*. 16:939-945.

Rougier, J.S., M. Albesa, H. Abriel, and P. Viard. 2011. Neuronal precursor cell-expressed developmentally down-regulated 4-1 (NEDD4-1) controls the sorting of newly synthesized Ca(V)1.2 calcium channels. *J Biol Chem*. 286:8829-8838.

Rowe, S.M., and A.S. Verkman. 2013. Cystic fibrosis transmembrane regulator correctors and potentiators. *Cold Spring Harb Perspect Med*. 3.

Ruggiano, A., O. Foresti, and P. Carvalho. 2014. Quality control: ER-associated degradation: protein quality control and beyond. *J Cell Biol*. 204:869-879.

Sahu, R., S. Kaushik, C.C. Clement, E.S. Cannizzo, B. Scharf, A. Follenzi, I. Potolicchio, E. Nieves, A.M. Cuervo, and L. Santambrogio. 2011. Microautophagy of cytosolic proteins by late endosomes. *Dev Cell*. 20:131-139.

Sanders, S.L., K.M. Whitfield, J.P. Vogel, M.D. Rose, and R.W. Schekman. 1992. Sec61p and BiP directly facilitate polypeptide translocation into the ER. *Cell*. 69:353-365.

Santoro, N., N. Johansson, and D.J. Thiele. 1998. Heat shock element architecture is an important determinant in the temperature and transactivation domain requirements for heat shock transcription factor. *Mol Cell Biol*. 18:6340-6352.

Sardana, R., L. Zhu, and S.D. Emr. 2019. Rsp5 Ubiquitin ligase-mediated quality control system clears membrane proteins mistargeted to the vacuole membrane. *J Cell Biol*. 218:234-250.

Sato, B.K., D. Schulz, P.H. Do, and R.Y. Hampton. 2009. Misfolded membrane proteins are specifically recognized by the transmembrane domain of the Hrd1p ubiquitin ligase. *Mol Cell*. 34:212-222.

Schafer, A., and D.H. Wolf. 2009. Sec61p is part of the endoplasmic reticulum-associated degradation machinery. *EMBO J*. 28:2874-2884.

Schoebel, S., W. Mi, A. Stein, S. Ovchinnikov, R. Pavlovicz, F. DiMaio, D. Baker, M.G. Chambers, H. Su, D. Li, T.A. Rapoport, and M. Liao. 2017. Cryo-EM structure of the protein-conducting ERAD channel Hrd1 in complex with Hrd3. *Nature*. 548:352-355.

Schubert, U., L.C. Anton, I. Bacik, J.H. Cox, S. Bour, J.R. Bennink, M. Orlowski, K. Strebel, and J.W. Yewdell. 1998. CD4 glycoprotein degradation induced by human immunodeficiency virus type 1 Vpu protein requires the function of proteasomes and the ubiquitin-conjugating pathway. *J Virol*. 72:2280-2288.

Schuberth, C., and A. Buchberger. 2005. Membrane-bound Ubx2 recruits Cdc48 to ubiquitin ligases and their substrates to ensure efficient ER-associated protein degradation. *Nat Cell Biol*. 7:999-1006.

Schuck, S., C.M. Gallagher, and P. Walter. 2014. ER-phagy mediates selective degradation of endoplasmic reticulum independently of the core autophagy machinery. *J Cell Sci*. 127:4078-4088.

Schuck, S., W.A. Prinz, K.S. Thorn, C. Voss, and P. Walter. 2009. Membrane expansion alleviates endoplasmic reticulum stress independently of the unfolded protein response. *J Cell Biol*. 187:525-536.

Schultz, M.L., K.L. Krus, S. Kaushik, D. Dang, R. Chopra, L. Qi, V.G. Shakkottai, A.M. Cuervo, and A.P. Lieberman. 2018. Coordinate regulation of mutant NPC1 degradation by selective ER autophagy and MARCH6-dependent ERAD. *Nat Commun*. 9:3671.

Senft, D., and Z.A. Ronai. 2015. UPR, autophagy, and mitochondria crosstalk underlies the ER stress response. *Trends Biochem Sci*. 40:141-148.

Sewell, A.K., F. Yokoya, W. Yu, T. Miyagawa, T. Murayama, and D.R. Winge. 1995. Mutated yeast heat shock transcription factor exhibits elevated basal transcriptional activation and confers metal resistance. *J Biol Chem*. 270:25079-25086.

Shao, S., and R.S. Hegde. 2016. Target Selection during Protein Quality Control. *Trends Biochem Sci*. 41:124-137.

Singh, S., and A. Mittal. 2016. Transmembrane Domain Lengths Serve as Signatures of Organismal Complexity and Viral Transport Mechanisms. *Sci Rep*. 6:22352.

Smith, M., and S. Wilkinson. 2017. ER homeostasis and autophagy. *Essays Biochem*. 61:625-635.

Smith, M.D., M.E. Harley, A.J. Kemp, J. Wills, M. Lee, M. Arends, A. von Kriegsheim, C. Behrends, and S. Wilkinson. 2018. CCPG1 Is a Non-canonical Autophagy Cargo Receptor Essential for ER-Phagy and Pancreatic ER Proteostasis. *Dev Cell*. 44:217-232 e211.

Snider, J., G. Thibault, and W.A. Houry. 2008. The AAA+ superfamily of functionally diverse proteins. *Genome Biol*. 9:216.

Sommer, T., and S. Jentsch. 1993. A protein translocation defect linked to ubiquitin conjugation at the endoplasmic reticulum. *Nature*. 365:176-179.

Spear, E.D., and D.T. Ng. 2003. Stress tolerance of misfolded carboxypeptidase Y requires maintenance of protein trafficking and degradative pathways. *Mol Biol Cell*. 14:2756-2767.

Stagg, H.R., M. Thomas, D. van den Boomen, E.J. Wiertz, H.A. Drabkin, R.M. Gemmill, and P.J. Lehner. 2009. The TRC8 E3 ligase ubiquitinates MHC class I molecules before dislocation from the ER. *J Cell Biol*. 186:685-692.

Stagg, S.M., C. Gurkan, D.M. Fowler, P. LaPointe, T.R. Foss, C.S. Potter, B. Carragher, and W.E. Balch. 2006. Structure of the Sec13/31 COPII coat cage. *Nature*. 439:234-238.

Staub, O., S. Dho, P. Henry, J. Correa, T. Ishikawa, J. McGlade, and D. Rotin. 1996. WW domains of Nedd4 bind to the proline-rich PY motifs in the epithelial Na+ channel deleted in Liddle's syndrome. *EMBO J*. 15:2371-2380.

Stewart, E.V., S.J. Lloyd, J.S. Burg, C.C. Nwosu, R.E. Lintner, R. Daza, C. Russ, K. Ponchner, C. Nusbaum, and P.J. Espenshade. 2012. Yeast sterol regulatory element-binding protein (SREBP) cleavage requires Cdc48 and Dsc5, a ubiquitin regulatory X domain-containing subunit of the Golgi Dsc E3 ligase. *J Biol Chem*. 287:672-681.

Stewart, E.V., C.C. Nwosu, Z. Tong, A. Roguev, T.D. Cummins, D.U. Kim, J. Hayles, H.O. Park, K.L. Hoe, D.W. Powell, N.J. Krogan, and P.J. Espenshade. 2011. Yeast SREBP cleavage activation requires the Golgi Dsc E3 ligase complex. *Mol Cell*. 42:160-171.

Stirling, C.J., J. Rothblatt, M. Hosobuchi, R. Deshaies, and R. Schekman. 1992. Protein translocation mutants defective in the insertion of integral membrane proteins into the endoplasmic reticulum. *Mol Biol Cell*. 3:129-142.

Stoller, J.K., and L.S. Aboussouan. 2012. A review of alpha1-antitrypsin deficiency. *Am J Respir Crit Care Med*. 185:246-259.

Stolz, A., S. Besser, H. Hottmann, and D.H. Wolf. 2013. Previously unknown role for the ubiquitin ligase Ubr1 in endoplasmic reticulum-associated protein degradation. *Proc Natl Acad Sci U S A*. 110:15271-15276.

Stringer, D.K., and R.C. Piper. 2011. A single ubiquitin is sufficient for cargo protein entry into MVBs in the absence of ESCRT ubiquitination. *J Cell Biol*. 192:229-242.

Subramanian, A., A. Capalbo, N.R. Iyengar, R. Rizzo, A. di Campli, R. Di Martino, M. Lo Monte, A.R. Beccari, A. Yerudkar, C. Del Vecchio, L. Glielmo, G. Turacchio, M. Pirozzi, S.G. Kim, P. Henklein, J. Cancino, S. Parashuraman, D. Diviani, F. Fanelli, M. Sallese, and A. Luini. 2019. Auto-regulation of Secretory Flux by Sensing and Responding to the Folded Cargo Protein Load in the Endoplasmic Reticulum. *Cell*. 176:1461-1476 e1423.

Sun, Z., and J.L. Brodsky. 2017. Guardians of the ERAD Galaxy. *Cell*. 171:267-268.

Sun, Z., and J.L. Brodsky. 2018. The degradation pathway of a model misfolded protein is determined by aggregation propensity. *Mol Biol Cell*. 29:1422-1434.

Sweeney, P., H. Park, M. Baumann, J. Dunlop, J. Frydman, R. Kopito, A. McCampbell, G. Leblanc, A. Venkateswaran, A. Nurmi, and R. Hodgson. 2017. Protein misfolding in neurodegenerative diseases: implications and strategies. *Transl Neurodegener*. 6:6.

Tamarappoo, B.K., B. Yang, and A.S. Verkman. 1999. Misfolding of mutant aquaporin-2 water channels in nephrogenic diabetes insipidus. *J Biol Chem*. 274:34825-34831.

Tansey, W.P. 2007. Pulse-chase assay for measuring protein stability in yeast. *CSH Protoc*. 2007:pdb prot4641.

Tao, Y.X., and P.M. Conn. 2014. Chaperoning G protein-coupled receptors: from cell biology to therapeutics. *Endocr Rev*. 35:602-647.

Tao, Y.X., and P.M. Conn. 2018. Pharmacoperones as Novel Therapeutics for Diverse Protein Conformational Diseases. *Physiol Rev*. 98:697-725.

Taxis, C., F. Vogel, and D.H. Wolf. 2002. ER-golgi traffic is a prerequisite for efficient ER degradation. *Mol Biol Cell*. 13:1806-1818.

Teckman, J.H., and D.H. Perlmutter. 1996. The endoplasmic reticulum degradation pathway for mutant secretory proteins alpha1-antitrypsin Z and S is distinct from that for an unassembled membrane protein. *J Biol Chem*. 271:13215-13220.

Teckman, J.H., and D.H. Perlmutter. 2000. Retention of mutant alpha(1)-antitrypsin Z in endoplasmic reticulum is associated with an autophagic response. *Am J Physiol Gastrointest Liver Physiol*. 279:G961-974.

Tewari, R., C. Bachert, and A.D. Linstedt. 2015. Induced oligomerization targets Golgi proteins for degradation in lysosomes. *Mol Biol Cell*. 26:4427-4437.

Theesfeld, C.L., and R.Y. Hampton. 2013. Insulin-induced gene protein (INSIG)-dependent sterol regulation of Hmg2 endoplasmic reticulum-associated degradation (ERAD) in yeast. *J Biol Chem*. 288:8519-8530.

Tooze, J., M. Hollinshead, T. Ludwig, K. Howell, B. Hoflack, and H. Kern. 1990. In exocrine pancreas, the basolateral endocytic pathway converges with the autophagic pathway immediately after the early endosome. *J Cell Biol*. 111:329-345.

Travers, K.J., C.K. Patil, L. Wodicka, D.J. Lockhart, J.S. Weissman, and P. Walter. 2000. Functional and genomic analyses reveal an essential coordination between the unfolded protein response and ER-associated degradation. *Cell*. 101:249-258.

Trombetta, E.S., and A.J. Parodi. 2003. Quality control and protein folding in the secretory pathway. *Annu Rev Cell Dev Biol*. 19:649-676.

Tsai, J., and M.G. Douglas. 1996. A conserved HPD sequence of the J-domain is necessary for YDJ1 stimulation of Hsp70 ATPase activity at a site distinct from substrate binding. *J Biol Chem*. 271:9347-9354.

Tsuchiya, H., F. Ohtake, N. Arai, A. Kaiho, S. Yasuda, K. Tanaka, and Y. Saeki. 2017. In Vivo Ubiquitin Linkage-type Analysis Reveals that the Cdc48-Rad23/Dsk2 Axis Contributes to K48-Linked Chain Specificity of the Proteasome. *Mol Cell*. 66:488-502 e487.

Uttenweiler, A., H. Schwarz, H. Neumann, and A. Mayer. 2007. The vacuolar transporter chaperone (VTC) complex is required for microautophagy. *Mol Biol Cell*. 18:166-175.

Valastyan, J.S., and S. Lindquist. 2014. Mechanisms of protein-folding diseases at a glance. *Dis Model Mech*. 7:9-14.

Vashist, S., W. Kim, W.J. Belden, E.D. Spear, C. Barlowe, and D.T. Ng. 2001. Distinct retrieval and retention mechanisms are required for the quality control of endoplasmic reticulum protein folding. *J Cell Biol*. 155:355-368.

Vashist, S., and D.T. Ng. 2004. Misfolded proteins are sorted by a sequential checkpoint mechanism of ER quality control. *J Cell Biol*. 165:41-52.

Veit, G., R.G. Avramescu, A.N. Chiang, S.A. Houck, Z. Cai, K.W. Peters, J.S. Hong, H.B. Pollard, W.B. Guggino, W.E. Balch, W.R. Skach, G.R. Cutting, R.A. Frizzell, D.N. Sheppard, D.M. Cyr, E.J. Sorscher, J.L. Brodsky, and G.L. Lukacs. 2016. From CFTR biology toward combinatorial pharmacotherapy: expanded classification of cystic fibrosis mutations. *Mol Biol Cell*. 27:424-433.

Vembar, S.S., and J.L. Brodsky. 2008. One step at a time: endoplasmic reticulum-associated degradation. *Nat Rev Mol Cell Biol*. 9:944-957.

Venkat, S., and A.D. Linstedt. 2017. Manganese-induced trafficking and turnover of GPP130 is mediated by sortilin. *Mol Biol Cell*. 28:2569-2578.

Wahlman, J., G.N. DeMartino, W.R. Skach, N.J. Bulleid, J.L. Brodsky, and A.E. Johnson. 2007. Real-time fluorescence detection of ERAD substrate retrotranslocation in a mammalian in vitro system. *Cell*. 129:943-955.

Wallis, J.W., G. Chrebet, G. Brodsky, M. Rolfe, and R. Rothstein. 1989. A hyper-recombination mutation in S. cerevisiae identifies a novel eukaryotic topoisomerase. *Cell*. 58:409-419.

Wang, F., L.A. Durfee, and J.M. Huibregtse. 2013. A cotranslational ubiquitination pathway for quality control of misfolded proteins. *Mol Cell*. 50:368-378.

Wang, F., W. Song, G. Brancati, and L. Segatori. 2011a. Inhibition of endoplasmic reticulum-associated degradation rescues native folding in loss of function protein misfolding diseases. *J Biol Chem*. 286:43454-43464.

Wang, Q., Y. Liu, N. Soetandyo, K. Baek, R. Hegde, and Y. Ye. 2011b. A ubiquitin ligase-associated chaperone holdase maintains polypeptides in soluble states for proteasome degradation. *Mol Cell*. 42:758-770.

Wang, S., and D.T. Ng. 2010. Evasion of endoplasmic reticulum surveillance makes Wsc1p an obligate substrate of Golgi quality control. *Mol Biol Cell*. 21:1153-1165.

Wang, S., G. Thibault, and D.T. Ng. 2011c. Routing misfolded proteins through the multivesicular body (MVB) pathway protects against proteotoxicity. *J Biol Chem*. 286:29376-29387.

Wangeline, M.A., N. Vashistha, and R.Y. Hampton. 2017. Proteostatic Tactics in the Strategy of Sterol Regulation. *Annu Rev Cell Dev Biol*. 33:467-489.

Ward, C.L., S. Omura, and R.R. Kopito. 1995. Degradation of CFTR by the ubiquitin-proteasome pathway. *Cell*. 83:121-127.

Watanabe, R., and H. Riezman. 2004. Differential ER exit in yeast and mammalian cells. *Curr Opin Cell Biol*. 16:350-355.

Weber, A., I. Cohen, O. Popp, G. Dittmar, Y. Reiss, T. Sommer, T. Ravid, and E. Jarosch. 2016. Sequential Poly-ubiquitylation by Specialized Conjugating Enzymes Expands the Versatility of a Quality Control Ubiquitin Ligase. *Mol Cell*. 63:827-839.

Welsh, M.J., and A.E. Smith. 1993. Molecular mechanisms of CFTR chloride channel dysfunction in cystic fibrosis. *Cell*. 73:1251-1254.

Werner, E.D., J.L. Brodsky, and A.A. McCracken. 1996. Proteasome-dependent endoplasmic reticulum-associated protein degradation: an unconventional route to a familiar fate. *Proc Natl Acad Sci U S A*. 93:13797-13801.

Wiertz, E.J., T.R. Jones, L. Sun, M. Bogyo, H.J. Geuze, and H.L. Ploegh. 1996a. The human cytomegalovirus US11 gene product dislocates MHC class I heavy chains from the endoplasmic reticulum to the cytosol. *Cell*. 84:769-779.

Wiertz, E.J., D. Tortorella, M. Bogyo, J. Yu, W. Mothes, T.R. Jones, T.A. Rapoport, and H.L. Ploegh. 1996b. Sec61-mediated transfer of a membrane protein from the endoplasmic reticulum to the proteasome for destruction. *Nature*. 384:432-438.

Winzeler, E.A., D.D. Shoemaker, A. Astromoff, H. Liang, K. Anderson, B. Andre, R. Bangham, R. Benito, J.D. Boeke, H. Bussey, A.M. Chu, C. Connelly, K. Davis, F. Dietrich, S.W. Dow, M. El Bakkoury, F. Foury, S.H. Friend, E. Gentalen, G. Giaever, J.H. Hegemann, T. Jones, M. Laub, H. Liao, N. Liebundguth, D.J. Lockhart, A. Lucau-Danila, M. Lussier, N. M'Rabet, P. Menard, M. Mittmann, C. Pai, C. Rebischung, J.L. Revuelta, L. Riles, C.J. Roberts, P. Ross-MacDonald, B. Scherens, M. Snyder, S. Sookhai-Mahadeo, R.K. Storms, S. Veronneau, M. Voet, G. Volckaert, T.R. Ward, R. Wysocki, G.S. Yen, K. Yu, K. Zimmermann, P. Philippsen, M. Johnston, and R.W. Davis. 1999. Functional characterization of the S. cerevisiae genome by gene deletion and parallel analysis. *Science*. 285:901-906.

Wolf, D.H., and A. Schafer. 2005. CPY* and the power of yeast genetics in the elucidation of quality control and associated protein degradation of the endoplasmic reticulum. *Curr Top Microbiol Immunol*. 300:41-56.

Wolins, N., H. Bosshart, H. Kuster, and J.S. Bonifacino. 1997. Aggregation as a determinant of protein fate in post-Golgi compartments: role of the luminal domain of furin in lysosomal targeting. *J Cell Biol*. 139:1735-1745.

Xie, W., K. Kanehara, A. Sayeed, and D.T. Ng. 2009. Intrinsic conformational determinants signal protein misfolding to the Hrd1/Htm1 endoplasmic reticulum-associated degradation system. *Mol Biol Cell*. 20:3317-3329.

Xu, C., and D.T. Ng. 2015a. Glycosylation-directed quality control of protein folding. *Nat Rev Mol Cell Biol*. 16:742-752.

Xu, C., and D.T. Ng. 2015b. O-mannosylation: The other glycan player of ER quality control. *Semin Cell Dev Biol*. 41:129-134.

Xu, C., S. Wang, G. Thibault, and D.T. Ng. 2013. Futile protein folding cycles in the ER are terminated by the unfolded protein O-mannosylation pathway. *Science*. 340:978-981.

Yamamoto, K., R. Fujii, Y. Toyofuku, T. Saito, H. Koseki, V.W. Hsu, and T. Aoe. 2001. The KDEL receptor mediates a retrieval mechanism that contributes to quality control at the endoplasmic reticulum. *EMBO J*. 20:3082-3091.

Yamasaki, A., T. Hara, I. Maejima, M. Sato, K. Sato, and K. Sato. 2014. Rer1p regulates the ER retention of immature rhodopsin and modulates its intracellular trafficking. *Sci Rep*. 4:5973.

Yang, X., F.M. Arines, W. Zhang, and M. Li. 2018. Sorting of a multi-subunit ubiquitin ligase complex in the endolysosome system. *Elife*. 7.

Yang, Y.S., and S.M. Strittmatter. 2007. The reticulons: a family of proteins with diverse functions. *Genome Biol*. 8:234.

Ye, Y., H.H. Meyer, and T.A. Rapoport. 2003. Function of the p97-Ufd1-Npl4 complex in retrotranslocation from the ER to the cytosol: dual recognition of nonubiquitinated polypeptide segments and polyubiquitin chains. *J Cell Biol*. 162:71-84.

Youker, R.T., P. Walsh, T. Beilharz, T. Lithgow, and J.L. Brodsky. 2004. Distinct roles for the Hsp40 and Hsp90 molecular chaperones during cystic fibrosis transmembrane conductance regulator degradation in yeast. *Mol Biol Cell*. 15:4787-4797.

Zhang, S., C. Xu, K.E. Larrimore, and D.T.W. Ng. 2017. Slp1-Emp65: A Guardian Factor that Protects Folding Polypeptides from Promiscuous Degradation. *Cell*. 171:346-357 e312.

Zhang, Y., G. Nijbroek, M.L. Sullivan, A.A. McCracken, S.C. Watkins, S. Michaelis, and J.L. Brodsky. 2001. Hsp70 molecular chaperone facilitates endoplasmic reticulum-associated protein degradation of cystic fibrosis transmembrane conductance regulator in yeast. *Mol Biol Cell*. 12:1303-1314.

Zhao, S., and H.D. Ulrich. 2010. Distinct consequences of posttranslational modification by linear versus K63-linked polyubiquitin chains. *Proc Natl Acad Sci U S A*. 107:7704-7709.

Zhao, Y., J.A. Macgurn, M. Liu, and S. Emr. 2013. The ART-Rsp5 ubiquitin ligase network comprises a plasma membrane quality control system that protects yeast cells from proteotoxic stress. *Elife*. 2:e00459.